8-2018

Constructing Fragment-Density Functionals

Kaili Jiang
Purdue University

CONSTRUCTING FRAGMENT-DENSITY FUNCTIONALS

A Dissertation

Submitted to the Faculty

of

Purdue University

by

Kaili Jiang

In Partial Fulfillment of the

Requirements for the Degree

of

Doctor of Philosophy

August 2018

Purdue University

West Lafayette, Indiana

THE PURDUE UNIVERSITY GRADUATE SCHOOL
STATEMENT OF DISSERTATION APPROVAL

Dr. Adam Wasserman, Chair

Department of Chemistry

Dr. Erica Carlson

Department of Physics and Astronomy

Dr. Hisao Nakanishi

Department of Physics and Astronomy

Dr. Onna Malis

Department of Physics and Astronomy

Approved by:

Dr. John P. Finley

Department of Physics and Astronomy

ACKNOWLEDGMENTS

I would like to thank every member in the Wasserman group who I have had a chance to work with during my Ph.D.. Especially thanks to Jonathan Nafziger and Martín Mosquera, who have laid down the foundations of my research. Thanks to Daniel Jensen, Carlos Borca, Kelsie Niffenegger, Ben Fasig, Alicia Hernández, Sara Gómez, Adam Kline, Yanal Ouies, Kui Zhang, and Victor Chavez. It has been a pleasure to work with you. Thanks to Prof. Adam Wasserman, our kind and supportive advisor. I would also like to thank Prof. Kieron Burke, who supported my post-doc application, and the United States Department of Energy who funded my research.

I would like to thank everyone in the Purdue board game group, who provides pleasure after work during these years. Thanks to Isaac Childres. I like your games!

Finally, I would like to thank my parents for the tremendous support over my life. Thank you for standing behind me even during my worst days!

TABLE OF CONTENTS

Page

LIST OF TABLES

Table Page

LIST OF FIGURES

Figure Page

ABBREVIATIONS

2OA	two-orbital approximation
DFT	density-functional theory
ENS	ensemble treatment
FDE	frozen-density embedding
FOO	fractionally occupied orbitals
GGA	generalized gradient approximation
HOMO	highest occupied molecular orbital
KE	kinetic energy
KS	Kohn-Sham
KSCED	Kohn-Sham equations with constrained electron density
LDA	local-density approximation
NAKE	non-additive non-interacting kinetic energy
NAKP	non-additive non-interacting kinetic potential
OF	orbital-free
P-DFT	partition-density-functional theory
SCF	self-consistent field
S-DFT	subsystem-density-functional theory
TF	Thomas-Fermi
vW	von Weizsäcker
XC	exchange-correlation

ABSTRACT

Jiang, Kaili PhD, Purdue University, August 2018. Constructing Fragment-Density Functionals. Major Professor: Adam Wasserman.

Approximations of the non-additive non-interacting kinetic energy (NAKE) as an explicit functional of the density are the basis of fragment-based methods that provide improved computational efficiency over standard Kohn-Sham calculations. However, within most fragment-based formalisms, there is no unique NAKE, making it difficult to develop general, robust approximations to it. In partition density-functional theory (P-DFT), the ambiguity of the NAKE is removed and approximate functionals may be more meaningfully compared to exact quantities. We demonstrate that the decomposable approximations constructed from approximations to the non-interacting kinetic energy fail to reproduce accurate NAKE and discuss promising avenues for constructing fragment density-functionals for the NAKE: (1) By re-parametrizing decomposable conjoint functionals for weakly-bonded systems; (2) By designing non-decomposable functionals for weak and covalent bonds that satisfy exact constraints of the partition energy without fitting. We derive two Virial relations for P-DFT which can be useful in constructing functionals for the NAKE.

1. INTRODUCTION

The electronic-structure problem is central to quantum chemistry. In most cases, this is a many-body problem in which the analytically exact solution is unachievable. Numerical methods are used in these cases, and the choice of the method is based on the required accuracy and computational efficiency of the problem in interest. Wavefunction methods based on solving the Shrödinger equation can be numerically exact, but only feasible for very small systems due to the computational cost scales exponentially with the number of electrons. Density-functional theory (DFT), on the other hand, becomes one of the most commonly used numerical methods in quantum chemistry and solid-state physics because it has a good balance between the accuracy and the computational efficiency for molecules and solids.

The most widely used formalism of DFT is Kohn-Sham DFT (KS-DFT) [1]. In KS-DFT, a fictitious system of non-interacting electrons is constructed with the electron density of the fictitious system equal to the ground state density of the real system in the exact case. The external potential is replaced by the KS potential to compensate for the interactions between the electrons. The ground state energy is written in the form of a functional of the density. In principle, KS-DFT is exact when the exact functionals are used. However, in practical calculations, a small component of the total energy called the exchange-correlation (XC) energy needs to be approximated.

KS-DFT greatly improves the computational efficiency comparing with wavefunction methods, but is still slow for large systems. Fragment-based DFT methods, in which the whole system is further divided into non-interacting fragments, are designed to further improve the efficiency. Partition-DFT (P-DFT) [2–4] is one of them. P-DFT works as an analog of KS-DFT. A fragment KS-DFT calculation is run for each fragment. A global partition potential, in addition to the fragment KS potential, is introduced to compensate for the interactions between the fragments. The

advantage of P-DFT lies in the following aspects. First, by partitioning a large system into smaller fragments, the computational cost can be reduced. Second, different functional approximations can be used in different fragments. For example, more accurate approximations can be used in the fragments we are more interested in, or approximations optimized only for certain types of systems can be used in the matching fragments. Third, with fragment-density functional approximations, P-DFT can achieve a better accuracy than the standard KS-DFT. Lastly, the quantities obtained from P-DFT calculations can be used to improve the understandings of the behavior of atom in molecules and to construct quantities like pseudo-potentials.

There are of course challenges for P-DFT. One of them is the non-additive non-interacting kinetic energy (NAKE). The NAKE is a component of the partition energy and eventually contributes to the total energy. It is defined as the difference between the non-interacting kinetic energy (KE), i.e. the KE of the non-interacting electrons, of the whole system and the sum of the non-interacting KE of the fragments. However, in most cases, it is difficult to use this definition directly to calculate the exact NAKE in P-DFT, because the exact non-interacting KE of the whole system is only known as an explicit functional of the molecular KS orbitals, which are not calculated in P-DFT. In P-DFT, the NAKE can be obtained either by using numerically exact but very computationally expensive inversion methods [5–10], or with efficient but possibly inaccurate explicit functional approximations. The former is useful to obtain benchmark results, but its high computational cost will completely nullify the efficiency advantage of P-DFT in practical calculations. Therefore, accurate explicit approximations to the NAKE is required to make P-DFT useful in practice. One easy way to construct approximations to the NAKE is to directly apply the approximations to the non-interacting KE, which have been intensively studied in orbital-free DFT (OF-DFT) [11], into the definition of the NAKE. NAKE approximations constructed this way are called decomposable approximations. Another way is to construct non-decomposable approximations as a functional of the fragment densities. These approximations typically behave better for the NAKE than decomposable

approximations because they can utilize the fragment density and can be fine-tuned to reproduce the exact behavior of the NAKE.

P-DFT also has a big advantage compared to other fragment-based DFT formalisms in studying the NAKE. In most fragment-based DFT formalisms, the NAKE is not unique, which means it depends on the choice of the initial fragment densities and the method of convergence [4] . This introduces difficulties to study the exact behavior and comparing different approximation of the NAKE. The non-uniqueness of the NAKE is removed in P-DFT, making developing general, robust approximations less difficult.

One more thing that is worth mentioning is the meaning of the term "exact". Typically DFT calculations are done with the self-consistent field (SCF) method in which the density and the potential are updated iteratively until the self-consistency is reached. That means if approximated functionals are used, the density at self-consistency will be different than the density of the real system. In this dissertation, the term "exact NAKE" means the NAKE is exact for a given set of fragment densities, which in most cases are different than the exact fragment densities. However this does not reduce the meaningfulness of my work, as first of all my work is about studying the exact behavior of the NAKE as a functional of fragment densities and improving the approximations to the NAKE, it does not matter if the fragment densities are exact or not, and second the error in the density is pretty small even with the simplest XC approximation, the local-density approximation (LDA), such that the density-driven error is typically much smaller than the functional-driven error [12].

This dissertation concerns about the exact behavior of the NAKE, the performance of the existing decomposable approximation of the NAKE, and constructing NAKE approximations with fragment-density functionals for weakly-interacting systems and covalent bonds. Here is an outline of the chapters:

- **Density-Functional Theory** This chapter outlines the formalism of DFT and the KS equations, and discuss the two types of errors in practical DFT calculations. This gives a background of P-DFT. This chapter contains work

from the review article entitled "The importance of being inconsistent", written by Adam Wasserman, Jonathan Nafziger, the author, Min-Cheol Kim, Eunji Sim, and Kieron Burke, published in Annual Review of Physical Chemistry [12].

- **Partition Density-Functional Theory** This chapter briefly introduces the development of fragment-based DFT methods and outlines a detailed formalism of P-DFT. It also discusses the two different treatments of fractional numbers of electrons commonly used in DFT. This chapter also contains work from "The importance of being inconsistent".

- **Non-additive Non-interacting Kinetic Energy** This chapter discusses the properties of the NAKE and the methods to obtain the NAKE in P-DFT calculations. It also discusses different types of approximations to the non-interacting KE that can be used to construct decomposable approximations to the NAKE.

- **Computational Details** This chapter discusses the computational details of the calculations in this dissertation and introduces the custom-built P-DFT software CADMium.

- **Rare-gas Dimers** This chapter discusses the exact behavior of the NAKE and its functional derivatives for rare-gas dimers. It also introduces two new approximations: R-PBE and two orbital approximation and shows how they improve the results compared with existing decomposable approximation. This chapter contains work from an article entitled "Non-additive non-interacting kinetic energy of rare gas dimers", written by the author, Jonathan Nafziger, and Adam Wasserman, published in the Journal of Chemical Physics [13].

- **Covalent Bonds** This chapter discusses the exact behavior of the NAKE and its functional derivatives for homo-nuclear dimers with covalent bonds, and introduces the covalent approximation. This chapter contains work from an article entitled "Accurate Reference Data for the Nonadditive, Noninteracting Kinetic Energy in Covalent Bonds", written by Jonathan Nafziger, the author,

and Adam Wasserman, published in the Journal of Chemical Theory and Computation [9].

- **Virial Theorem in P-DFT** This chapter derives the virial relations in P-DFT and verifies them numerically.

2. DENSITY-FUNCTIONAL THEORY

2.1 Time-Independent Schrödinger Equation

In quantum chemistry and materials science, the time-independent Schrödinger equation is sufficient for capturing the ground state behaviors of molecular systems. The Born-Oppenheimer approximation is usually used, in which case the position of all nuclei is considered to be fixed. The Hamiltonian of these systems can be written as:

$$\hat{H} = \hat{T} + \hat{V}_{\text{ee}} + \hat{V}_{\text{ext}}, \tag{2.1}$$

where the subscript e stands for the electron.

Throughout this dissertation atomic units are used, in which the mass, the charge of electron, and the reduced Planck's constant are equal to one ($m_{\text{e}} = e = \hbar = 1$). The kinetic energy operator is given by:

$$\hat{T} = -\frac{1}{2}\sum_{i=1}^{N} \nabla_i^2, \tag{2.2}$$

where N is the total number of electrons. The electron-electron interaction is represented by:

$$\hat{V}_{\text{ee}} = \frac{1}{2}\sum_{i}\sum_{j\neq i} \frac{1}{|\mathbf{r}_i - \mathbf{r}_j|}, \tag{2.3}$$

where the indices i and j runs over all N electrons. The electron-nuclei interaction is included in the external potential operator:

$$\hat{V}_{\text{ext}} = \sum_{i-1}^{N} v(\mathbf{r}_i). \tag{2.4}$$

For coulomb systems the potential is given by:

$$v(\mathbf{r}) = \sum_{\beta} \frac{Z_\beta}{|\mathbf{r} - \mathbf{R}_\beta|}, \tag{2.5}$$

where Z_β and $\mathbf{R}_\beta$ are the electric charge and the position of the βth nuclei, respectively.

With the Hamiltonian, the ground state wavefunction Ψ and the ground state energy E can be obtained by solving the time-independent Schrödinger equation:

$$\hat{H}\Psi(\mathbf{r}_1\sigma_1, \mathbf{r}_2\sigma_2, ..., \mathbf{r}_N\sigma_N) = E\Psi(\mathbf{r}_1\sigma_1, \mathbf{r}_2\sigma_2, ..., \mathbf{r}_N\sigma_N), \tag{2.6}$$

where $\mathbf{r}_i$ and σ_i are the spatial and the spin coordinate of electron i, respectively. The biggest issue of this wavefunction approach is its huge computational cost. For example, to run a calculation for a system with N electrons using a grid in real space which has M points in each dimension, one must compute and store M^{3N} values of Ψ. This exponential scaling of the computational cost means that wavefunction methods are only feasible for very small systems.

DFT provides another approach in which the wavefunction Ψ is replaced by the electronic density:

$$n(\mathbf{r}) = N \sum_\sigma \int \mathrm{d}x_2 ... \int \mathrm{d}x_N \Psi^*(\mathbf{r}\sigma, x_2, ..., x_N)\Psi(\mathbf{r}\sigma, x_2, ..., x_N), \tag{2.7}$$

where $x = (\mathbf{r}, \sigma)$. This reduces the number of spatial coordinates from $3N$ to 3, making the computation feasible.

2.2 Hohenberg-Kohn Theorems

One problem of DFT is whether the electronic density can preserve all the necessary information of the system. This is solved by Hohenberg and Kohn in 1964 [14].

The first Hohenberg-Kohn theorem proves that the external potential $v(\mathbf{r})$ is unique (up to a constant) for a given density $n(\mathbf{r})$.

The second Hohenberg-Kohn theorem states that there exists a universal functional $F[n(\mathbf{r})]$, such that the ground state energy E for a given external potential $v(\mathbf{r})$ can be written as:

$$E = \min_n \{F[n] + \int \mathrm{d}^3 r \, v(\mathbf{r}) n(\mathbf{r})\}, \tag{2.8}$$

where the minimization is running over all $n(\mathbf{r})$ which satisfy the constraint

$$\int \mathrm{d}^3 r\, n(\mathbf{r}) = N, \tag{2.9}$$

where N is the total number of electrons in the system. This minimization can be done by solving the Euler-Lagrange equation

$$\frac{\delta F[n]}{\delta n(\mathbf{r})} + v(\mathbf{r}) - \mu = 0, \tag{2.10}$$

where μ is the Lagrange multiplier, and is also known as the chemical potential.

2.3 N and v-representability

There are still a few questions not answered by the Hohenberg-Kohn theorems. The first one is the N-representability problem: for arbitrarily given density $n(\mathbf{r})$ that integrate to the electron number N, can it be represented in the form of Eq. 2.7, i.e. is there an anti-symmetric N-body wavefunction integrates to that density? The answer to this problem is yes, as long as $n(\mathbf{r}) > 0$, $\forall \mathbf{r}$ [15, 16].

The other one is the v-representability problem: for arbitrary given N-representable density $n(\mathbf{r})$, is there a external potential $v(\mathbf{r})$ that $n(\mathbf{r})$ is ground state [17]? The first Hohenberg-Kohn theorem proves the uniqueness of $v(\mathbf{r})$ if it exists, but the existence of $v(\mathbf{r})$ still needs to be proved. It is known for discretized systems the density is ensemble v-representable, but in general case, there are densities in continuum systems that are not v-representable [15]. However, for interacting systems, the v-representability is not required to prove the Hohenberg-Kohn theorems thanks to the constrained search algorithm of Levy and Lieb [15, 18, 19].

2.4 Kohn-Sham Density-Functional Theory

Despite the Hohenberg-Kohn theorem stating the existence of a universal functional $F[n]$, it is very difficult to find the explicit form of it. KS-DFT provides a successful formalism to solve this problem by constructing a fictitious system (KS

system) of non-interacting electrons which yields to the same ground-state density of the real system [1].

First we write $F[n]$ as

$$F[n] = T_{\mathrm{S}}[n] + E_{\mathrm{H}}[n] + E_{\mathrm{X}}[n] + E_{\mathrm{C}}[n]. \tag{2.11}$$

The first term $T_{\mathrm{S}}[n]$ represents the non-interacting kinetic energy, where the subscript s denotes single electron. It is defined by:

$$T_{\mathrm{S}}[n] = \min_{\Psi \to n} \langle \Psi | \hat{T} | \Psi \rangle , \tag{2.12}$$

where Ψ is any N-electron antisymmetric wavefunction. The minimization runs over all Ψ which yields to the density n. The Ψ satisfies this minimization, which we denote as Φ_n here onwards, is usually a single Slater determinant of the single electron wavefunctions ϕ_i, which are also known as orbitals.

The second term $E_{\mathrm{H}}[n]$ is the Hartree energy:

$$E_{\mathrm{H}}[n] = \frac{1}{2} \int \mathrm{d}^3 r \int \mathrm{d}^3 r' \, \frac{n(\mathbf{r}) n(\mathbf{r}')}{|\mathbf{r} - \mathbf{r}'|}. \tag{2.13}$$

The last two terms of $E_{\mathrm{X}}[n]$ and $E_{\mathrm{C}}[n]$ are the exchange and the correlation energy, respectively:

$$E_{\mathrm{X}}[n] = \langle \Phi_n | \hat{V}_{\mathrm{ee}} | \Phi_n \rangle - E_{\mathrm{H}}[n], \tag{2.14}$$

$$E_{\mathrm{C}}[n] = \langle \Psi_n | \hat{T} + \hat{V}_{\mathrm{ee}} | \Psi_n \rangle - \langle \Phi_n | \hat{T} + \hat{V}_{\mathrm{ee}} | \Phi_n \rangle , \tag{2.15}$$

where Ψ_n is the wavefunction that yields to the density $n(\mathbf{r})$ and minimizes the expectation value of the Hamiltonian $\hat{H}$. They are often come together as the XC energy $E_{\mathrm{XC}}[n] = E_{\mathrm{X}}[n] + E_{\mathrm{C}}[n]$. Typically, approximations for $E_{\mathrm{XC}}[n]$ are used in KS-DFT calculations. Since $E_{\mathrm{XC}}[n]$ is a very small portion of $F[n]$, even the crude st approximations can give decent results.

Substitute Eq. 2.11 into Eq. 2.10, we get

$$\frac{\delta T_{\mathrm{S}}[n]}{\delta n(\mathbf{r})} + v_{\mathrm{S}}(\mathbf{r}) - \mu = 0, \tag{2.16}$$

where

$$v_{\mathrm{S}}(\mathbf{r}) = v_{\mathrm{H}}(\mathbf{r}) + v_{\mathrm{XC}}(\mathbf{r}) + v(\mathbf{r}) = \frac{\delta E_{\mathrm{H}}[n]}{\delta n(\mathbf{r})} + \frac{\delta E_{\mathrm{XC}}[n]}{\delta n(\mathbf{r})} + v(\mathbf{r}). \tag{2.17}$$

The density satisfying the Eq. 2.16 can be obtained by solving the corresponding single electron Schrödinger equations

$$\left\{ -\frac{1}{2}\nabla^2 + v_{\mathrm{S}}(\mathbf{r}) \right\} \phi_i(\mathbf{r}) = \epsilon_i \phi_i(\mathbf{r}). \tag{2.18}$$

These equations are also known as Kohn-Sham equations. The orbitals are implicit functionals of the density:

$$n(\mathbf{r}) = \sum_i f_i |\phi_i(\mathbf{r})|^2, \tag{2.19}$$

where f_i can be 0, 1, or 2 for unoccupied, half occupied, or fully occupied orbitals, respectively.

2.5 Orbital-Free Density-Functional Theory

The computational cost of KS-DFT typically scales as $O(N^3)$, with N being an appropriate measure of the size of the system. This is a significant improvement over wavefunction methods, but still impractical for large systems. A majority of the computational cost of KS-DFT comes from the introduction of the orbitals. Each orbital requires 3 additional degrees of freedom, and in addition to that, there are costs associated with orbital manipulation such as orbital orthonormalization and orbital localization [11]. One way to further reduce the computational cost is to use OF approach. In OF-DFT, the Eq. 2.16 is solved directly. This requires an explicit expression of the non-interacting KE and a functional of density. OF-DFT has a linear-scaling $O(N)$, which is a great improvement comparing with KS-DFT. However, the exact explicit expression of the non-interacting KE is still unknown, and unlike XC energy, the non-interacting KE contributes a large portion towards $F[n]$. Therefore the accuracy of the approximations to the non-interacting KE has a big impact on the accuracy of OF-DFT calculations. Unfortunately, approximations to the non-interacting KE are still lacking accuracy and transferability for all kinds of

systems in diverse scenarios, which becomes the biggest limitation of OF-DFT [11]. On the other hand, the approximations to the non-interacting KE proposed during the development of OF-DFT can be used in constructing approximations to the NAKE. Details of these approximations can be found in Section 4.7.

2.6 Functional and Density-driven Errors

When approximated functionals are used in DFT calculations, the density that minimizes Eq. 2.8 will also be approximate. Therefore, the energy error of the approximated functional can be decomposed into two parts

$$\Delta E = \tilde{E}[\tilde{n}] - E[n] = \Delta E_{\text{F}} + \Delta E_{\text{D}}, \tag{2.20}$$

where $\tilde{E}$ and $\tilde{n}$ are approximated functional of E and approximated density of n, respectively. ΔE_{F} is the functional-driven error

$$\Delta E_{\text{F}} = \tilde{E}[n] - E[n], \tag{2.21}$$

and ΔE_{D} is the density-driven error

$$\Delta E_{\text{D}} = \tilde{E}[\tilde{n}] - \tilde{E}[n]. \tag{2.22}$$

Most DFT calculations have $\Delta E_{\text{F}} \gg \Delta E_{\text{D}}$. They are called normal DFT calculations, in which the energy error does not change much if the calculation is done non-self-consistently. However, some DFT calculations are abnormal, in which $\Delta E_{\text{F}} \lesssim \Delta E_{\text{D}}$. For those calculations, the energy error can be massively reduced if the calculation is done non-self-consistently with more accurate densities.

3. PARTITION DENSITY-FUNCTIONAL THEORY

3.1 Fragment-based Density-Functional Methods

Another way to improve the $O(N^3)$ computational efficiency of KS-DFT is to divide the density of a large system into smaller fragments:

$$n(\mathbf{r}) = \sum_{\alpha} n_{\alpha}(\mathbf{r}). \tag{3.1}$$

In 1972, Gordon and Kim [20] made the first fragment-based DFT calculation of the binding curve of rare-gas dimers. The calculation was done non-self-consistently with the total density constructed from the Hartree-Fock density of isolated fragments using Eq. 3.1 based on the fact that the distortion of the fragment density from the fragment-fragment interaction of rare-gas dimers can be neglected. In 1986, self-consistent calculations with the Gordon-Kim model was done by Senatore and Subbaswamy [21].

In the 1990s, two fragment-based DFT formalisms, subsystem-DFT (S-DFT) [22] and frozen-density embedding (FDE) [23] were developed. FDE was initially not fully self-consistent, as the density of one fragment is frozen, but was later made self-consistent using the freeze-and-thaw cycles [24], making it equivalent with S-DFT. The fragment density of these two formalisms can be obtained by solving the fragment Kohn-Sham equations with constrained electron density (KSCED): [25]

$$\{-\frac{1}{2}\nabla^2 + v_{\alpha}^{\mathrm{KSCED}}[n_{\alpha}](\mathbf{r})\}\phi_{i,\alpha}(\mathbf{r}) = \varepsilon_{i,\alpha}\phi_{i,\alpha}(\mathbf{r}), \tag{3.2}$$

where

$$v_{\alpha}^{\mathrm{KSCED}}[n_{\alpha}](\mathbf{r}) = \frac{\delta T_{\mathrm{S}}^{\mathrm{nad}}[\{n_{\alpha}\}]}{\delta n_{\alpha}(\mathbf{r})} + v_{\mathrm{H}}[n](\mathbf{r}) + v_{\mathrm{XC}}[n](\mathbf{r}) + v[n](\mathbf{r}), \tag{3.3}$$

and $T_{\mathrm{S}}^{\mathrm{nad}}[\{n_{\alpha}\}]$ is the NAKE.

When the NAKE and its functional derivatives are evaluated exactly, the solutions of the KSCED equations can reproduce the KS density of the whole system given the

same approximation of the XC energy are used in both cases. These solutions of the KSCED equations are referred to as the exact solutions to the KSCED equations, which is not unique. Nafziger and Wasserman showed that any set of non-interacting v-representable densities $\{n_\alpha\}$ that satisfies Eq. 3.1 will be an exact solution to the KSCED equations [4]. The resulting fragment densities depend on the initial guess of the densities and the method of convergence. However, the solution of the KSCED equations becomes unique when approximated NAKE is used, because different sets of $\{n_\alpha\}$ that satisfies Eq. 3.1 will lead to different total energy in this case. This non-uniqueness leads to some difficulties in studying the exact behaviors of the NAKE.

P-DFT is another formalism of fragment-based DFT that can reproduce the KS result so long as the exact NAKE and the same approximation of the XC energy are used. In P-DFT, the fragments are non-interacting with the partition potential v_p introduced to compensate for the interactions between the fragments. There are two major differences between P-DFT and standard S-DFT or FDE. First, the non-uniqueness is removed in P-DFT by enforcing the partition potential to be global. Second, fractional occupation numbers $N_\alpha = \int \mathrm{d}^3r\, n_\alpha(\mathbf{r})$ are allowed in P-DFT, which leads to localized fractional densities when the occupation numbers are optimized. It is worth mentioning later on re-formalisms of S-DFT and FDE were developed to remove the non-uniqueness [7] and to allow non-integer occupation numbers [26] by imposing similar methods used in P-DFT.

3.2 Fractional Occupation Numbers

There are two treatments to deal with fractional occupation numbers: ensemble treatment (ENS) and fractionally occupied orbitals (FOO). P-DFT typically uses ENS, but there is nothing fundamental to prevent the use of FOO.

With ENS, the number of electrons in each fragment ensemble component is $N_{j\alpha\sigma}$, where j, α, σ are the ensemble component index, fragment index, spin index, respec-

tively. $N_{j\alpha\sigma}$ must be an integer. The occupation number for a given spin is given by

$$N_{\alpha\sigma} = \sum_j f_{j\alpha} N_{j\alpha\sigma}, \tag{3.4}$$

where $f_{j\alpha}$ are the ensemble coefficients which satisfy $\sum_j f_{j\alpha} = 1$. The fragment densities are the ensemble average of its component densities:

$$n_{\alpha\sigma}(\mathbf{r}) = \sum_j f_{j\alpha} n_{j\alpha\sigma}(\mathbf{r}), \tag{3.5}$$

and any density functional should also be evaluated using the ensemble average:

$$F[n_{\alpha\uparrow}, n_{\alpha\downarrow}] = \sum_j f_{j\alpha} F[n_{j\alpha\uparrow}, n_{j\alpha\downarrow}]. \tag{3.6}$$

A special case is the spin unpolarized fragment density with the occupation number $N_\alpha = p_\alpha + \mu_\alpha$, where p_α is an integer and $0 \leq \mu_\alpha < 1$, then [27]

$$n_\alpha(\mathbf{r}) = (1 - \nu_\alpha) n_{p_\alpha}(\mathbf{r}) + \nu_\alpha n_{p_\alpha+1}(\mathbf{r}), \tag{3.7}$$

and

$$F[n_\alpha] = (1 - \nu_\alpha) F[n_{p_\alpha}] + \nu_\alpha F[n_{p_\alpha+1}]. \tag{3.8}$$

With FOO, the highest occupied molecular orbital (HOMO) of each spin can be fractionally occupied. The fragment densities are given by

$$n_{\alpha\sigma}(\mathbf{r}) = \sum_i f_{i\alpha\sigma} |\phi_{i\alpha\sigma}(\mathbf{r})|^2, \tag{3.9}$$

where $\phi_{i\alpha\sigma}(\mathbf{r})$ is the ith Kohn-Sham fragment orbital of spin σ of fragment α. $f_{i\alpha\sigma}$ can take values from $0 \leq f_{i\alpha\sigma} \leq 1$ depending on whether the given orbital is unoccupied, partially occupied, or fully occupied. Any density functional should be evaluated directly from the fragment densities.

The primary difference between ENS and FOO is that in the case of ENS, functionals are evaluated on spin densities with integer numbers of electrons in each spin, whereas in FOO, functionals are evaluated on non-integer spin densities. Cohen *et* al. showed that the exact energy functional will yield the same energy in both cases as

long as the total density is the same [28]. However, when approximated functionals are used, these two treatments can lead to different results because most approximations do not scale linearly with fractional numbers of electrons. Please refer to Sec. 7.1 for a detailed mathematical explanation of the impact of the choice of FOO or ENS with approximated NAKE. Some numerical examples can also be found in Chapter 7.

3.3 Fragment Equations

In this section, the fragment equations of P-DFT under the ENS treatment will be derived. In P-DFT, the system is divided into N_f isolated fragments. Each fragment is under the influence of the fragment external potential $v_\alpha(\mathbf{r})$ which sums up to the total external potential

$$v(\mathbf{r}) = \sum_{\alpha=1}^{N_\mathrm{f}} v_\alpha(\mathbf{r}). \tag{3.10}$$

The total density $n(\mathbf{r})$ is divided among the fragments, by minimizing the sum of the fragment energies [3]

$$E_\mathrm{f}[n_\uparrow, n_\downarrow] = \min_{\{n_\alpha\}} \sum_{\alpha=1}^{N_\mathrm{f}} E_\alpha[n_{\alpha\uparrow}, n_{\alpha\downarrow}], \tag{3.11}$$

under two constraints

$$\sum_{\alpha=1}^{N_\mathrm{f}} n_{\alpha\sigma}(\mathbf{r}) = n_\sigma(\mathbf{r}), \tag{3.12}$$

and

$$\int \mathrm{d}^3 r \sum_{\alpha=1}^{N_\mathrm{f}} \sum_{\sigma} n_{\alpha\sigma}(\mathbf{r}) = N. \tag{3.13}$$

The first constraint means the sum of the fragment densities must match the molecular density. The second constraint means the sum of the fragment densities should integrate into the total number of electrons in the system. This constrained minimization can be replaced by an unconstrained minimization of $G[n_\uparrow, n_\downarrow]$ by introducing two

Lagrangian multipliers, the partition potential $v_{\rm p} = [v_{{\rm p},\uparrow}(\mathbf{r}), v_{{\rm p},\downarrow}(\mathbf{r})]$ and the molecular chemical potential μ.

$$\begin{aligned} G[n_\uparrow, n_\downarrow] &= \sum_{\alpha=1}^{N_{\rm f}} E_\alpha[n_{\alpha\uparrow}, n_{\alpha\downarrow}] + \sum_\sigma \int {\rm d}^3 r\, v_{{\rm p},\sigma}(\mathbf{r}) \left(\sum_{\alpha=1}^{N_{\rm f}} n_{\alpha\sigma} - n_\sigma(\mathbf{r}) \right) \\ &\quad -\mu \left(\int {\rm d}^3 r \sum_{\alpha=1}^{N_{\rm f}} \sum_\sigma n_{\alpha\sigma}(\mathbf{r}) - N \right). \end{aligned} \tag{3.14}$$

$G[n_\uparrow, n_\downarrow]$ must be minimized with respect to every ensemble component in every fragment. The Euler-Lagrange equation with respect to the ensemble component $n_{j\alpha\sigma}$ is

$$\begin{aligned} 0 &= \frac{\delta G[n]}{\delta n_{j\alpha\sigma}(\mathbf{r})} \\ &= f_{j\alpha} \frac{\delta E_\alpha[n_{\alpha\uparrow}, n_{\alpha\downarrow}]}{\delta n_{j\alpha\sigma}(\mathbf{r})} + f_{j\alpha} v_{{\rm p},\sigma}(\mathbf{r}) - f_{j\alpha}\mu_m, \end{aligned} \tag{3.15}$$

or

$$\frac{\delta T_{\rm S}[n_{\alpha\uparrow}, n_{\alpha\downarrow}]}{\delta n_{j\alpha\sigma}(\mathbf{r})} + v_{{\rm s},\alpha\sigma}[n_{\alpha\uparrow}, n_{\alpha\downarrow}](\mathbf{r}) + v_{{\rm p},\sigma}(\mathbf{r}) - \mu = 0, \tag{3.16}$$

where the non-interacting KE of fragment α is defined as

$$T_{\rm S}[n_{\alpha\uparrow}, n_{\alpha\downarrow}] = \min_{\phi_{i,j\alpha\sigma} \to n_{j\alpha\sigma}} \sum_j \sum_\sigma \sum_i f_{j\alpha} \left\langle \phi_{i,j\alpha\sigma} \right| -\frac{1}{2}\nabla^2 \left| \phi_{i,j\alpha\sigma} \right\rangle, \tag{3.17}$$

and the fragment KS potential

$$v_{{\rm s},\alpha\sigma}[n_{j\alpha\sigma}](\mathbf{r}) = v_{\rm H}[n_{j\alpha}](\mathbf{r}) + v_{\rm XC}[n_{\alpha\uparrow}, n_{\alpha\downarrow}](\mathbf{r}) + v_\alpha(\mathbf{r}). \tag{3.18}$$

Using the analogy as in section 2.4, we can obtain $n_{j\alpha\sigma}(\mathbf{r})$ satisfying Eq. 3.16 by solving the fragment KS equations [4]

$$\left\{ -\frac{1}{2}\nabla^2 + v_{{\rm s},\alpha\sigma}[n_{j\alpha\sigma}](\mathbf{r}) + v_{{\rm p},\sigma}(\mathbf{r}) \right\} \phi_{i,j\alpha\sigma}(\mathbf{r}) = \epsilon_{i,j\alpha\sigma} \phi_{i,j\alpha\sigma}(\mathbf{r}). \tag{3.19}$$

The fragmental orbitals and fragmental density satisfy the following equation

$$n_{j\alpha\sigma}(\mathbf{r}) = \sum_i |\phi_{i,j\alpha\sigma}(\mathbf{r})|^2. \tag{3.20}$$

where the summation is over all occupied orbitals.

Through these equations, we can see the fragment density can be written as a functional of the partition potential and the occupation number

$$n_{\alpha\sigma} = n_{\alpha\sigma}[v_{{\rm p},\sigma}, N_{\alpha\sigma}]. \tag{3.21}$$

3.4 Partition Potential Optimization

The next step is to find the partition potential that correctly enforces the constraint. It has been established that there is a one-to-one mapping between the partition potential (up to a constant) and the ground state density of the whole system [29]. According to the Hohenberg-Kohn Theorems, we can get the ground state density by minimizing the total molecular energy

$$E[n_\uparrow, n_\downarrow] = E_{\mathrm{f}}[n_\uparrow, n_\downarrow] + E_{\mathrm{p}}[n_\uparrow, n_\downarrow], \tag{3.22}$$

under the constraint

$$\int \mathrm{d}^3 r \sum_\sigma n_\sigma(\mathbf{r}) = N. \tag{3.23}$$

where $E_{\mathrm{p}}[n_\uparrow, n_\downarrow]$ is the partition energy, which is defined by Eq. 3.22. It can be broken into components,

$$\begin{aligned} E_{\mathrm{p}}[\{n_{\alpha\uparrow}, n_{\alpha\downarrow}\}] = T_{\mathrm{S}}^{\mathrm{nad}}[\{n_{\alpha\uparrow}, n_{\alpha\downarrow}\}] + V_{\mathrm{ext}}^{\mathrm{nad}}[\{n_\alpha\}] \\ + E_{\mathrm{H}}^{\mathrm{nad}}[\{n_\alpha\}] + E_{\mathrm{XC}}^{\mathrm{nad}}[\{n_{\alpha\uparrow}, n_{\alpha\downarrow}\}], \end{aligned} \tag{3.24}$$

where the four components are known as the NAKE, the non-additive external energy, the non-additive Hartree energy, the non-additive XC energy, respectively. They are defined as

$$T_{\mathrm{S}}^{\mathrm{nad}}[\{n_{\alpha\uparrow}, n_{\alpha\downarrow}\}] = T_{\mathrm{S}}[n_\uparrow, n_\downarrow] - \sum_{\alpha=1}^{N_{\mathrm{f}}} T_{\mathrm{S}}[n_{\alpha\uparrow}, n_{\alpha\downarrow}], \tag{3.25}$$

$$V_{\mathrm{ext}}^{\mathrm{nad}}[\{n_\alpha\}] = \int \mathrm{d}^3 r \left\{ n(\mathbf{r}) v(\mathbf{r}) - \sum_{\alpha=1}^{N_{\mathrm{f}}} n_\alpha(\mathbf{r}) v_\alpha(\mathbf{r}) \right\}, \tag{3.26}$$

$$E_{\mathrm{H}}^{\mathrm{nad}}[\{n_\alpha\}] = E_{\mathrm{H}}[n] - \sum_{\alpha=1}^{N_{\mathrm{f}}} E_{\mathrm{H}}[n_\alpha], \tag{3.27}$$

$$E_{\mathrm{XC}}^{\mathrm{nad}}[\{n_{\alpha\uparrow}, n_{\alpha\downarrow}\}] = E_{\mathrm{XC}}[n_\uparrow, n_\downarrow] - \sum_{\alpha=1}^{N_{\mathrm{f}}} E_{\mathrm{XC}}[n_{\alpha\uparrow}, n_{\alpha\downarrow}], \tag{3.28}$$

The constrained minimization of Eq. 3.22 can be done by solving the Euler-Lagrange equation

$$\frac{\delta E_{\mathrm{f}}[n_\uparrow, n_\downarrow]}{\delta n_\sigma(\mathbf{r})} + \frac{\delta E_{\mathrm{p}}[n_\uparrow, n_\downarrow]}{\delta n_\sigma(\mathbf{r})} - \mu = 0. \tag{3.29}$$

Let us consider the first term. Using the chain rule, Eq. 3.5, Eq. 3.12, and Eq. 3.15, we get

$$\begin{aligned}
\frac{\delta E_{\rm f}[n_\uparrow, n_\downarrow]}{\delta n_\sigma} &= \sum_{\alpha=1}^{N_{\rm f}} \frac{\delta E_\alpha[n_{\alpha\uparrow}, n_{\alpha\downarrow}]}{\delta n_\sigma} \\
&= \sum_{\alpha=1}^{N_{\rm f}} \sum_j \sum_{\sigma'} \int {\rm d}^3 r' \, f_{j\alpha} \frac{\delta E_\alpha[n_{\alpha\uparrow}, n_{\alpha\downarrow}]}{\delta n_{j\alpha\sigma'}(\mathbf{r}')} \frac{\delta n_{j\alpha\sigma'}(\mathbf{r}')}{\delta n_\sigma(\mathbf{r})} \\
&= \sum_{\alpha=1}^{N_{\rm f}} \sum_j \sum_{\sigma'} \int {\rm d}^3 r' \, (\mu_m - v_{{\rm p},\sigma'}(\mathbf{r}')) f_{j\alpha} \frac{\delta n_{j\alpha\sigma'}(\mathbf{r}')}{\delta n_\sigma(\mathbf{r})} \\
&= \sum_{\sigma'} \int {\rm d}^3 r' \, (\mu - v_{{\rm p},\sigma'}(\mathbf{r}')) \frac{\delta n_{\sigma'}(\mathbf{r}')}{\delta n_\sigma(\mathbf{r})} \\
&= \mu - v_{{\rm p},\sigma}(\mathbf{r}). \qquad (3.30)
\end{aligned}$$

Combining Eq. 3.29 and Eq. 3.30, we can find the partition potential is the functional derivative of the partition energy with respect to the density of the whole system

$$v_{{\rm p},\sigma}(\mathbf{r}) = \frac{\delta E_{\rm p}[n_\uparrow, n_\downarrow]}{\delta n_\sigma(\mathbf{r})}. \qquad (3.31)$$

3.5 Q-Functions

We can expand Eq. 3.31

$$\begin{aligned}
v_{{\rm p},\sigma}(\mathbf{r}) &= \sum_{\alpha=1}^{N_{\rm f}} \sum_j \sum_{\sigma'} \int {\rm d}^3 r' \, \frac{\delta E_{\rm p}[n_\uparrow, n_\downarrow]}{\delta n_{j\alpha\sigma'}(\mathbf{r}')} \frac{\delta n_{j\alpha\sigma'}(\mathbf{r}')}{\delta n_\sigma(\mathbf{r})} \\
&= \sum_{\alpha=1}^{N_{\rm f}} \sum_j \sum_{\sigma'} \int {\rm d}^3 r' \, v_{{\rm p},j\alpha\sigma'}(\mathbf{r}') Q_{j\alpha\sigma'\sigma}(\mathbf{r}', \mathbf{r}), \qquad (3.32)
\end{aligned}$$

where the fragment-dependent partition potential and the Q-functions are given by

$$v_{{\rm p},j\alpha\sigma'}(\mathbf{r}') = \frac{\delta E_{\rm p}[n_\uparrow, n_\downarrow]}{\delta n_{j\alpha\sigma'}(\mathbf{r}')}, \qquad (3.33)$$

and

$$Q_{j\alpha\sigma'\sigma}(\mathbf{r}', \mathbf{r}) = \frac{\delta n_{j\alpha\sigma'}(\mathbf{r}')}{\delta n_\sigma(\mathbf{r})}, \qquad (3.34)$$

respectively. The Q-function represents the mutual influence of fragments. It must satisfy the rule

$$\sum_{\alpha=1}^{N_{\rm f}} \sum_j Q_{j\alpha\sigma'\sigma}(\mathbf{r}', \mathbf{r}) = \delta_{\sigma'\sigma} \delta(\mathbf{r} - \mathbf{r}'). \qquad (3.35)$$

In practical calculations, the local-Q approximation is used [30]

$$Q^{\text{local}}_{j\alpha\sigma'\sigma}(\mathbf{r}', \mathbf{r}) = \frac{n_{j\alpha\sigma'}(\mathbf{r}')}{n_\sigma(\mathbf{r})}\delta_{\sigma'\sigma}\delta(\mathbf{r} - \mathbf{r}'). \tag{3.36}$$

It is worth mentioning for calculations with the exact partition energy, the choice of the Q-function does not affect the final result as long as Eq. 3.35 is satisfied. This is because for the exact partition energy at convergence, the functional derivative of the partition energy with respect to any of the fragment densities is the same. In cases where approximate non-additive functionals are used, the local-Q approximation has been shown to be close to the exact Q-function, especially at configurations where the bonds are stretched [4].

3.6 Algorithms

Typically, P-DFT calculations are done with SCF method where the fragment densities are updated iteratively until the self-consistency is reached. Figure 3.1 shows the flow chart of the P-DFT algorithm with the initial guess of the fragment densities $\{n^0_{\alpha\sigma}\}$ to be the required input.

In practical calculations, the NAKE and the non-additive XC energy are approximated. Thus the partition potential obtained through the algorithm in Figure 3.1 is not exact. To obtain the exact partition potential without the exact functional, one can use algorithms which involve solving the inverse problem. These algorithms are less computationally efficient, and usually require pre-computed target molecular density $n^{\text{target}}_\sigma(\mathbf{r})$ as an additional input. Figure 3.2 shows a general flow chart of the inversion algorithms [31].

The simplest method to compute $\delta v^i_{\text{p},\sigma}$ is to set it proportional to the difference between the current molecular density and the target molecular density

$$\delta v^i_{\text{p},\sigma}(\mathbf{r}) = \gamma\left[\sum_{\alpha=1}^{N_\text{f}} n^i_{\alpha\sigma}(\mathbf{r}) - n^{\text{target}}_\sigma(\mathbf{r})\right], \tag{3.37}$$

where γ is a positive coefficient that needs to be carefully chosen. The idea behind this method is very easy to understand: the partition potential needs to increase

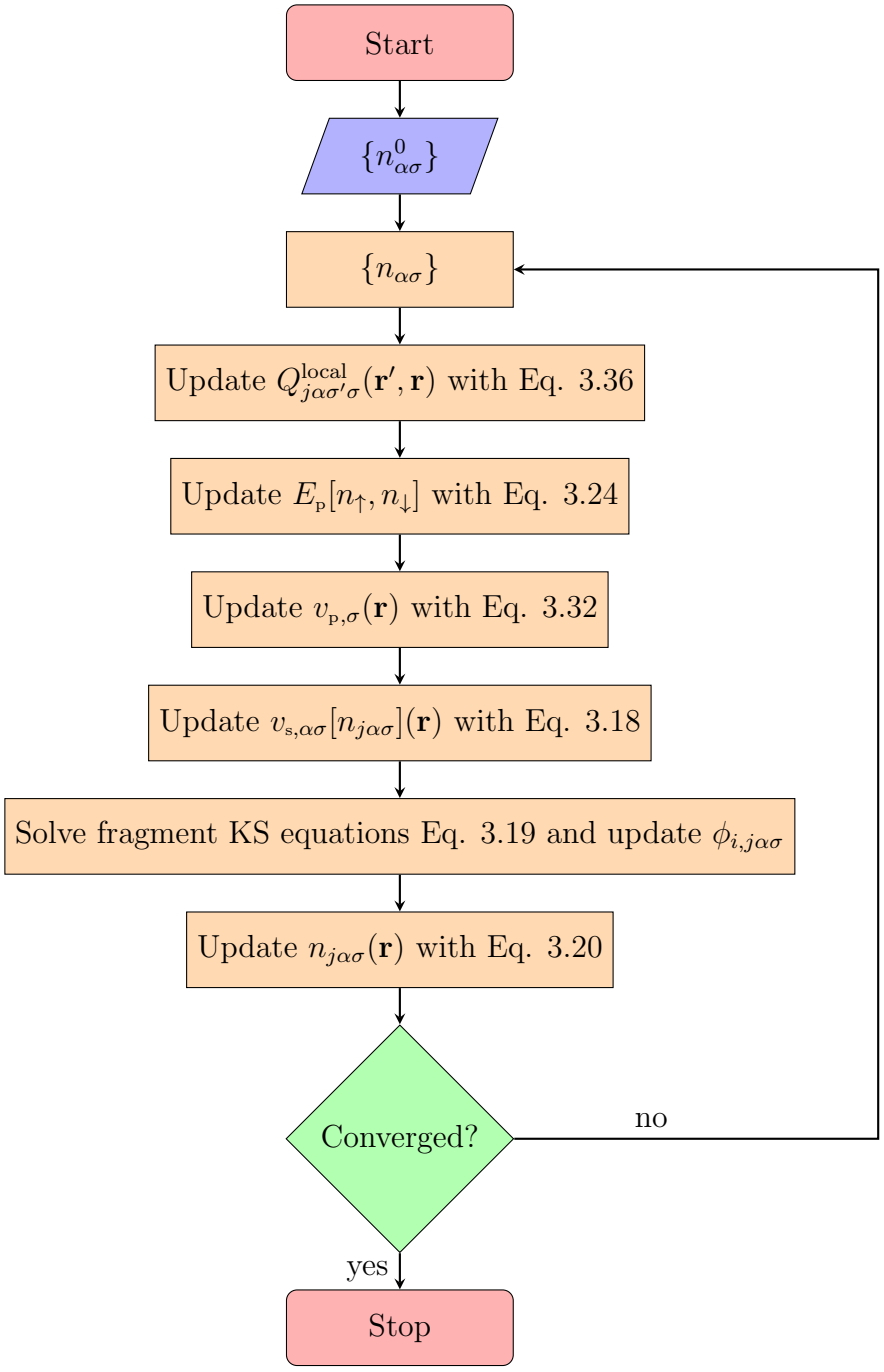

Figure 3.1. Flow chart of a P-DFT SCF calculation with the partition potential calculated approximately and the local-Q approximation used

in regions where the current density is larger than the target density so the new density in the next iteration can be pushed away from those regions, and vice versa. However, this method converges extremely slowly, especially when γ is small. On the other hand, it does not converge at all when γ is too large. The optimal γ is difficult to find and usually changes between iterations.

Alternatively, $\delta v^i_{\mathrm{p},\sigma}$ can be computed using the relative error in the molecular density

$$\delta v^i_{\mathrm{p},\sigma}(\mathbf{r}) = \gamma \left[\frac{\sum_{\alpha=1}^{N_\mathrm{f}} n^i_{\alpha\sigma}(\mathbf{r}) - n^{\mathrm{target}}_\sigma(\mathbf{r})}{n^{\mathrm{target}}_\sigma(\mathbf{r})} \right]. \tag{3.38}$$

Comparing with Eq. 3.37, Eq. 3.38 gives a higher importance in the asymptotic region where the molecular density is small. This usually ends up faster convergence, though γ still needs to be carefully chosen.

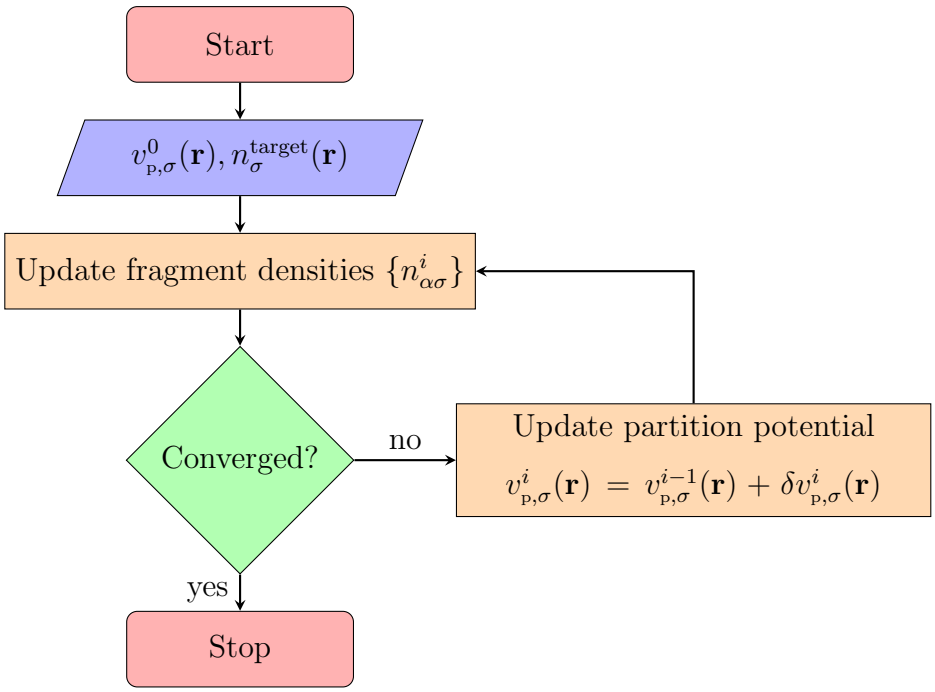

Figure 3.2. Simplified Flow chart of a P-DFT SCF cycle with the exact partition potential calculated by inversion.

4. NON-ADDITIVE NON-INTERACTING KINETIC ENERGY

4.1 Non-additive Non-interacting Kinetic Energy

One of the challenges in P-DFT is to calculate accurate partition potential, which often involves calculating accurate partition energy. Among the four components of the partition energy in Eq. 3.24, the explicit forms of the exact non-additive external and Hartree energy as a functional of fragment densities are already known. In most practical P-DFT calculations, decomposable approximations constructed from the approximation which is used in the fragment KS calculations are used for the non-additive XC energy. This generally works well because the non-additive XC energy is small comparing to the partition energy and using decomposable approximations this way will yield the same molecular density and ground state energy as the KS result using the corresponding XC approximation.

NAKE, however, is the component that needs to be taken care of. The difficulty in computing the exact NAKE using its definition Eq. 3.25 comes from calculating the molecular non-interacting KE. In most cases, the molecular non-interacting KE is only known as an explicit functional of the molecular KS orbitals. While avoiding calculating the molecular KS orbitals contributes the majority of computational cost reduction in P-DFT, it leads to issues in calculating the NAKE. A few algorithms have been developed to compute the exact molecular non-interacting KE as an implicit functional of the density, the details will be discussed in Section 4.6. These algorithms often require solving a very computational expensive inverse problem. Therefore, they are usually used to generate benchmark data to study the exact behavior of the NAKE, rather than in practical calculations. NAKE can be also obtained through explicit functional approximations. Any approximations to the

non-interacting KE can be plugged into Eq. 3.25 to generate an approximation of the NAKE. The approximations obtained in this way are called *decomposable* approximations [32]. Section 4.7 gives a detailed list of these approximations. Typically, decomposable approximations do not yield accurate results for the NAKE, because they are designed for approximate the non-interacting KE, thus not optimized for the NAKE, and also the lack of accuracy and transferability of these approximations means they typically do not yield accurate non-interacting KE, let alone the NAKE. Another type of approximation is the non-decomposable approximation. They cannot be expressed with Eq. 3.25. Generally, they yield better NAKE than the decomposable approximations due to the fact that they are optimized for the NAKE. Several non-decomposable approximations will be proposed in Chapter 6 and 7.

An S-DFT formalism was developed in which computing the NAKE is avoided by introducing a projection technique to keep the fragment KS orbitals from different fragments orthogonal to each other [33]. This formalism takes advantage of the non-uniqueness of the NAKE in S-DFT and thus not applicable for P-DFT.

4.2 NAKE for Spin-polarized Systems

The NAKE for spin-polarized systems can be calculated from the NAKE of spin-unpolarized densities using the spin-scaling of the KE functionals. The non-interacting KE of spin-polarized densities can be written as the sum of the non-interacting KE from the two spin channels

$$T_{\mathrm{S}}[n_\uparrow, n_\downarrow] = T_{\mathrm{S}}[n_\uparrow, 0] + T_{\mathrm{S}}[0, n_\downarrow]. \tag{4.1}$$

Applying this to a spin-unpolarized density. we get

$$T_{\mathrm{S}}^{\mathrm{unpol}}[n] = T_{\mathrm{S}}\left[\frac{n}{2}, \frac{n}{2}\right] = 2T_{\mathrm{S}}\left[\frac{n}{2}, 0\right], \tag{4.2}$$

or $T_{\mathrm{S}}[n, 0] = T_{\mathrm{S}}^{\mathrm{unpol}}[n]/2$. Applying this back to Eq. 4.1, we get

$$T_{\mathrm{S}}[n_\uparrow, n_\downarrow] = \frac{1}{2}(T_{\mathrm{S}}^{\mathrm{unpol}}[2n_\uparrow] + T_{\mathrm{S}}^{\mathrm{unpol}}[2n_\downarrow]). \tag{4.3}$$

Combining Eq. 3.25 and Eq. 4.1, we get the relation between the NAKE of spin-polarized densities and spin-unpolarized densities

$$T_{\rm S}^{\rm nad}[n_\uparrow, n_\downarrow] = \frac{1}{2}(T_{\rm S}^{\rm nad,unpol}[2n_\uparrow] + T_{\rm S}^{\rm nad,unpol}[2n_\downarrow]). \tag{4.4}$$

For the rest of the chapter, the discussion will be based on spin-unpolarized systems.

4.3 Unambiguous NAKE Density and NAKE per Particle

The non-interacting KE $T_{\rm S}$ can be written as a non-interacting KE density $\tau(\mathbf{r})$ integrated over real space

$$T_{\rm S} = \int {\rm d}^3r\, \tau(\mathbf{r}). \tag{4.5}$$

It is easy to see that the non-interacting KE density is not unique. Any functional that integrates over real space to 0, e.g., $\nabla^2 n(\mathbf{r})$, can be added to a valid non-interacting KE density to get another non-interacting KE density. Two commonly used non-interacting KE density are [34]

$$\tau^{\rm WFI}(\mathbf{r}) = -\frac{1}{2}\sum_{i=1}^{N} \phi_i^*(\mathbf{r})\nabla^2\phi_i(\mathbf{r}), \tag{4.6}$$

and

$$\tau^{\rm WFII}(\mathbf{r}) = \frac{1}{2}\sum_{i=1}^{N} |\nabla\phi_i(\mathbf{r})|^2. \tag{4.7}$$

The difference between the two choices is

$$\tau^{\rm WFI}(\mathbf{r}) = \tau^{\rm WFII}(\mathbf{r}) - \frac{1}{4}\nabla^2 n(\mathbf{r}). \tag{4.8}$$

Similarly, the NAKE density $\tau^{\rm nad}$ is defined as any function satisfies

$$T_{\rm S}^{\rm nad} = \int {\rm d}^3r\, \tau^{\rm nad}(\mathbf{r}). \tag{4.9}$$

Substitute into Eq. 3.25, we can get

$$\tau^{\rm nad}(\mathbf{r}) = \tau(\mathbf{r}) - \sum_{\alpha=1}^{N_f} \tau_\alpha(\mathbf{r}). \tag{4.10}$$

where $\tau(\mathbf{r})$ is the non-interacting KE density of the whole system while $\tau_\alpha(\mathbf{r})$ is the non-interacting KE density of fragment α. The ambiguity is partially removed for the NAKE density as long as the same expression is chosen for both $\tau(\mathbf{r})$ and $\tau_\alpha(\mathbf{r})$ because $\nabla^2 n = \sum_{\alpha=1}^{N_f} \nabla^2 n_\alpha$.

One issue of the NAKE density is that it is heavily localized in the nuclear regions. To better study the features in the binding region, we introduce the NAKE per particle $t_{\mathrm{S}}^{\mathrm{nad}}(\mathbf{r})$, which is defined as

$$t_{\mathrm{S}}^{\mathrm{nad}}(\mathbf{r}) = \frac{\tau^{\mathrm{nad}}(\mathbf{r})}{n(\mathbf{r})}. \tag{4.11}$$

4.4 Non-additive Non-interacting Kinetic Potential (NAKP)

Any effective approximation to the NAKE must perform well in two aspects, its value and its functional derivative [35]. The latter is called the NAKP $v_{\mathrm{t}}^{\mathrm{nad}}(\mathbf{r})$:

$$v_{\mathrm{t}}^{\mathrm{nad}}(\mathbf{r}) = \frac{\delta T_{\mathrm{S}}^{\mathrm{nad}}[\{n_\alpha\}]}{\delta n(\mathbf{r})}. \tag{4.12}$$

The NAKP is the kinetic component of the partition potential, it can be expanded as

$$v_{\mathrm{t}}^{\mathrm{nad}}(\mathbf{r}) = \frac{\delta T_{\mathrm{S}}[n]}{\delta n(\mathbf{r})} - \sum_{\alpha=1}^{N_{\mathrm{f}}} \sum_j f_{j\alpha} \int \mathrm{d}^3 r' \, \frac{\delta T_{\mathrm{S}}[n_{j\alpha}]}{\delta n_{j\alpha}(\mathbf{r}')} Q_{j\alpha}(\mathbf{r}', \mathbf{r}). \tag{4.13}$$

It has been shown that the improvements in approximations to the NAKE do not necessarily lead to the improvements in approximations to the NAKP [36,37]. Therefore, it is necessary to study the behavior of the NAKP.

In P-DFT, the NAKP is unique up to a constant. Therefore, P-DFT provides a suitable framework to analyze the behavior of the NAKP for various approximate KE functionals.

4.5 Scaling

Certain density scaling relations must be satisfied for an approximation to $T_{\mathrm{S}}[n]$ to be accurate.

The most commonly used scaling is uniform coordinate scaling

$$n_\eta(\mathbf{r}) = \eta^3 n(\eta\mathbf{r}), \tag{4.14}$$

where η is a scalar that multiplies the real space coordinates $\mathbf{r}$.

An alternative scaling relation is called density scaling

$$n_\gamma(\mathbf{r}) = \gamma n(\mathbf{r}). \tag{4.15}$$

An important concept in scaling is called homogeneity. For uniform coordinate scaling, a functional $X[n]$ has the degree of homogeneity m if it satisfies the relationship

$$X[n_\eta] = \eta^m X[n]. \tag{4.16}$$

For $m \neq 0$ it can be expressed using the integral expression

$$m = \frac{-\int \mathrm{d}^3 r\, n(\mathbf{r})\mathbf{r}\cdot\nabla\left(\dfrac{\delta X[n]}{\delta n(\mathbf{r})}\right)}{X[n]}. \tag{4.17}$$

Similarly, for density scaling, a functional $X[n]$ has the degree of homogeneity k if it satisfies the relationship

$$X[n_\gamma] = \gamma^k X[n]. \tag{4.18}$$

For $k \neq 0$ it can be expressed using the integral expression [38]

$$k = \frac{-\int \mathrm{d}^3 r\, n(\mathbf{r})\dfrac{\delta X[n]}{\delta n(\mathbf{r})}}{X[n]}. \tag{4.19}$$

4.6 Implicit Functionals

The exact NAKE and NAKP can be obtained as an implicit functional of the density [5, 6, 39].

From Eq. 2.16, we find

$$\frac{\delta T_\mathrm{S}[n]}{\delta n(\mathbf{r})} = -v_\mathrm{S}[n](\mathbf{r}) + \mu. \tag{4.20}$$

For any v-representable density, we can obtain the KS potential $v_{\rm S}[n](\mathbf{r})$ that yields the density n by solving the inverse problem. Substitute Eq. 4.20 into Eq. 4.13, we find

$$v_{\rm t}^{\rm nad}(\mathbf{r}) = -v_{\rm S}[n](\mathbf{r}) + \sum_{\alpha=1}^{N_{\rm f}} \sum_{j} f_{j\alpha} \int {\rm d}^3 r' \, v_{\rm S}[n_{j\alpha}](\mathbf{r}') Q_{j\alpha}(\mathbf{r}', \mathbf{r}) + \Delta\mu, \tag{4.21}$$

where $\Delta\mu$ is a constant shift of the potential that can be ignored.

There are a few algorithms to solve the inverse problem. One can construct a variational functional of the one-electron potential [40]. Another approach is directly searching for orbitals that solve the KS equations Eq. 2.18 under the constraint that the orbitals are normalized and yield the correct density [9].

4.7 Explicit Decomposable Functionals

4.7.1 Enhancement Factor

A LDA or generalized gradient approximation (GGA) level semi-local KE functional has a general form

$$T_{\rm S}[n] = \frac{3}{10}(3\pi^2)^{2/3} \int {\rm d}^3 r n(\mathbf{r})^{5/3} F(n, \nabla n), \tag{4.22}$$

where F is the enhancement factor, which is initially used as an analysis tool for exchange energy functionals, and later for KE functionals as well. To keep $F(n, \nabla n)$ invariant under uniform coordinate scaling, we introduce the reduced density gradient

$$s(\mathbf{r}) = \frac{|\nabla n(\mathbf{r})|}{2k_{\rm F}(\mathbf{r}) n(\mathbf{r})}, \tag{4.23}$$

where $k_{\rm F}(\mathbf{r}) = (3\pi^2 n(\mathbf{r}))^{1/3}$ is Fermi wave vector. Now the enhancement factor becomes

$$F(n, \nabla n) = F(s). \tag{4.24}$$

4.7.2 Exact Functionals

For two types of the systems the explicit form of the exact NAKE is known:

- Thomas-Fermi (TF) [41, 42]:

$$F^{\mathrm{TF}}(s) = 1. \tag{4.25}$$

  TF is exact for the homogeneous electron gas.

- von Weizsäcker (vW) [43]:

$$F^{\mathrm{vW}}(s) = \frac{5}{3}s^2. \tag{4.26}$$

  vW is exact for systems with only one orbital, i.e., systems with only one electron or spin-unpolarized systems with two electrons.

4.7.3 TFλW Functionals

One strategy to construct KE functionals is through a linear combination of TF and vW. They can be written in the general form [44, 45]

$$F(s) = F^{\mathrm{TF}}(s) + \lambda F^{\mathrm{vW}}(s). \tag{4.27}$$

In this dissertation, we consider the choices of λ listed in Table 4.1 [46–51], and refer to this type of KE functionals as TFλW functionals.

Table 4.1.
Choice of λ of TFλW functionals defined by the enhancement factor of Eq. (4.27)

Functional	λ
TFvW	1
GEA2	1/9
Golden	13/45
YT65	1/5
Baltin	5/9
Lieb	0.18590919

Among these functionals, it is worth mentioning that the second-order gradient expansion (GEA2) gives the correct NAKE for systems with slowly varying electron

densities. Therefore many functionals are constructed with the constraint that at $s \to 0$ limit these functionals yield the same result as GEA2.

4.7.4 Conjointness Conjecture

A large group of GGA KE functionals is constructed based on the "conjointness conjecture" [52,53]. With this strategy, the form of the enhancement factor of a GGA exchange energy functional is used, while the parameters can be either the same as the exchange energy functional, or re-parameterized by fitting or with physical constraints.

Many KE functionals conjoint PBE [54], which has the enhancement factor

$$F^{\mathrm{PBE}}(s) = 1 + \kappa - \frac{\kappa}{1 + \frac{\mu}{\kappa} s^2}. \tag{4.28}$$

The choice of parameters κ and μ of the functionals conjoint PBE are listed in Table 4.2. [55–57].

Table 4.2.
Choice of κ and μ of conjoint PBE functionals.

Functional	κ	μ
TW02I	0.8209	0.2335
TW02II	0.6774	0.2371
TW02III	0.8438	0.2319
TW02IV	0.8589	0.2309
APBEK	0.8040	0.238 89
revAPBEK	1.245	0.238 89
APBEKint	0.8040	$\frac{5/9 + 5s^2 \cdot 0.23889}{3 + 5s^2}$
revAPBEKint	1.245	$\frac{5/9 + 5s^2 \cdot 0.23889}{3 + 5s^2}$

LLP [53] and FR(B88) [58] both conjoint B88, which has the enhancement factor [59]

$$F^{\mathrm{B88}}(s) = 1 + \frac{\alpha(bs)^2}{1 + \gamma bs \sinh^{-1}(bs)}, \tag{4.29}$$

where $b = 2(3\pi^2)^{1/3}$ is not a parameter.

T92 has a similar enhancement factor [60]

$$F^{\mathrm{T92}}(s) = F^{\mathrm{B88}}(s) - \frac{Dbs}{1 + 2^{5/3} bs}, \tag{4.30}$$

where $D = 0.072$.

The choice of the parameters α and γ of the functionals conjoint B88 are listed in Table 4.3.

Table 4.3.
Choice of α and γ of conjoint B88 functionals.

Functional	α	γ
LLP	0.004 418 8	0.0253
FR(B88)	0.004 596	0.027 74
T92	0.0055	0.0253

Other functionals using conjointness conjecture are:

LC94, conjoint PW91, has the enhancement factor [61]

$$F^{\mathrm{LC94}}(s) = \frac{1 + A_1 s \sinh^{-1}(As) + (A_2 - A_3 e^{-A_4 s^2}) s^2}{1 + A_1 s \sinh^{-1}(As) + B_1 s^4}, \tag{4.31}$$

where $A_1 = 0.093907$, $A_2 = 0.26608$, $A_3 = 0.0809615$, $A_4 = 100.00$, $A = 76.320$, $B_1 = 0.5776 \times 10^{-4}$.

FR(PW86), conjoint PW86, has the enhancement factor [58]

$$F^{\mathrm{FR(PW86)}}(s) = (1 + c_1 s^2 + c_2 s^4 + 0.2 s^6)^{1/15}, \tag{4.32}$$

where $c_1 = 2.208$, $c_2 = 9.27$.

4.7.5 Other Functionals

LP is a LDA functional with the enhancement factor [62]

$$F^{\mathrm{LP}}(s) = \frac{5}{(36\pi)^{1/3}}. \tag{4.33}$$

OL1 and OL2 are proposed based on the uniform coordinate scaling properties of $T_{\mathrm{s}}[n]$ [63]. The enhancement factors are:

$$F^{\mathrm{OL1}}(s) = 1 + \frac{5}{27}s^2 + dbs, \tag{4.34}$$

where $d = 0.00187$, and

$$F^{\mathrm{OL2}}(s) = 1 + \frac{5}{27}s^2 + \frac{Dbs}{1 + 2^{5/3}bs}, \tag{4.35}$$

where $D = 0.0245$.

P82 has the enhancement factor [64–66]

$$F^{\mathrm{P82}}(s) = 1 + \frac{5}{27(1 + (s/\zeta)^6)}s^2, \tag{4.36}$$

where $\zeta = 1$.

The following four functionals are all fractions with both numerators and denominators polynomials of s^2 and yield the same result as GEA2 at $s \to 0$ limit.

P92 has the enhancement factor [67]

$$F^{\mathrm{P92}}(s) = \frac{1 + 88.3960s^2 + 16.3683s^4}{1 + 88.2108s^2}. \tag{4.37}$$

VSK98 has the enhancement factor [68]

$$F^{\mathrm{VSK98}}(s) = \frac{1 + 0.95x + 9ax^3}{1 - 0.05x + ax^2}, \tag{4.38}$$

where $x = (5/27)s^2$, $a = 0.396$.

VJKS00 has the enhancement factor [69]

$$F^{\mathrm{VJKS00}}(s) = \frac{1 + a_1s^2 + a_3s^6}{1 + a_2s^2 + a_3s^4}, \tag{4.39}$$

where $a_1 = 0.8944$, $a_2 = 0.6511$, $a_3 = 0.0431$.

E00 has the enhancement factor [70]

$$F^{\mathrm{E00}}(s) = \frac{135 + 28s^2 + 5s^4}{135 + 3s^2}. \tag{4.40}$$

5. COMPUTATIONAL DETAILS

5.1 CADMium

Most of the calculations in this dissertation are done with our own all-electron real-space code CADMium written in MATLAB. CADMium is designed to run KS-DFT and P-DFT calculations for diatomics. However, it is capable to run calculations for any systems as long as the external potential has azimuthal symmetry. Up to two fragments are supported for P-DFT calculations. Like many other calculations for diatomic systems [71–75], prolate spheroidal grids are used in CADMium, where the two nuclei of the dimer are located at the foci. CADMium uses Libxc [76, 77] as the library for the XC functionals. The NAKE can be calculated either with functional approximations from Libxc or stocked in CADMium, or with an inversion procedure described in section 4.6.

CADMium is capable to reproduce the same results of other well-recognized DFT codes. Table 5.1 provides a comparison for the rare-gas dimers between P-DFT and KS-DFT calculations performed on the same grid using CADMium and with KS-DFT results from NWChem [78]. The NWChem calculations are done with aug-cc-pVTZ basis sets, and the basis set superposition error correction is not included. This table shows that the differences between the P-DFT and the KS-DFT binding energies from CADMium are in the order of 10^{-8} Ha or less in all cases. The differences between the KS-DFT binding energies from CADMium and from NWChem are in the order of $10^{-5} \sim 10^{-6}$ Ha, which is mostly due to the difference between using finite basis sets (NWChem) and a real-space grid (CADMium). P-DFT calculations with the inversion procedures in CADMium accurately reproduce the KS-DFT results from other well-known packages. The NAKE generated with the inversion procedures in

CADMium is used as the benchmark for the numerically "exact" LDA NAKE in this dissertation.

Table 5.1.
Comparison of binding energy at the equilibrium using KS-DFT and P-DFT with inversion calculations in CADMium, and KS-DFT calculations from NWChem. The aug-cc-pVTZ basis set is used for NWChem calculations.

System	$E_{\mathrm{b,KS}}$ (mHa)	$E_{\mathrm{b,inv}}$ (mHa)	$E_{\mathrm{b,KS}} - E_{\mathrm{b,inv}}$ (nHa)	$E_{\mathrm{b,NWChem}}$ (mHa)	$E_{\mathrm{b,KS}} - E_{\mathrm{b,NWChem}}$ (μHa)
He_2	−0.3550	−0.3550	−13.5040	−0.3591	4.0604
Ne_2	−0.7372	−0.7372	11.6920	−0.7847	47.5650
Ar_2	−1.1175	−1.1175	−15.4400	−1.1186	1.1200
HeNe	−0.5495	−0.5494	−9.1450	−0.5653	15.8160
HeAr	−0.5442	−0.5442	3.2844	−0.5489	4.7381
NeAr	−0.8770	−0.8770	11.2960	−0.8994	22.3530

5.2 Other Details

LDA is used as the XC functional throughout this paper, and the equilibrium stands for the LDA equilibrium separation. Although LDA is the simplest XC functional and is known to severely overestimate the binding energy of systems such as rare-gas dimers [79], the errors in LDA are almost entirely functional-driven rather than density-driven. With a different XC functional, PBE, the binding energy for He_2 at the LDA equilibrium distance is 0.07 mHa, but it is −0.36 mHa with LDA. However, the NAKE at that separation is 0.89 mHa with PBE and 0.99 mHa with LDA. This $\sim 10\%$ difference remains almost the same throughout all separations. As argued further in Sec. 6.1.1, the conclusions of our work should only depend min-

imally on this choice of XC functional. By "exact" NAKE in this dissertation, we refer to the one that reproduces the LDA results, including all of its errors.

The CCSD calculations in this dissertation are done with NWChem, with the aug-cc-pVDZ basis sets used for Li_2 and 6-31G** basis sets used for Na_2.

6. RARE-GAS DIMERS

The exact behavior of the NAKE and the performance of NAKE approximations varies for different types of systems. In this chapter, we will focus on rare-gas dimers, which is a simple type of weakly-interacting system where the bond type is Van der Waals. The NAKE of rare-gas dimers is very small compared to the total energy due to the small overlap of the fragment densities. Also, the fragment densities are very similar to the densities of corresponding isolated rare-gas atoms due to the nature of week interacting, so that a majority of the error in the approximated NAKE are functional driven.

There are a few facts that make the calculation of rare-gas dimers easier. First, all rare-gas dimers are spin-unpolarized. Also, all the fragments are closed-shell which means there are no fractional numbers of charge and spin.

6.1 Behavior of Numerically Exact $T_{\mathrm{S}}^{\mathrm{nad}}$ and Its Derivatives

6.1.1 Asymptotic Behavior

Figure 6.1, top panel, shows the LDA NAKE *vs.* inter-nuclear separation (R) for He_2, Ne_2 and HeNe. It is apparent that for each of these systems the NAKE is always positive and behaves as a nearly exponential function of the separation. In order to explore this behavior further, we numerically calculate the logarithmic derivative of the NAKE *vs.* the separation (Figure 6.1, bottom panel). A perfectly exponential function would have a constant logarithmic derivative, but the figure shows the logarithmic derivative varying in a small range: The NAKE is a nearly exponential function of R, i.e. $T_{\mathrm{S}}^{\mathrm{nad}}[\{n_\alpha\}] \sim e^{-kR}$. The best fit to the exponential decay constant (k) is reported in Table 6.1.

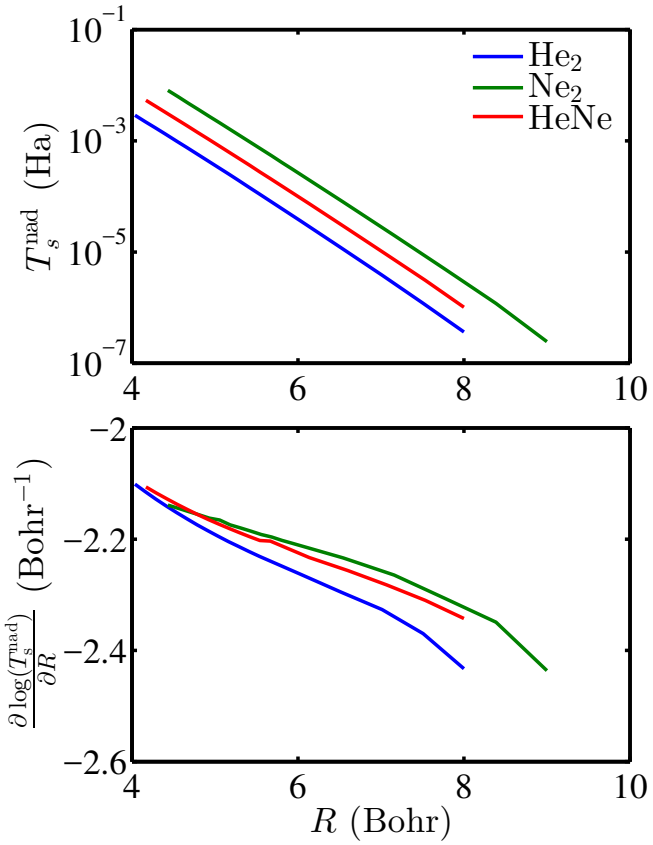

Figure 6.1. Top: The LDA NAKE *vs.* inter-nuclear separation for three rare-gas dimers. Bottom: logarithmic derivative of the NAKE *vs.* inter-nuclear separation for the same systems.

Table 6.1.
The decay constant k of the rare-gas dimers obtained by fitting the NAKE data into $T_{\rm S}^{\rm nad}[\{n_\alpha\}] = Ce^{-kR}$. Units in Bohr^{-1}.

System	Decay constant
He_2	2.2508
Ne_2	2.2549
Ar_2	1.8701
HeNe	2.2277
HeAr	1.9681
NeAr	1.9837

One might wonder whether this nearly exponential behavior is a feature of the LDA NAKE and would disappear with a van der Waals-inclusive XC functional [80, 81]. We suspect this is not the case: Although such functionals would provide dramatic improvements in the binding energies, they would not change the densities enough to affect the observed NAKE behavior reported here. We carried our analogous PBE calculations in He_2 and observed that the decay constant differs by only $\sim 1\%$ in spite of dramatic differences in the corresponding binding energy. As mentioned in Sec. 5.2, the overestimation of binding energies by local and semi-local functionals in these systems is mostly functional-driven. The behavior of the NAKE, which depends on the detailed behavior of fragment and total *densities*, varies only minimally with the choice of XC functional.

6.1.2 Behavior of NAKE per Particle

Figure 6.2 shows that the main feature of the exact NAKE per particle for the rare-gas dimers is a double peak with a well in the middle located in the center region, where the densities of the two fragments overlap. This feature is a result of the fragment densities slightly polarizing toward the bonding region (as compared

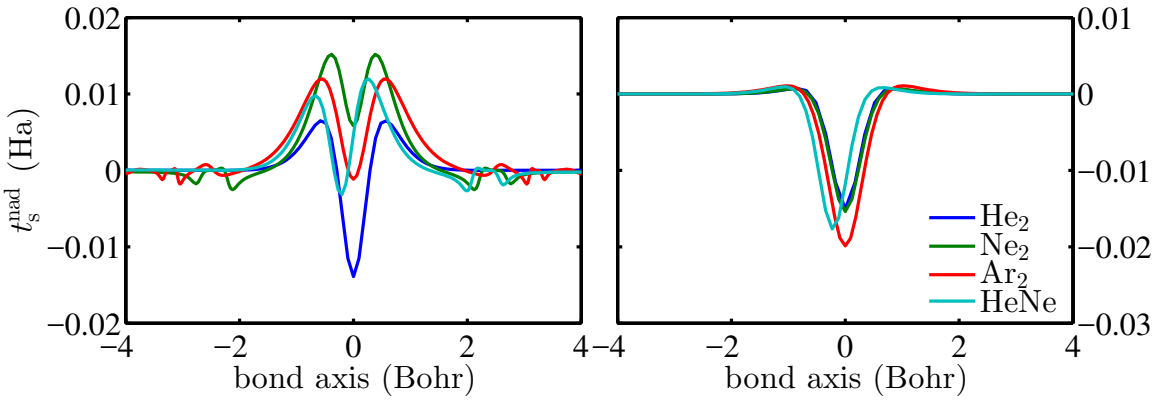

Figure 6.2. The numerically exact LDA NAKE per particle on the bond axis for select rare-gas dimers, where $x = 0$ is the bond midpoint. Left: equilibrium. Right: large separation.

to the isolated fragment densities). As the separation of the nuclei of the dimers increases, the peaks move farther apart and become much smaller, while the well becomes wider and deeper. Note with HeNe, the minima of the well is slightly away from the bond mid-point, which is a result of the unsymmetrical fragment densities. Also, small features exist in the region of the Ne and Ar nuclei. This is due to the non-spherical symmetry of the p orbitals in Ne and Ar. Those features are visible at the equilibrium but can be hardly seen at larger separations.

6.1.3 Behavior of NAKP

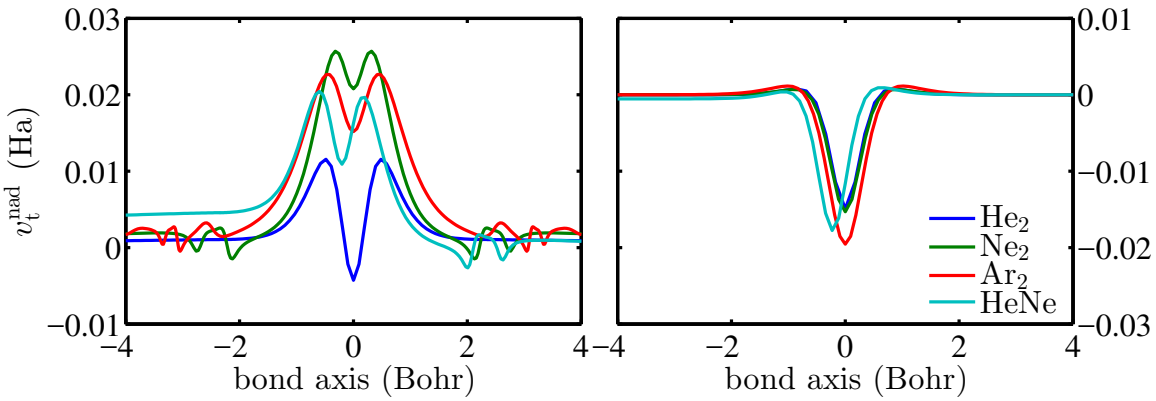

Figure 6.3. The exact NAKP on the bond axis for rare-gas dimers, where $x = 0$ is the bond mid-point. Left: equilibrium. Right: large separation.

Similar to the behavior of the NAKE per particle, figure 6.3 shows that the exact NAKP also has the feature of a double peak with a single well for all the systems we considered. The depth of the wells is smaller compared to that of the NAKE per particle at the equilibrium, but of about the same size at the larger separations. The exact NAKP also shows some small features in the region of the Ne and the Ar nuclei. The difference in the level between the left and the right side of asymmetrical systems is due to the difference in the chemical potential between the two atoms.

6.2 Re-parametrization of PBE Enhancement Factor

Some KE functionals are constructed by fitting into accurate non-interacting KE data of a set of systems. For example, the TW02 functionals are fitted into the non-interacting KE data for rare-gas atoms [82]. If we re-parameterized them by fitting into a set of accurate NAKE data, we should expect the performance of approximating the NAKE will be improved.

In this work, we choose the PBE form of the enhancement factor in Eq. 4.28 which is used in the TW02 functionals and re-parameterize it by fitting to our accurate set of NAKE data for rare-gas dimers. The re-parametrization is done in the following way. For each rare-gas dimer, we choose 13 different separations evenly distributed between $R_{\rm eq} - 1/4\,$Bohr and $R_{\rm eq} + 1/2\,$Bohr, where $R_{\rm eq}$ is the equilibrium separation. We then look for the κ and μ that minimize the error Δ

$$\Delta = \sum_{\text{Systems}} \sum_{R_i} \left(\frac{\tilde{T}^{\rm nad}_{\rm s,R_i} - T^{\rm nad}_{\rm s,R_i}}{T^{\rm nad}_{\rm s,R_i}} \right)^2 , \tag{6.1}$$

where $\tilde{T}^{\rm nad}_{\rm s,R_i}$ is the non-self-consistent NAKE evaluated from the exact P-DFT density using the re-parameterized enhancement factor and R_i is the ith separation.

Table 6.2.
Parameters κ and μ obtained by fitting into the NAKE data of rare-gas dimers

Fitting set	κ	μ
He_2	2.0654	0.010 42
Ne_2	2.3234	0.027 48
Ar_2	2.2049	0.019 06
HeNe	2.0158	0.020 52
HeAr	2.0301	0.013 03
NeAr	2.0777	0.028 08
He_2, Ne_2, Ar_2, HeNe, HeAr, NeAr	1.9632	0.019 79

The results are shown in Table 6.2. The optimal value of κ is close to 2 for all systems, which is much larger than the typical κ value of the conjoint PBE functionals optimized for the non-interacting KE listed in table 4.2. Laricchia *et al.* [57] suggest that a large value of κ in revAPBEK is needed to obtain improved embedding energies in frozen density embedding calculations. Our results show that to obtain accurate NAKE in P-DFT calculations, the value of κ needs to be even larger than that of revAPBEK. On the other hand, the optimal value of μ is much smaller and varies between $0.01 - 0.03$ for different systems. The last set of κ and μ in Table 6.2 is named R-PBE.

6.2.1 Asymptotic Behavior with Different Choices of Parameters

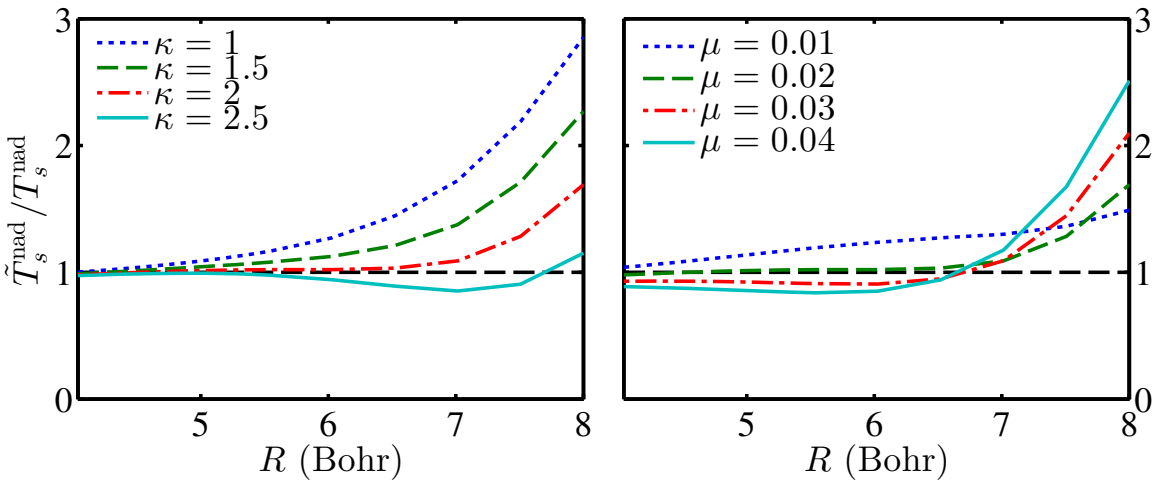

Figure 6.4. The ratio of the approximated and the exact NAKE of different choices of κ and μ in the PBE enhancement factor versus the inter-nuclear separation for He_2. Left: fixed $\mu = 0.02$. Right: fixed $\kappa = 2.0$.

Figure 6.4 shows how the parameters κ and μ in the PBE enhancement factor affect the asymptotic behavior of the NAKE for He_2. Overall with a generally wide range of κ and μ, the PBE enhancement factor can reproduce the nearly exponential

asymptotic behavior except at very large separations. The parameter κ mostly controls the decay constant. As we can see from the figure, the NAKE with different κ starts at the same point at small separations, but diverges as the dimer stretches. As mentioned in the previous section, in order to reproduce the exact decay constant, a large value of κ needs to be chosen. On the other hand, μ shifts the NAKE value up and down near the equilibrium and controls how the curve bends at large separations. A small value of μ is required to keep the asymptotic behavior exponential.

6.2.2 Behavior of NAKE per Particle

Figure 6.5 shows the NAKE per particle with selected approximate KE functionals of He_2, Ne_2 and HeNe on the bond axis. In general, most of the approximations fail to accurately reproduce the feature of a double peak with a single well, and none of the approximations reproduce the correct features observed around the Ne nuclei. TF has a single peak and vW has a very deep and wide well in the center for both equilibrium and large separations. However, the TFλW functionals do not reproduce the double-peak feature because the well in vW is wider than the peak in TF. TW02I does reproduce the double-peak feature, resembling the exact result at equilibrium, but at large separations, the peak becomes higher and the well becomes narrower than it should. Although R-PBE fails to reproduce this feature at the equilibrium because the two peaks overlap, it does reproduce the feature at large separations with the well of a more accurate width than TW02I.

6.2.3 Behavior of NAKP

Figure 6.6 shows the NAKP with selected approximate KE functionals of He_2, Ne_2 and HeNe on the bond axis. The behavior of the NAKP with approximate functionals is very similar to the behavior of the NAKE per particle of those functionals. The most noticeable difference is in TW02I. While it matches the exact result fairly accurately for the behavior of the NAKE per particle, in the case of the NAKP it yields much

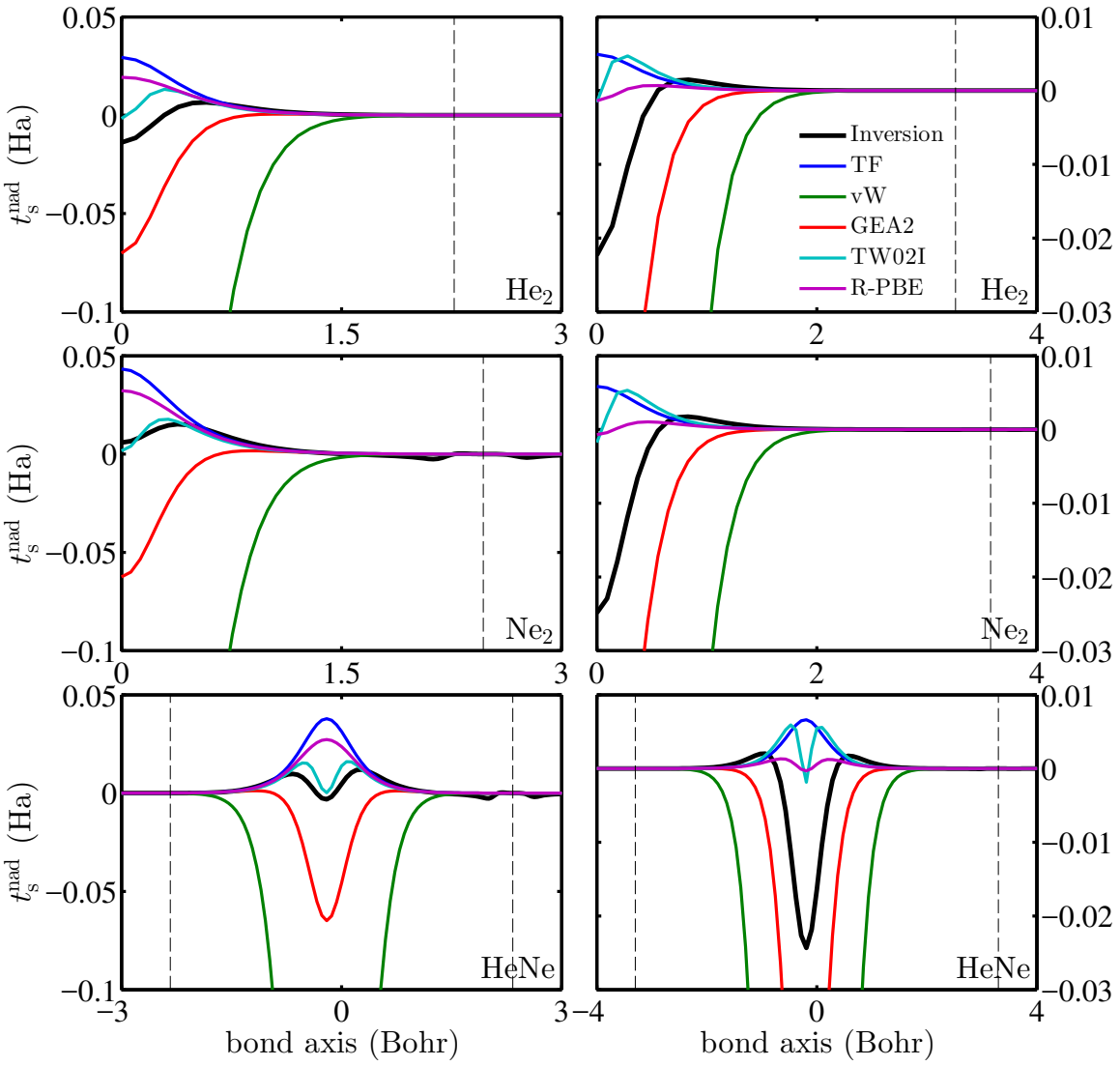

Figure 6.5. The LDA NAKE per particle for various rare-gas dimers on the bond axis. The left column shows the NAKE per particle at equilibrium and the right column at a larger separation. Only the right half is shown for all systems except HeNe due to symmetry. Dashed lines indicate the locations of nuclei, and $x = 0$ is the bond mid-point.

higher peaks and a much deeper well compared to the inversion results. On the other hand, R-PBE reproduces the feature of a double peak with a single well at large separations, but the width and the depth of the well are smaller than they should be.

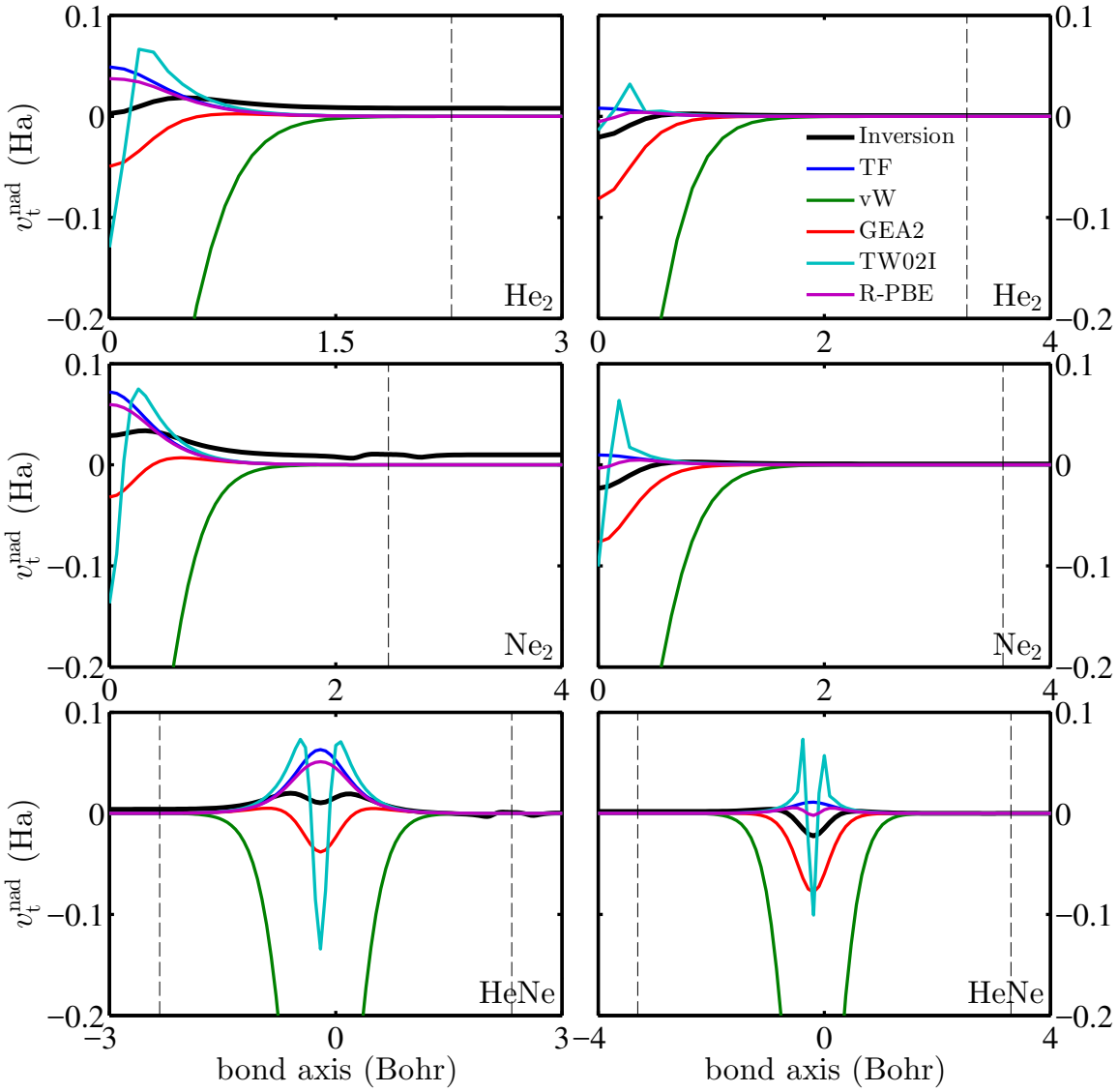

Figure 6.6. The NAKP for various rare-gas dimers on the bond axis. The left column shows the NAKP at the equilibrium and the right column shows that at a larger separation. Only the right half is shown for all systems except HeNe due to symmetry. Dashed lines indicate the locations of nuclei, and $x = 0$ is the bond mid-point.

Overall, similar to the behavior of the NAKE per particle, none of the approximate functionals capture the correct behavior at all separations.

6.2.4 NAKE and Self-consistent Density at Equilibrium

In this section, the performance of the KE functionals at the equilibrium is studied for six rare-gas dimers: He_2, Ne_2, Ar_2, HeNe, HeAr and NeAr. To measure how well an approximate KE functional performs in different regions with only one number, we calculated the error in the self-consistent density using

$$N_{\text{err}} = \int \mathrm{d}^3 r \, |n(\mathbf{r}) - n_{\text{approx}}(\mathbf{r})|. \tag{6.2}$$

Table 6.3 shows the "exact" LDA NAKE at equilibrium, and Figure 6.7 shows the error in the NAKE and the error in the self-consistent density of selected approximate KE functionals. Tables with a full list of approximate functionals can be found in Tables A.1 - A.4 in the appendix. The functional "setting $T_{\text{S}}^{\text{nad}} = 0$" is used as a reference. A functional should at least perform better than setting $T_{\text{S}}^{\text{nad}} = 0$ to be considered as "good".

Table 6.3.
The numerically "exact" LDA NAKE at equilibrium for rare-gas dimers.

System	$T_{\text{S}}^{\text{nad}}$ (Ha)
He_2	9.929×10^{-4}
Ne_2	2.750×10^{-3}
Ar_2	4.050×10^{-3}
HeNe	1.845×10^{-3}
HeAr	1.802×10^{-3}
NeAr	3.152×10^{-3}

Due to the small overlap between the fragment density at equilibrium, setting $T_{\text{S}}^{\text{nad}} = 0$ yields relatively small errors, which is $\sim 1\,\text{mHa}$ for the NAKE, and ~ 0.01 for the self-consistent density. All functionals using the conjointness conjecture give an error in the NAKE of less than 1mHa and an error in the density of less than 0.01.

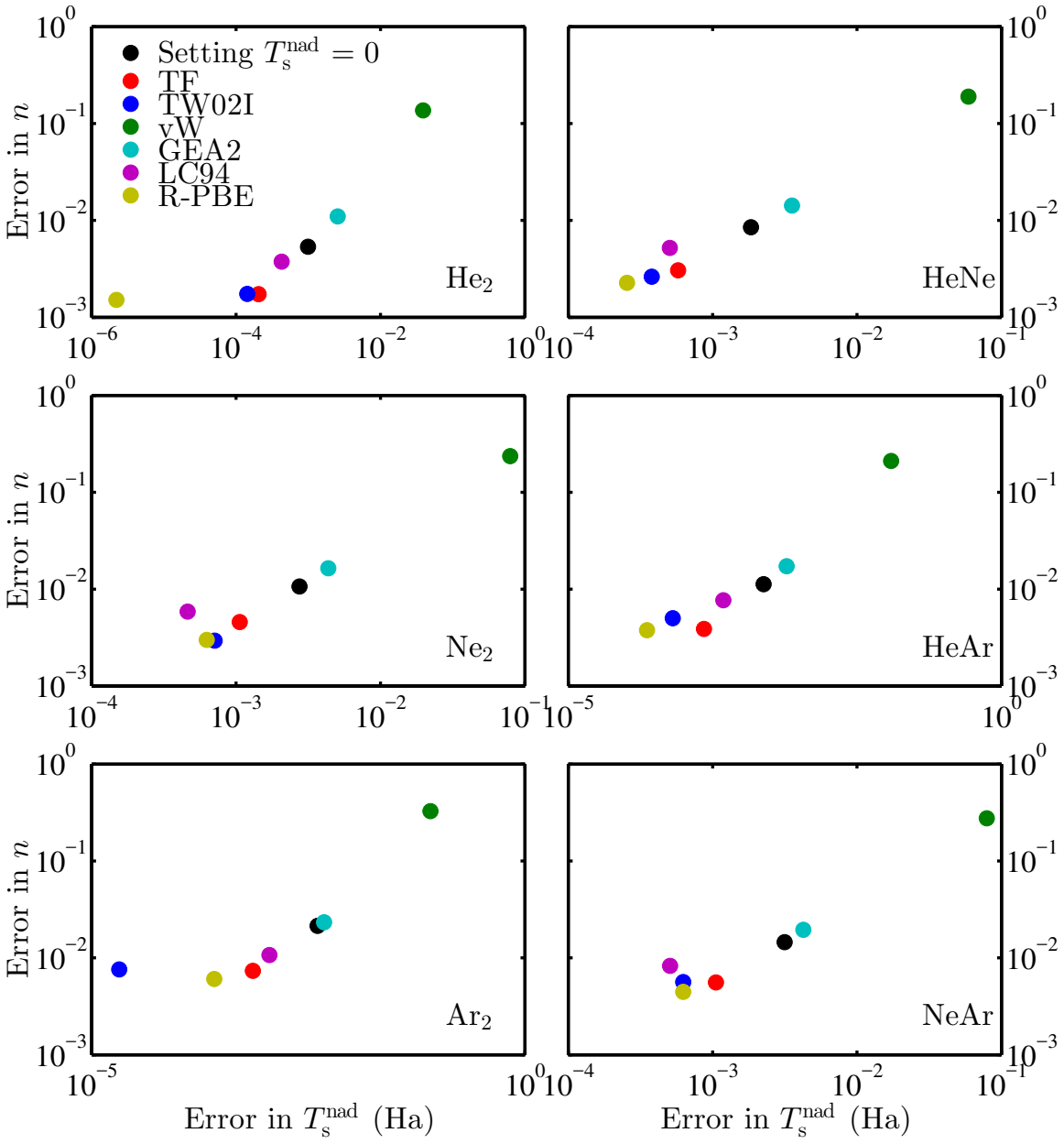

Figure 6.7. The error in the NAKE and in the self-consistent density as defined in Eq.(6.2) for various KE functionals.

In terms of the NAKE, R-PBE achieves the best result for He_2 and LC94 for Ne_2 and HeNe, while TW02II achieves the best result in terms of the density, followed by R-PBE. It is worth noting that although revAPBEK yields better results than APBEK

in terms of the NAKE as in Ref [57], it yields worse self-consistent densities. On the other hand, vW yields errors that are $20 - 40$ times larger than setting $T_{\rm S}^{\rm nad} = 0$, making all TFλW functionals "bad".

6.2.5 Dissociation

The dissociation curve can be used as a measure of the performance of approximate KE functionals as the dimers are stretched. Overall, conjoint PBE functionals yield better dissociation curves for the rare-gas dimers than other approximate KE functionals. Figure 6.8 shows the dissociation curve with conjoint PBE functionals for rare-gas dimers. TW02I, TW02III, TW02IV, APBEK and APBEKint yield very similar results, so only TW02I is shown, and revAPBEKint yields a similar dissociation curve to revAPBEK.

R-PBE errors are smaller than 0.1 Bohr for the equilibrium bond lengths of He_2, Ar_2, and HeAr. For Ne_2, HeNe and NeAr, the R-PBE equilibrium bond length is larger than the exact result. revAPBEK yields an accurate equilibrium bond length for Ne_2, TW02I for HeNe and HeAr, and TW02II for He_2 and HeAr. In terms of the binding energy, R-PBE matches the exact dissociation curve for He_2, and has an error of less than 0.1 mHa for HeAr, and it still outperforms the other conjoint PBE functionals for the other rare-gas dimers, especially at large separations. Although revAPBEK and revAPBEKint have accurate binding energies near the equilibrium, they overbind in all systems, while TW02II underbinds in all systems. Overall, R-PBE performs the best in dissociation for the rare-gas dimers.

6.3 Two-orbital approximation (2OA)

In two-orbital homo-nuclear diatomics, one Kohn-Sham orbital has gerade symmetry while the other orbital has ungerade symmetry. By treating the fragment densities of these systems as if they represented localized molecular orbitals, we can construct approximations to the gerade and ungerade KS molecular orbitals. We be-

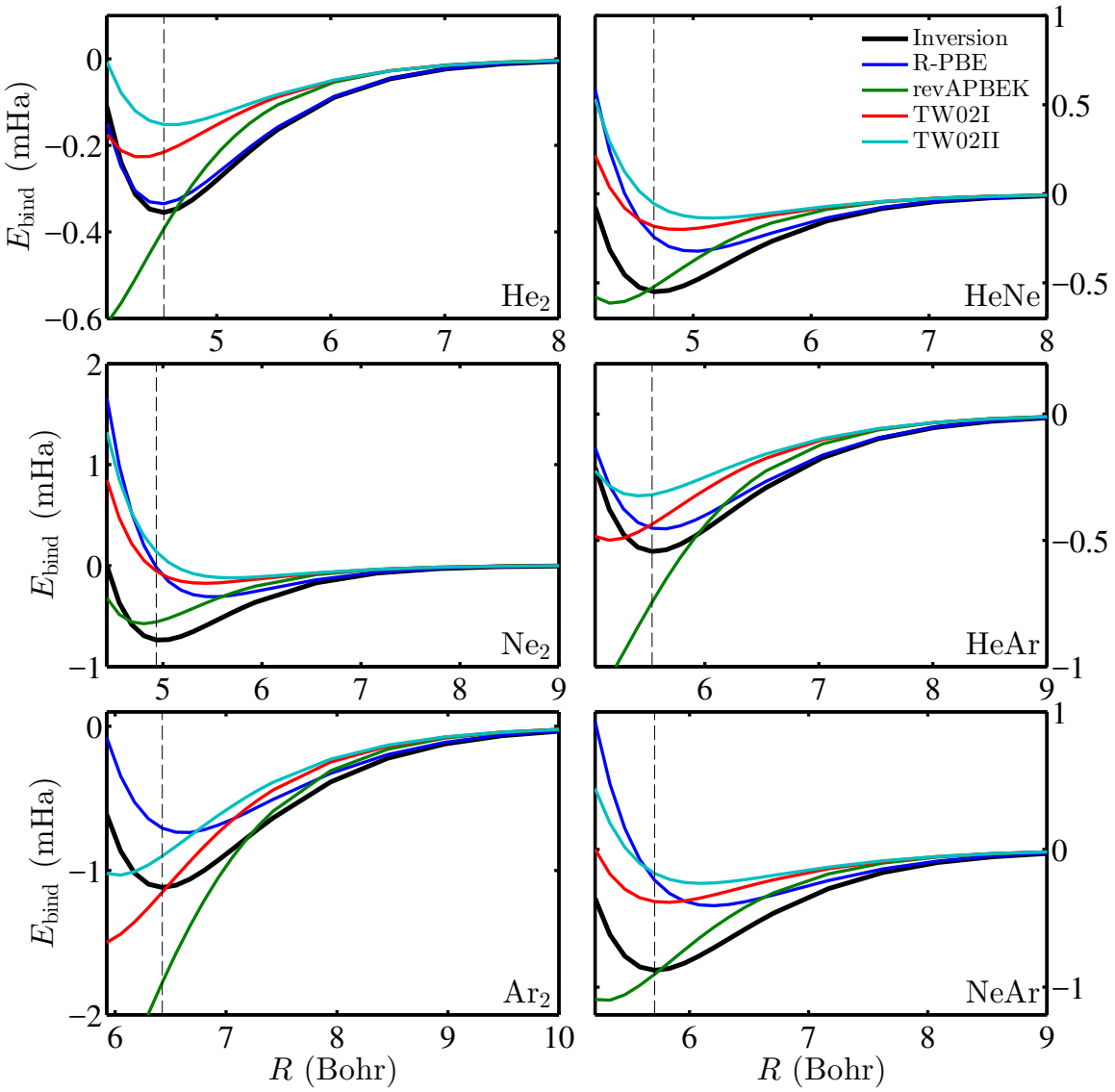

Figure 6.8. Binding Curves for rare-gas dimers with functionals conjoint PBE used as $T_{\rm S}^{\rm nad}[\{n_\alpha\}]$. R is the internuclear separation and $E_{\rm bind}$ is the binding energy. Dashed lines indicate the equilibrium separation.

gin by studying this idea with non-self-consistent post-P-DFT calculations. In this case, each fragment orbital has the same asymptotic behavior as the HOMO, which is

the ungerade orbital. Because of this, we construct an approximation to the ungerade orbital first:

$$\phi_{\rm u}(\mathbf{r}) \approx N(n_1(\mathbf{r})^{\frac{1}{2}} - n_2(\mathbf{r})^{\frac{1}{2}}). \tag{6.3}$$

This approximate orbital will have the correct symmetry and be properly normalized by setting $N = 1/(\int {\rm d}^3r\,(n_1(\mathbf{r})^{\frac{1}{2}} - n_2(\mathbf{r})^{\frac{1}{2}})^2)^{\frac{1}{2}}$. After the normalization, we can construct the remaining gerade orbital from the remaining density.

$$\phi_{\rm g}(\mathbf{r}) \approx \left(\frac{n(\mathbf{r})}{2} - \phi^2_{\rm ug}(\mathbf{r})\right)^{\frac{1}{2}}. \tag{6.4}$$

This approximation becomes exact as the inter-nuclear separation goes to infinity, but it still does quite well in the bonding region even at relatively short bond lengths. These approximate orbitals then lead to approximate KEs that can be used to construct NAKEs:

$$\begin{aligned} T_{\rm S}^{\rm nad,2OA}[n_1,n_2] &= -\frac{1}{2}\sum_{i={\rm u,g}}\int {\rm d}^3r\,\phi_i(\mathbf{r})\nabla^2\phi_i(\mathbf{r}) \\ &\quad +\frac{1}{2}\sum_{i=1,2}\int {\rm d}^3r\,n_i^{1/2}(\mathbf{r})\nabla^2 n_i^{1/2}(\mathbf{r}). \end{aligned} \tag{6.5}$$

This approximation can only be expected to give reasonable results for He_2, but it is interesting to note that it captures the asymptotic behavior of all other rare-gas dimers better than any other approximate functional.

6.3.1 Asymptotic Behavior

As we noted in Sec. 6.1.1, the exact NAKE behaves as a nearly exponential function of the inter-nuclear separation for all the rare-gas dimers. The 2OA of Eq.(6.5) satisfies this exact condition, as shown numerically in Figure 6.9, where the y-axis is in the logarithmic scale. The 2OA not only reproduces the nearly exponential behavior but also has the same decay constant compared to the exact NAKE. On the other hand, most of the other approximations either do not reproduce the nearly

exponential behavior or reproduce the nearly exponential behavior but with a different decay constant (FR(B88) and LLP reproduce the asymptotic behavior, but their decay constants are not as accurate as 2OA).

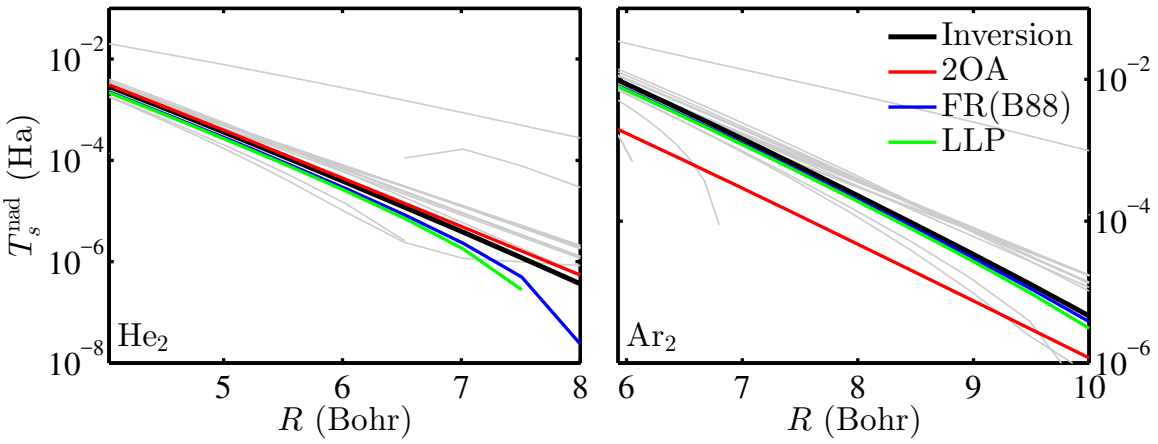

Figure 6.9. The approximate NAKE *vs.* the inter-nuclear separation for the rare-gas dimers. The curves in gray correspond to approximate functionals in Libxc, all of which fail to reproduce the exact asymptotic behavior. The "best"ones, FR(B88) and LLP, are highlighted alongside the 2OA.

Figure 6.10 compares the ratio between the exact NAKE and the 2OA. For each system, the ratio is almost a constant regardless of the inter-nuclear separation. This indicates that we can multiply 2OA by a single system-dependent parameter M and obtain an approximation that accurately reproduces the NAKE for all rare-gas dimers:

$$T_{\rm S}^{\rm nad,M}[n_1, n_2] \equiv M T_{\rm S}^{\rm nad,2OA}[n_1, n_2]. \tag{6.6}$$

We refer to 2OA with the parameter M as scaled-2OA here onwards. For He$_2$, we expect M to be slightly less than 1 because the non-interacting KE follows a variational principle and therefore the correct non-interacting KE for the two orbitals of the helium dimer must be less than the non-interacting KE of our approximate orbitals.

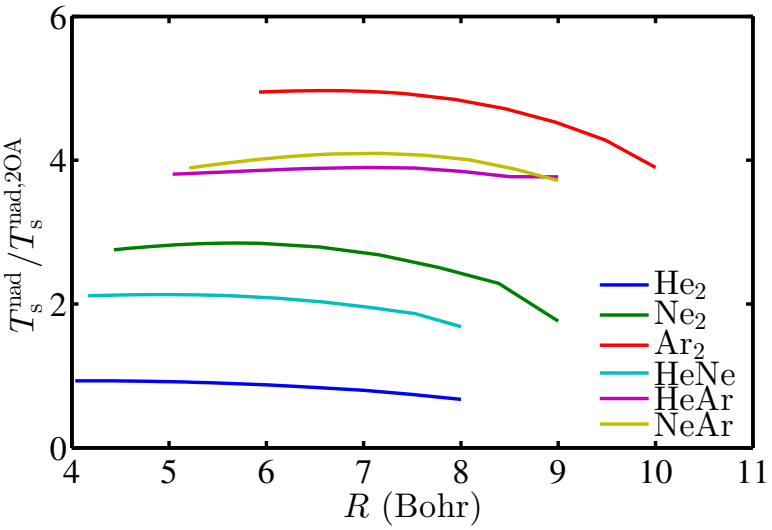

Figure 6.10. The ratio between the NAKE from inversion and 2OA vs the inter-nuclear separation for the rare-gas dimers.

We optimized M by minimizing the square of the difference between the NAKE from scaled-2OA and inversion. Only the data between $R_{eq} - 0.5$ Bohr and $R_{eq} + 0.5$ Bohr are used for the minimization, where R_{eq} is the equilibrium separation. The results are shown in Table 6.4.

Table 6.4.
The optimized M for the rare-gas dimers.

System	M
He_2	0.93
Ne_2	2.80
Ar_2	4.96
HeNe	2.12
HeAr	3.83
NeAr	3.96

6.3.2 Dissociation

Figure 6.11 compares the binding curve for inversion, TF, 2OA and scaled-2OA. As expected, the 2OA only works well in the case of He_2. However, it is impressive that the scaled-2OA binding curves accurately match the exact binding curves in *all* these cases.

6.4 Concluding Remarks

We have provided uniquely defined numerically exact NAKE reference data as well as NAKE data from approximate KE functionals for the rare-gas dimers. We also introduced two new NAKE functional approximations: R-PBE, a conjoint PBE functional re-parameterized with the NAKE data for the rare-gas dimers; and 2OA, a simple, physically-motivated, non-decomposable NAKE approximation constructed from two orbitals that are explicit functionals of the fragment densities.

Our NAKE data obtained from highly accurate inversion procedure with P-DFT calculation show that the "exact" LDA NAKE for the rare-gas dimers has a nearly exponential asymptotic behavior, which is not well reproduced by the approximate KE functionals. Our new approximations significantly improve this asymptotic behavior. For R-PBE, this is a result of fitting into the NAKE data. Although 2OA was not intended to approximate systems with more than two orbitals, it also reproduces the asymptotic behavior extremely well for all the rare-gas dimers.

We also provided the data of the NAKE per particle and the NAKP, two quantities that can be used to measure the performance of NAKE approximations in different regions. None of the approximations matches the exact result accurately for these quantities. However, R-PBE can reproduce the main feature of a double peak and a central well, but the size of these features is incorrect at large separations.

As for the NAKE and the self-consistent density at the equilibrium, approximations that use the conjointness-conjecture strategy generally produce better results while approximations based on the linear combinations of TF and vW functionals

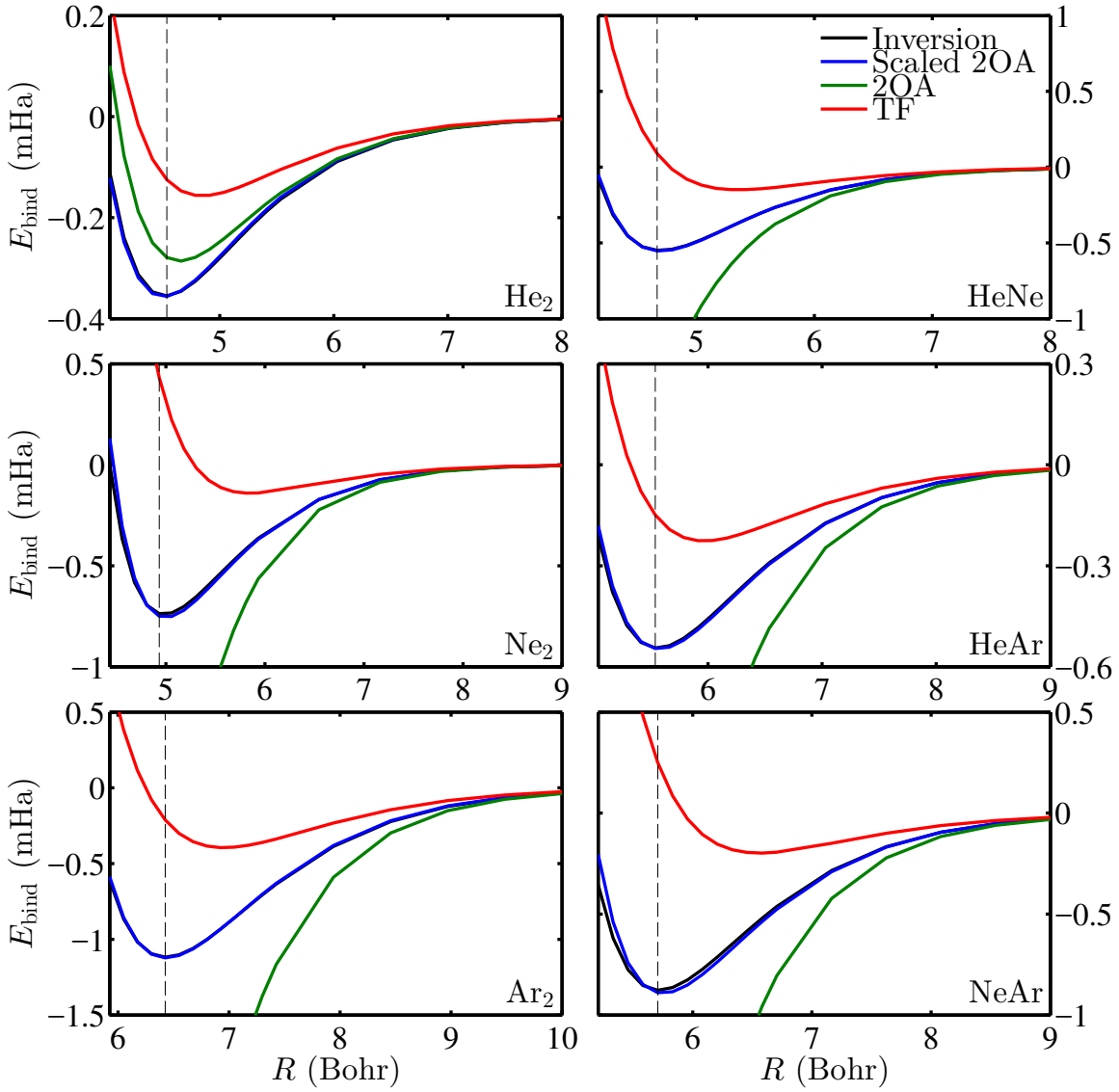

Figure 6.11. Binding Curves for rare-gas dimers with 2OA, scaled-2OA and TF. R is the inter-nuclear separation and E_{bind} is the binding energy. The curves of 2OA and scaled-2OA are from non-self-consistent P-DFT calculations. Dashed lines indicate the equilibrium separation.

produce worse results even than setting $T_{\text{s}}^{\text{nad}} = 0$. For the NAKE of rare-gas dimers, R-PBE provides the maximum accuracy attainable from conjoint PBE functionals.

We expect R-PBE and 2OA to be applicable to weakly-interacting systems, and should then be useful for large-scale simulations of nano-porous carbon-based materials. Work along these lines is ongoing. Our work also suggests that re-parameterizing existing approximations for the non-interacting KE with our benchmark data for the NAKE is a promising path. However, further improvement of approximate functionals for the NAKE remains an important open challenge.

7. COVALENT BONDS

In this chapter, we will examine the behavior of the NAKE for covalent bonds, which are more common in chemistry. There are a few differences between weekly-interacting systems and covalent bonds: the stronger overlap between the fragment densities in covalent bonds not only means the NAKE is much larger, and therefore the accuracy of the approximations can significantly impact the total energy, but also the density-driven error can play a more important role in some cases; also while all rare-gas dimers are spin-unpolarized, closed-shell systems, many dimers involving covalent bonds are spin-polarized with fractional charges and spins.

7.1 Impact of FOO and ENS with Approximated NAKE

In the cases of many covalent bonds, the choice of ENS or FOO can impact the result NAKE when approximated functionals are used. This is because most of the approximated functionals fail to reproduce the exact behavior that the NAKE should scale linearly with the density when the total number of electrons goes from N to $N+1$, where N is any non-negative integer. Here we give a mathematical explanation of how ENS and FOO yield to different NAKE per particle in core regions with approximated functionals.

Consider a diatomic system partitioned into two fragments labeled with L and R. Under FOO treatment, the NAKE per particle can be written as

$$\begin{aligned} t_{\mathrm{S}}^{\mathrm{nad,FOO}}[n_L, n_R](\mathbf{r}) &= \frac{1}{2}\sum_{\sigma} t_{\mathrm{S}}^{\mathrm{unpol}}[2(n_{L\sigma} + n_{R\sigma})](\mathbf{r}) \\ &\quad -\frac{1}{2}\sum_{\sigma} t_{\mathrm{S}}^{\mathrm{unpol}}[2n_{L\sigma}](\mathbf{r}) - \frac{1}{2}\sum_{\sigma} t_{\mathrm{S}}^{\mathrm{unpol}}[2n_{R\sigma}](\mathbf{r}). \end{aligned} \tag{7.1}$$

The fragment densities typically have exponential asymptotic behavior [4], which means at large separations, in the core region of the left nucleus, $n_R \ll n_L$ and $\nabla n_R \ll$

∇n_L. With a LDA or GGA level approximation, the influence to the molecular $t_{\rm S}$ from the right fragment can be ignored:

$$t_{\rm S}^{\rm unpol}[2(n_{L\sigma}+n_{R\sigma})](\mathbf{r}\to\mathbf{R}_L)\approx t_{\rm S}^{\rm unpol}[2n_{L\sigma}](\mathbf{r}\to\mathbf{R}_L). \tag{7.2}$$

The $t_{\rm S}$ of the right fragment in the left region can also be ignored:

$$t_{\rm S}^{\rm unpol}[2n_{R\sigma}](\mathbf{r}\to\mathbf{R}_L)\approx 0. \tag{7.3}$$

Therefore,

$$t_{\rm S}^{\rm nad,FOO}[n_L,n_R](\mathbf{r}\to\mathbf{R}_L)\approx 0. \tag{7.4}$$

The same math can be done in the core region of the right nucleus. This means the approximated NAKE per particle will have no feature in the core regions. However, this is not the case with ENS treatment. The NAKE per particle under ENS treatment can be written as

$$\begin{aligned} t_{\rm S}^{\rm nad,ENS}[n_L,n_R](\mathbf{r}) &= \frac{1}{2}\sum_{\sigma} t_{\rm S}^{\rm unpol}[2(n_{L\sigma}+n_{R\sigma})](\mathbf{r}) \\ &\quad -\frac{1}{2}\sum_{i,\sigma} f_{iL}t_{\rm S}^{\rm unpol}[2n_{iL\sigma}](\mathbf{r}) \\ &\quad -\frac{1}{2}\sum_{i,\sigma} f_{iR}t_{\rm S}^{\rm unpol}[2n_{iR\sigma}](\mathbf{r}). \end{aligned} \tag{7.5}$$

Since $t_{\rm S}[n]$ is not a linear functional of n for LDA or GGA level approximations, we have

$$t_{\rm S}^{\rm unpol}[2n_{L\sigma}](\mathbf{r}\to\mathbf{R}_L)\neq\sum_i f_{iL}t_{\rm S}^{\rm unpol}[2n_{iL\sigma}](\mathbf{r}\to\mathbf{R}_L). \tag{7.6}$$

The $t_{\rm S}$ of the right fragment in the left region can still be ignored:

$$t_{\rm S}^{\rm unpol}[2n_{iR\sigma}](\mathbf{r}\to\mathbf{R}_L)\approx 0. \tag{7.7}$$

Therefore,

$$\begin{aligned} t_{\rm S}^{\rm nad,ENS}[n_L,n_R](\mathbf{r}\to\mathbf{R}_L) &\approx \frac{1}{2}\sum_{\sigma} t_{\rm S}^{\rm unpol}[2(n_{L\sigma})](\mathbf{r}\to\mathbf{R}_L) \\ &\quad -\frac{1}{2}\sum_{i,\sigma} f_{iL}t_{\rm S}^{\rm unpol}[2n_{iL\sigma}](\mathbf{r}\to\mathbf{R}_L) \\ &\neq 0. \end{aligned} \tag{7.8}$$

This means the approximated NAKE per particle under ENS will have features in the core regions. In fact, in Section 7.3 we will show that these features are very significant.

7.2 Behavior of NAKE vs Separation

Figure 7.1 displays the NAKE versus bond length R of several diatomic systems with covalent bonds. In all cases, the NAKE displays a minimum separation, and except for H_2, this separation is significantly outside the equilibrium separation. Thus, at equilibrium distances, the NAKE constitutes a repulsive force, whereas at very large separations, it acts in an attractive manner. In contrast, for H_2 the minimum in the NAKE is at roughly the same distance as the equilibrium.

Figure 7.1 also shows the TF and vW NAKE calculated non-self-consistently using the same fragment density from the exact NAKE with both ENS and FOO treatments. Thus all errors are functional-driven. It can be seen that the approximate functionals evaluated on both ENS and FOO are quite inaccurate, except for the case of H_2 where vW is exact. Neither ENS nor FOO has a minimum as displayed by the exact NAKE. Instead, all the approximate functionals yield values that decrease monotonically with separation.

There is also a very large difference between the two treatments with approximate functionals. These differences are due to the incorrect treatment of fractional spins by approximate density functionals. It is interesting to note that, close to equilibrium, TF and many other NAKE approximations not showing in Figure 7.1 with ENS significantly outperforms the same functionals evaluated with FOO. At large separations, the reverse becomes true as FOO becomes more accurate while there is a significant error with ENS. This unphysical behavior of ENS at large separations is due to the static-correlation error [83] of the NAKE approximations. vW evaluated with FOO performs especially well at large separations, and it is the only approximated functional gives the correct negative sign with FOO. It performs especially

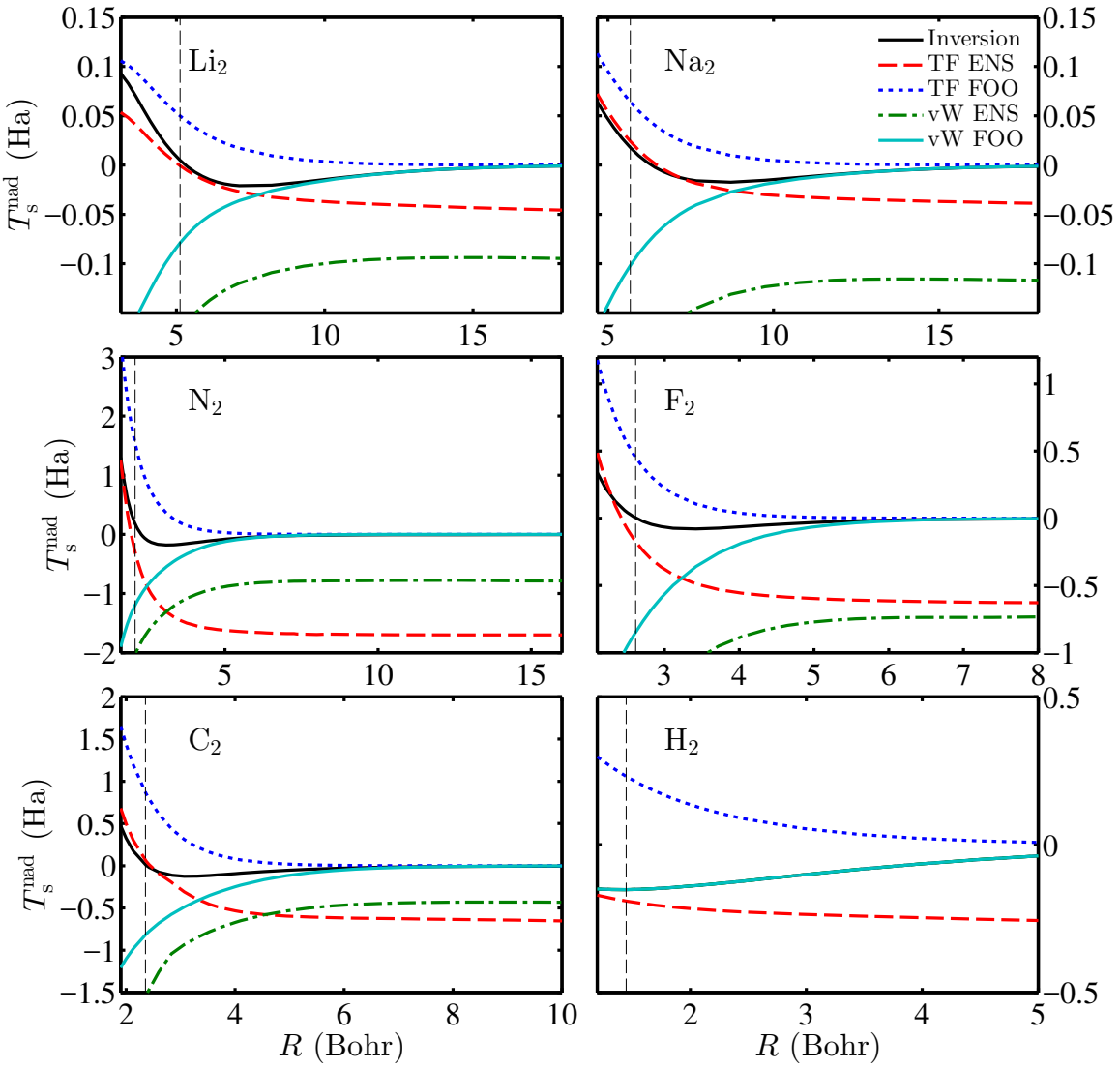

Figure 7.1. Exact NAKE vs bond length R for covalent dimers and some approximate kinetic energy functionals evaluated with the same fragment density use ENS and FOO. The black dashed straight lines represent the equilibrium separation.

well for Li_2 and Na_2 as it is nearly exact at separations larger than twice the equilibrium distance, because these systems have only one valence orbital. Also unlike other approximate functionals, vW evaluated with FOO outperforms vW evaluated

with ENS at all separations, except for the case of H_2, where vW evaluated with both treatments are the same as the exact result.

7.3 Behavior of NAKE per Particle

The top panels of Figures 7.2-7.6 show the exact NAKE per particle with the ENS treatment for Li_2, Na_2, N_2, C_2, and F_2, as well as the TF and vW NAKE per particle with both ENS and FOO treatments evaluated non-self-consistently with the same fragment densities obtained from the inversion calculation.

The exact NAKE per particle has significant features in both binding region and core regions for the equilibrium configuration, while for the stretched configuration, the features in the core regions are much less significant than those in the binding region. The TF and vW NAKE per particle evaluated with the ENS treatment displays features in both binding region and core regions, and the features are much more significant than the exact one in both equilibrium configuration and stretched configuration. On the other hand, the TF and vW NAKE per particle evaluated with the FOO treatment has features only in the binding region, as explained in Sec 7.1.

In stretched Li_2 and Na_2, the vW NAKE per particle is identical with the exact one in all but the core regions with both ENS and FOO treatment, because in the non-core regions the density is dominated by the only valence orbital for alkali dimers, and vW is exact for one orbital. It is worth mentioning the similarity will disappear if the vW NAKE per particle is evaluated self-consistently, because in this case, the density-driven error will dominate in the non-core region. The similarity of the vW NAKE per particle and the exact one in the non-core regions is also observed in some non-alkali dimers like N_2 and F_2. However, in C_2, the exact NAKE per particle has a peak feature in the binding region which is not reproduced by vW.

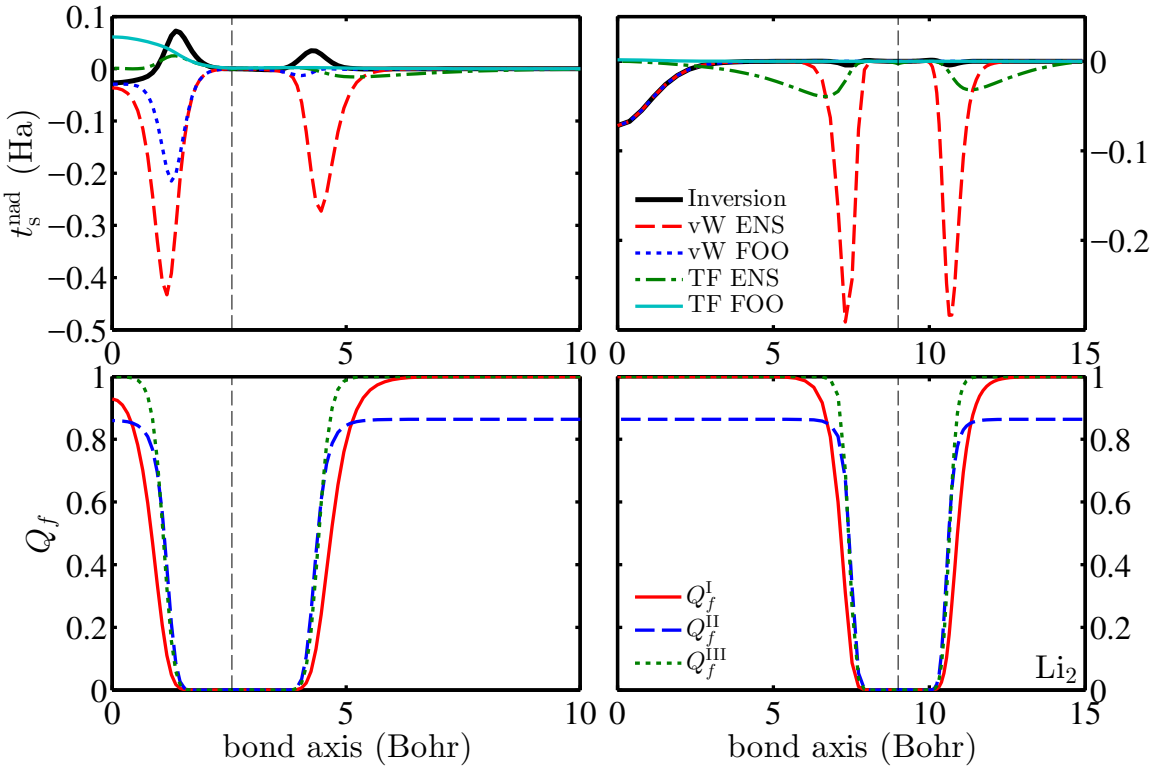

Figure 7.2. Top panels: the NAKE per particle for Li_2. Bottom panels: Three choices of switching functions. Left panels: LDA equilibrium. Right panels: stretched configuration. The plots are evaluated along the bond axis. Only the right half is plotted due to the mirror symmetry. The black dashed straight lines represent the position of the nuclei.

7.4 NAKE and Self-consistent Density at Equilibrium

Figure 7.7 shows the error in the NAKE and self-consistent density for H_2 and Li_2 at equilibrium configuration of selected decomposable NAKE functionals. Tables of complete data can be found in Tables A.5 - A.6 in the appendix. The errors in the self-consistent density are evaluated in the same way as explained in Eq. 6.2, except only the density for one spin component is used. The errors in the density for the other spin component is the same due to the spin symmetry of these systems. ENS treatment is used considering ENS outperforms FOO at equilibrium. It is worth noting that

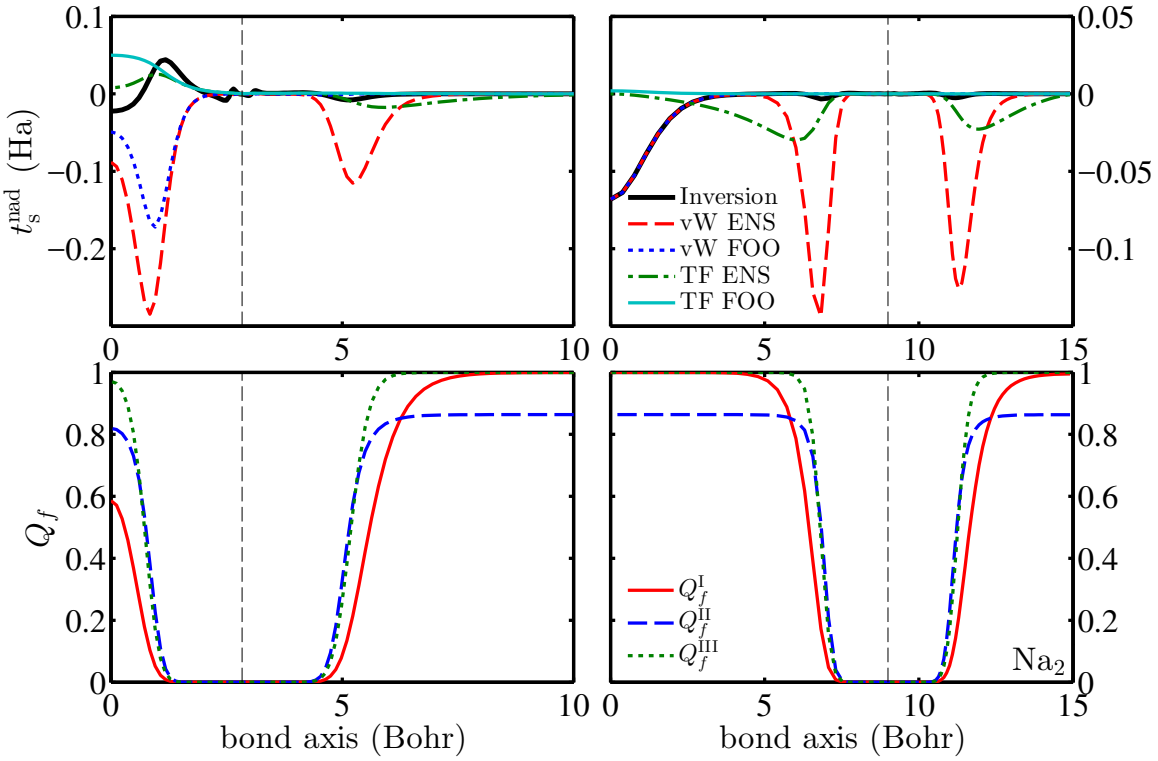

Figure 7.3. Same as figure 7.2 with results for Na_2.

unlike previous sections in this chapter, the NAKE is calculated self-consistently so that both functional-driven and density-driven errors are included.

Unlike rare-gas dimers, where some approximations are on par with or better than setting $T_S^{nad} = 0$, existing decomposable approximations perform poorly for covalent bonds, as setting $T_S^{nad} = 0$ is the best approximation for Li_2, and better than all but vW for H_2. One of the reasons for this behavior is that the exact NAKE is very close to 0 at equilibrium, as shown in Figure 7.1. Another reason is that covalent bonds tend to have more rapidly varying electron densities, while most of these approximations are more accurate with slower varying electron densities.

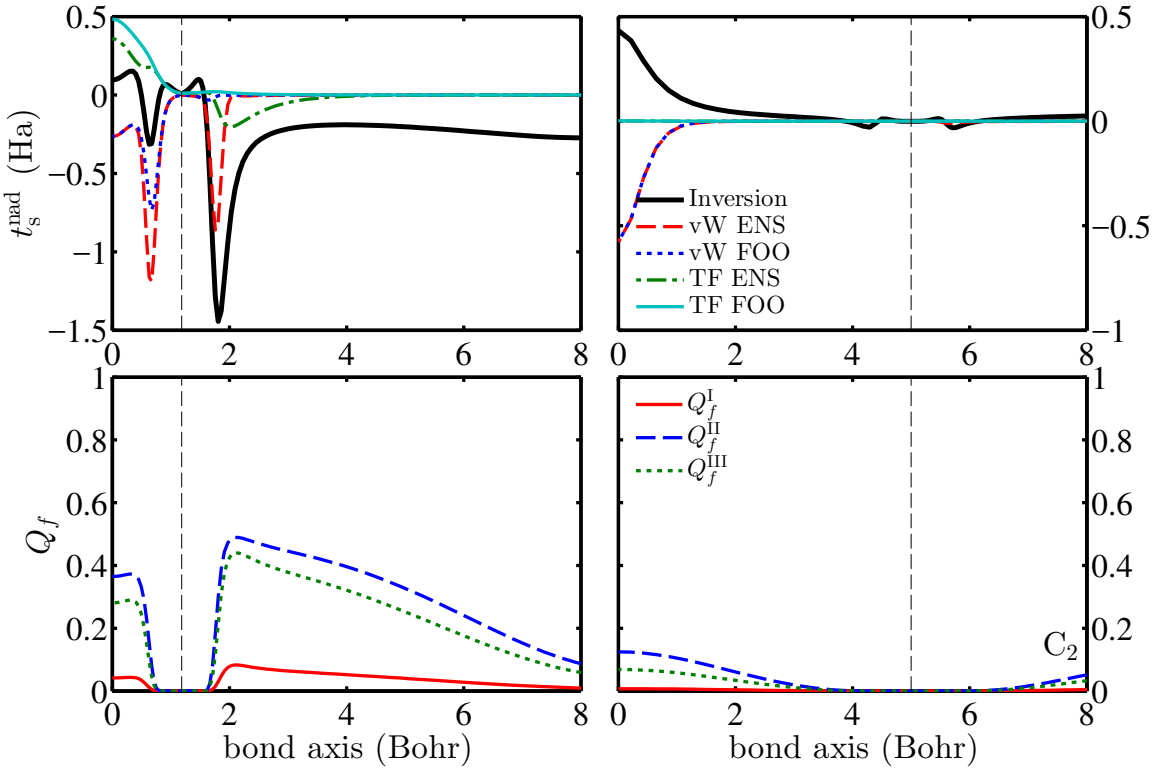

Figure 7.4. Same as figure 7.2 with results for C_2.

7.5 Covalent Approximation

The covalent approximation is constructed by taking the advantage of the similarities between the vW and the exact NAKE per particle in the non-core regions for alkali dimers. It is a non-decomposable NAKE approximation which uses a mixture of the TF and vW functional with the vW functional only used in the regions where only one orbital dominates. The mixing factor is determined by a switching function $Q_f(\mathbf{r})$. To achieve the exact result for the stretched bonds, both vW and TF NAKE per particle are evaluated with the FOO treatment. The combined NAKE per particle can be written as the following:

$$\begin{aligned} t_{\rm S}^{\rm nad}[\{n_\alpha\}](\mathbf{r}) &= Q_f(\mathbf{r}) t_{\rm S}^{\rm nad,vW,FOO}[\{n_\alpha\}](\mathbf{r}) \\ &\quad + (1 - Q_f(\mathbf{r})) t_{\rm S}^{\rm nad,TF,FOO}[\{n_\alpha\}](\mathbf{r}). \end{aligned} \tag{7.9}$$

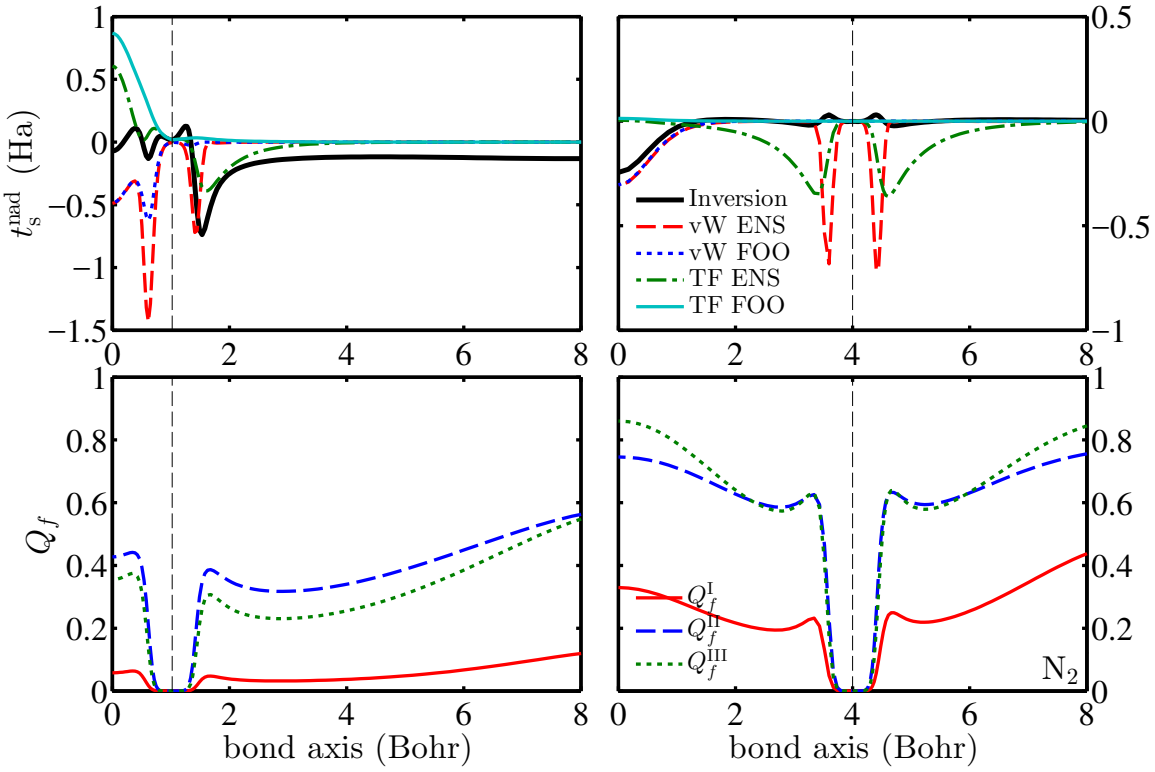

Figure 7.5. Same as figure 7.2 with results for N_2.

A few attempts have been made to determine typical types of regions. Sun *et al.* use parameters calculated from the exact non-interacting KE density and the non-interacting KE density approximated by TF and vW [84]. Lastra *et al.*, on the other hand, use a switching function of the fragment densities, its gradient and Laplacian [85].

In constructing the switching function $Q_f(\mathbf{r})$ the following requirements need to be met:

- $0 \leq Q_f(\mathbf{r}) \leq 1$.
- $Q_f(\mathbf{r}) = 1$ in the one orbital limit.
- $Q_f(\mathbf{r}) = 0$ in the uniform gas limit.

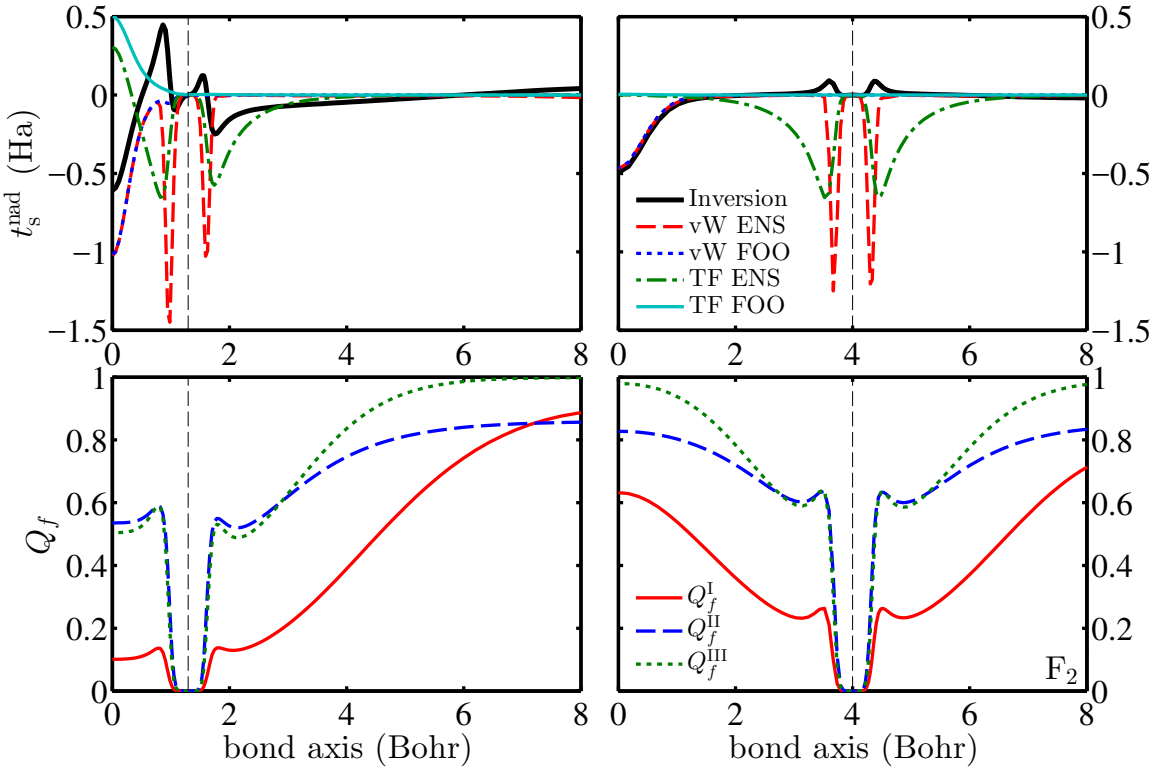

Figure 7.6. Same as figure 7.2 with results for F_2.

However to meet the uniform gas limit requirement $Q_f(\mathbf{r})$ must be a function of $\nabla n(\mathbf{r})$. As the covalent approximation is constructed to represent the NAKE for the covalent bonds which are dominated by one orbital and the densities are not slowly-varying, it is more important to have $Q_f(\mathbf{r})$ to satisfy the one orbital limit requirement rather than the uniform gas requirement.

Hereby we propose the following three choices of $Q_f(\mathbf{r})$:

$$Q_f^{\mathrm{I}}(\mathbf{r}) = \prod_{\alpha=1}^{N_\mathrm{f}} \left(1 + \sum_i f_{i\alpha} \sum_\sigma \frac{n_{i\alpha\sigma}(\mathbf{r})}{n_{i\alpha}(\mathbf{r})} \log_2 \frac{n_{i\alpha\sigma}(\mathbf{r})}{n_{i\alpha}(\mathbf{r})} \right), \tag{7.10}$$

$$Q_f^{\mathrm{II}}(\mathbf{r}) = \prod_{\alpha=1}^{N_\mathrm{f}} \left(1 - \cosh^{-2}(\frac{2m_\alpha}{n_\alpha}) \right), \tag{7.11}$$

$$Q_f^{\mathrm{III}}(\mathbf{r}) = \prod_{\alpha=1}^{N_\mathrm{f}} \left(\frac{1}{2} - \frac{1}{2} \cos(\frac{\pi m_\alpha}{n_\alpha}) \right), \tag{7.12}$$

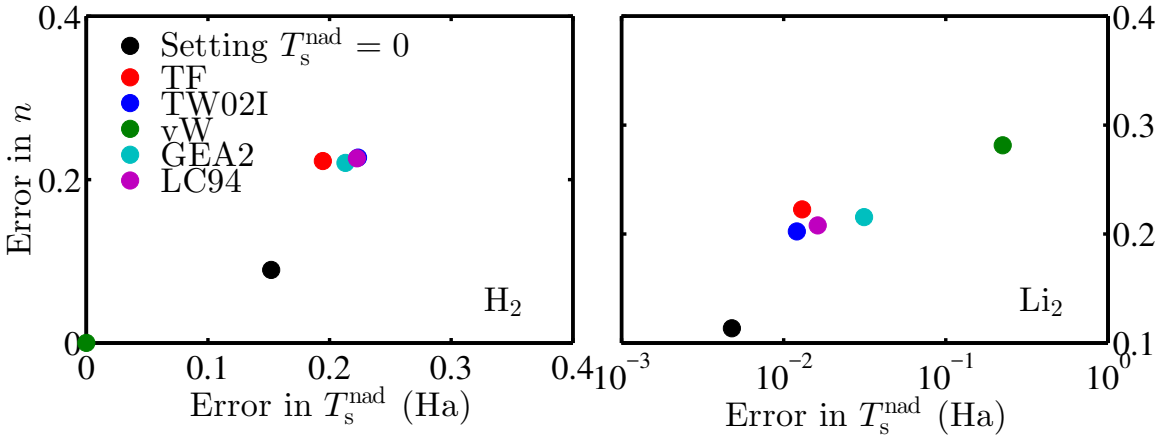

Figure 7.7. The error in the NAKE and in the self-consistent density as defined in Eq.(6.2) of various KE functionals. ENS treatment is used.

where $m_\alpha(\mathbf{r}) = \sum_i f_{i\alpha}|n_{i\alpha\uparrow}(\mathbf{r}) - n_{i\alpha\downarrow}(\mathbf{r})|$. These choices of $Q_f(\mathbf{r})$ are constructed based on the fact that with the ENS treatment, in the core regions the spin up and spin down fragment densities are almost the same; while in the binding region, the spin fragment densities of the two spin components are different with $m_\alpha(\mathbf{r})/n_\alpha(\mathbf{r}) = 1$ in the one orbital limit. Therefore, the covalent approximation is a mixture of the ENS and the FOO treatment with Eq. 3.5 used to connect the fragment densities of the two treatments.

The bottom panels of Figures 7.2-7.6 show the three choices of the switching function for Li_2, Na_2, N_2, C_2, and F_2. All three choices of the switching function go to 0 in core regions where the vW NAKE per particle does not match the exact NAKE per particle. For Li_2 and Na_2, Q_f^{I} and Q_f^{III} go to 1 in non-core regions as these regions are dominated by only one orbital. For N_2, C_2, and F_2, $Q_f(\mathbf{r})$ varies between 0 to 1 in non-core regions and Q_f^{I} has a significantly smaller value than Q_f^{II} and Q_f^{III}.

7.6 Results of Covalent Approximation

7.6.1 NAKE vs Bond Length

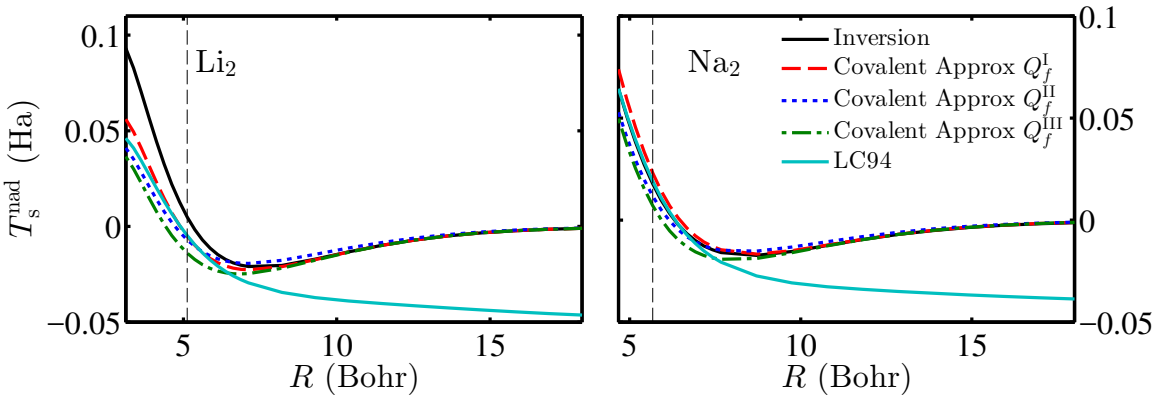

Figure 7.8. NAKE vs bond length R for Li_2 and Na_2. The black dashed straight lines represent the equilibrium separation.

Figure 7.8 displays the NAKE versus bond length R for Li_2 and Na_2. The approximated NAKEs are evaluated non-self-consistently with the density obtained from the inversion calculation. LC94 calculated with the ENS treatment is included for comparison with existing decomposable approximations. Covalent approximation with all three choices of the switching function yield very accurate NAKE for stretched bonds beyond the minimum of the NAKE. At shorter bond length near the equilibrium, $Q_f^{\rm I}$ yields more accurate NAKE than the other two choices of the switching function, and also outperforms LC94.

Figure 7.9 displays the same data for N_2, F_2, and C_2. Covalent approximation still yields very accurate NAKE for stretched bonds, but begins to diverge at a bond length farther away from the equilibrium compared to Li_2 and Na_2. That is expected because these dimers have more than one valence orbital. For N_2 and F_2, $Q_f^{\rm II}$ and $Q_f^{\rm III}$ significantly outperform $Q_f^{\rm I}$ while $Q_f^{\rm II}$ is slightly more accurate than $Q_f^{\rm III}$. For

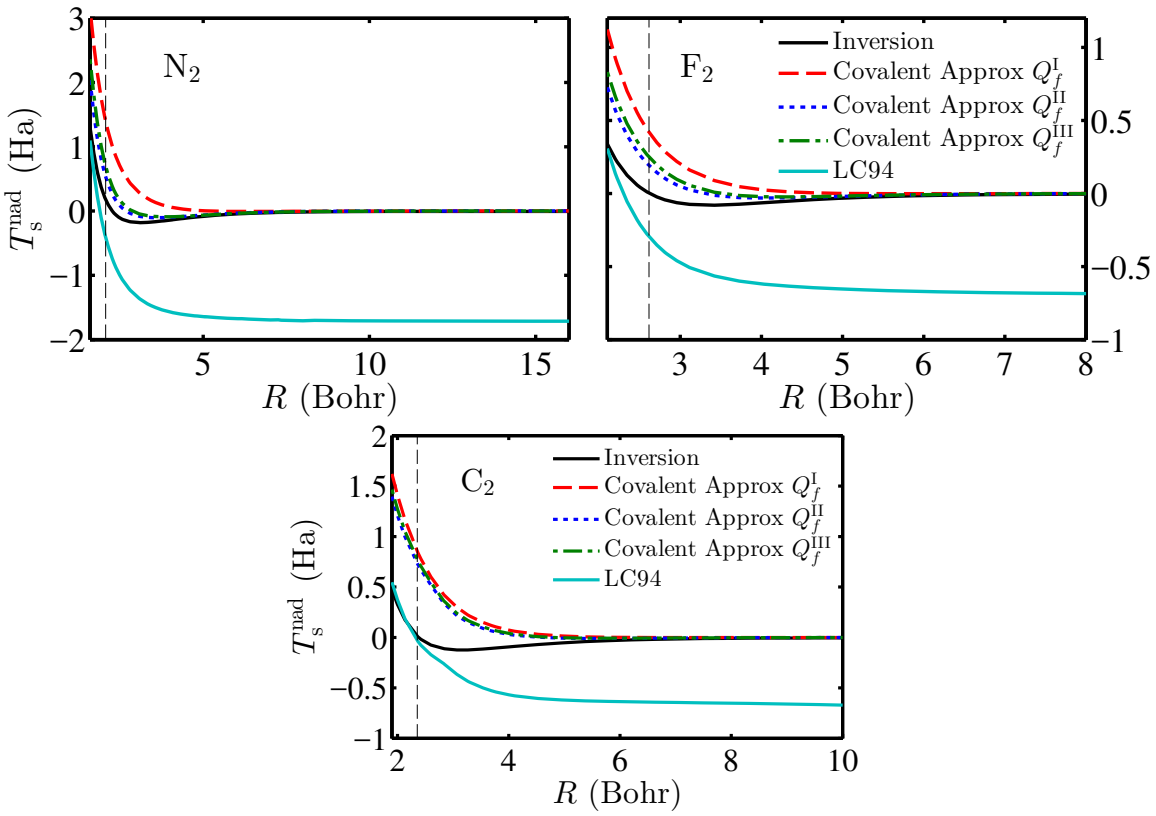

Figure 7.9. NAKE vs bond length R for N_2, F_2, and C_2. The black dashed straight lines represent the equilibrium separation.

C_2, all three choices of switching function do not perform well near the equilibrium bond length.

7.6.2 Binding Curves

In this section, we demonstrate the potential of combining the covalent approximation with the overlap approximation [86] to solve the static-correlation error with efficient P-DFT calculations. Overlap approximation is a correction to the non-additive exchange-correlation energy that keeps the KS behavior near the equilibrium but corrects the delocalization and static-correlation errors at large separations.

Figure 7.10 shows the binding curves of Li_2 and Na_2. All calculations are done self-consistently. The CCSD result is used as a benchmark for the exact binding

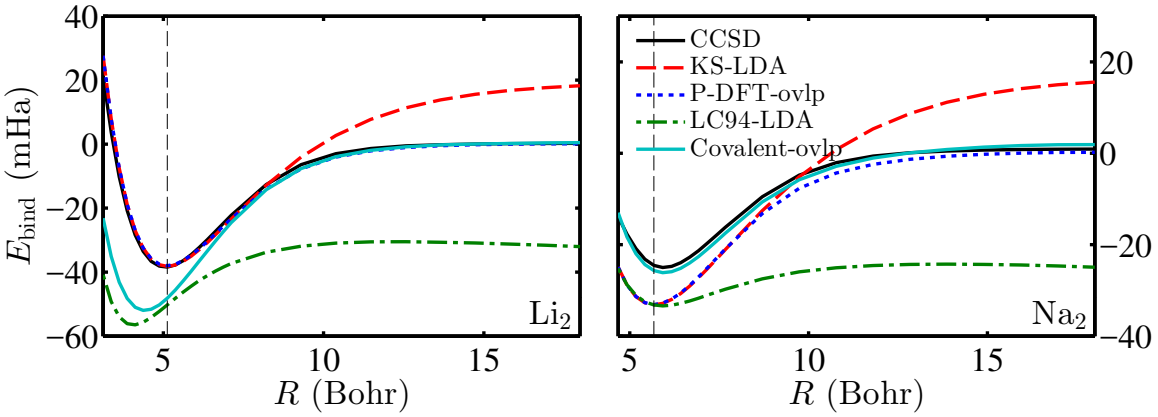

Figure 7.10. Binding curves for Li_2 and Na_2. KS-LDA: KS-DFT with LDA as XC functional. P-DFT-ovlp: P-DFT with LDA XC functional plus corrections from overlap approximation, and the NAKE is evaluated with inversion. LC94-LDA: P-DFT with LC94 as NAKE and LDA as XC. Covalent-ovlp: P-DFT with covalent approximation with Q_f^{I} as NAKE and LDA plus overlap approximation correction as XC. The black dashed straight lines represent the equilibrium separation.

curve. P-DFT with the overlap approximation and accurate NAKE from inversion method yields accurate binding energy for stretched bonds while keeping the same binding energy as KS-DFT near equilibrium. P-DFT combining covalent approximation and overlap approximation also yields similarly accurate binding energy at large bond length. It is worth noting combining these two approximations yields a better result than KS-LDA for Na_2 near the equilibrium as well, although mainly due to error cancellation. The accurate binding energy at large bond length from the self-consistent result means the covalent approximation not only minimizes the functional-driven error, but also the density-driven error.

7.7 Concluding Remarks

Constructing accurate NAKE functional approximations for covalent bonds is a huge challenge. In this work, we examined the exact behavior of the vW NAKE per

particle in the region dominated by one orbital. We proposed the covalent approximation based on this exact behavior by mixing the vW and TF functionals with the mixing factor determined by a switching function $Q_f(\mathbf{r})$ of the spatial coordinate to determine different types of regions. We provided three carefully chosen $Q_f(\mathbf{r})$ that satisfies two out of the three exact requirements. Covalent approximation also uses a mixture of the two treatments handling fractional spins: ENS and FOO, to obtain the exact behavior of FOO for stretched bonds and the similar accuracy of ENS near the equilibrium bond length. We tested covalent approximation with a few dimers with covalent bonds. It reproduces the exact NAKE for stretched bonds, and near the equilibrium, it outperforms existing decomposable approximations for alkali dimers. We also demonstrated the potential to solve the delocalization and static-correlation errors with efficient P-DFT calculations by combining the covalent approximation with the overlap approximation.

Future work includes improving the behavior of the covalent approximation near the equilibrium bond length. One possibility is to enforce the uniform gas limit to the switching function. Another direction is to replace TF with a better approximation in the core regions.

8. VIRIAL RELATIONS IN P-DFT

8.1 Derivation of the Virial Relations

The Virial theorem provides the relationship between the kinetic and the potential energy for a given system. It is considered to be one of the most powerful quantum-mechanical theorems. Research has been done in regards to the Virial relations for KS-DFT [87–89], which gives us insights into the relations between the KE, non-interacting KE, and KS potentials. In this section, we will derive two Virial relations for P-DFT.

In classical mechanics, the Virial theorem for a time-independent system with N particles can be written as:

$$2\sum_{i=1}^{N} K_i = -\sum_{i=1}^{N} \mathbf{F}_i \cdot \mathbf{r}_i, \tag{8.1}$$

where K_i is the kinetic energy and $\mathbf{F}_i$ is total force on the ith particle. For a system of interacting electrons at ground state with density $n(\mathbf{r})$, Eq. 8.1 becomes

$$2K = \int \mathrm{d}^3 r\, n(\mathbf{r})\mathbf{r} \cdot \nabla v_{\mathrm{tot}}(\mathbf{r}), \tag{8.2}$$

or

$$2K + V_{\mathrm{ee}} = \int \mathrm{d}^3 r\, n(\mathbf{r})\mathbf{r} \cdot \nabla v(\mathbf{r}), \tag{8.3}$$

where $K = \langle \Psi | \hat{T} | \Psi \rangle$ is the kinetic energy of the system.

Similarly, for a KS system with non-interacting electrons, in which $V_{\mathrm{ee}} = 0$, we can replace the kinetic energy of Eq. 8.3 with the non-interacting KE and the external potential $v(\mathbf{r})$ with the KS potential, to obtain the Virial relation of KS systems

$$2T_{\mathrm{S}} = \int \mathrm{d}^3 r\, n(\mathbf{r})\mathbf{r} \cdot \nabla v_{\mathrm{S}}(\mathbf{r}). \tag{8.4}$$

This virial relation not only works for exact functionals, but also for approximated XC functionals as long as the self-consistency is reached.

The many-electron wavefunctions of the fragment ensembles satisfy the Shrödinger equation:

$$\left[\hat{H}_\alpha + \int \mathrm{d}^3r\, v_\mathrm{p}(\mathbf{r})\hat{n}(\mathbf{r})\right] |\psi_{j\alpha}\rangle = E_{j\alpha}\, |\psi_{j\alpha}\rangle\,, \tag{8.5}$$

where $\hat{H}_\alpha = \hat{T} + \hat{V}_\mathrm{ee} + \int \mathrm{d}^3r\, v_\alpha(\mathbf{r})\hat{n}(\mathbf{r})$. The Virial relations for the fragments can be obtained by averaging the ensembles weighted by the ensemble coefficients

$$2K_\alpha + V_{\mathrm{ee},\alpha} = \int \mathrm{d}^3r\, n_\alpha(\mathbf{r})\mathbf{r}\cdot\nabla[v_\alpha(\mathbf{r}) + v_\mathrm{p}(\mathbf{r})], \tag{8.6}$$

where $K_\alpha = \sum_j f_{j\alpha}\, \langle\psi_{j\alpha}|\, \hat{T}\, |\psi_{j\alpha}\rangle$ and $V_{\mathrm{ee},\alpha} = \sum_j f_{j\alpha}\, \langle\psi_{j\alpha}|\, \hat{V}_\mathrm{ee}\, |\psi_{j\alpha}\rangle$. Similar procedure can be done to the KS fragments to obtain the following relation

$$2T_{\mathrm{s},\alpha} = \int \mathrm{d}^3r\, n_\alpha(\mathbf{r})\mathbf{r}\cdot\nabla[v_{\mathrm{s},\alpha}(\mathbf{r}) + v_\mathrm{p}(\mathbf{r})]. \tag{8.7}$$

Subtract Eq. 8.7 from Eq. 8.6 we get

$$T_{\mathrm{c},\alpha} = -E_{\mathrm{XC},\alpha} - \int \mathrm{d}^3r\, n_\alpha(\mathbf{r})\mathbf{r}\cdot\nabla v_{\mathrm{XC},\alpha}(\mathbf{r}), \tag{8.8}$$

where $T_{\mathrm{c},\alpha} = K_\alpha - T_{\mathrm{S},\alpha}$ is the correlation KE of fragment α [87].

If we sum up Eq. 8.6 over all fragments, we get

$$2K_\mathrm{f} + V_{\mathrm{ee,f}} = \sum_\alpha \int \mathrm{d}^3r\, n_\alpha(\mathbf{r})\mathbf{r}\cdot\nabla[v_\alpha(\mathbf{r}) + v_\mathrm{p}(\mathbf{r})], \tag{8.9}$$

where $K_\mathrm{f} = \sum_\alpha K_\alpha$ and $V_{\mathrm{ee,f}} = \sum_\alpha V_{\mathrm{ee},\alpha}$. Combining Eq. 8.3 and Eq. 8.9 and rearrange terms we obtain the Virial relations for P-DFT

$$\begin{aligned} K^\mathrm{nad} &= V_\mathrm{ext}^\mathrm{nad}[n] + \sum_\alpha \int \mathrm{d}^3r\, n_\alpha(\mathbf{r})\mathbf{r}\cdot\nabla v_{\mathrm{ext},\alpha}^\mathrm{r}(\mathbf{r}) \\ &\quad -E_\mathrm{p}[n] - \int \mathrm{d}^3r\, n(\mathbf{r})\mathbf{r}\cdot\nabla v_\mathrm{p}(\mathbf{r}), \end{aligned} \tag{8.10}$$

where $V_\mathrm{ext}^\mathrm{nad}[n]$ is the non-additive external energy defined by Eq. 3.26, $v_{\mathrm{ext},\alpha}^\mathrm{nad}(\mathbf{r}) = \frac{\delta V_\mathrm{ext}^\mathrm{nad}}{\delta n_\alpha(\mathbf{r})} = v(\mathbf{r}) - v_\alpha(\mathbf{r})$, and $K^\mathrm{nad} = K - K_\mathrm{f}$ is the non-additive KE.

Eq. 8.10 gives the expression of the non-additive KE in terms of the quantities that can be obtained through P-DFT calculations. It can also be used to verify if the result from a P-DFT calculation is correct.

K^{nad} can also be constructed with the NAKE and the non-additive correlation KE $T_{\mathrm{c}}^{\mathrm{nad}}$

$$K^{\mathrm{nad}} = T_{\mathrm{S}}^{\mathrm{nad}} + T_{\mathrm{c}}^{\mathrm{nad}}, \tag{8.11}$$

where $T_{\mathrm{c}}^{\mathrm{nad}} = T_{\mathrm{c}} - \sum_{\alpha} T_{\mathrm{c},\alpha}$.

Alternatively, we can obtain a different Virial relation for P-DFT by subtracting Eq. 8.7 from Eq. 8.4

$$2T_{\mathrm{S}}^{\mathrm{nad}} = \int \mathrm{d}^3 r \left\{ n(\mathbf{r})\mathbf{r} \cdot \nabla[v_{\mathrm{S}}(\mathbf{r}) - v_{\mathrm{p}}(\mathbf{r})] - \sum_{\alpha} n_{\alpha}(\mathbf{r})\mathbf{r} \cdot \nabla v_{\mathrm{s},\alpha}(\mathbf{r}) \right\}. \tag{8.12}$$

Eq. 8.12 gives an alternative way to obtain the NAKE in P-DFT calculations.

8.2 Numerical Verification

Table 8.1 shows the well match between the non-additive KE $K_{\mathrm{I}}^{\mathrm{nad}}$ which is calculated through wavefunctions for H_2^+ and through Eq. 8.11 for other systems, and $K_{\mathrm{II}}^{\mathrm{nad}}$ calculated through the Virial relation Eq.8.10. The main source of the error comes from taking the gradient of the potentials, which contains cusps and singularities.

Table 8.2 shows the similar result for the NAKE, where $T_{\mathrm{s,I}}^{\mathrm{nad}}$ is obtained from the inversion method and $T_{\mathrm{s,II}}^{\mathrm{nad}}$ is calculated through the Virial relation Eq. 8.12. Again, the Virial relation is well preserved for all systems.

Table 8.3 shows the comparison in the NAKE of He_2 when approximated functionals for the NAKE are used. The calculations are done self-consistently and the difference in $T_{\mathrm{s,II}}^{\mathrm{nad}}$ compared to the exact result mainly comes from the NAKP, a component of the partition potential, is calculated using the approximated NAKE functional as well. For most approximated NAKE functionals, the Virial relation Eq. 8.12 is not well preserved. This is expected because the fragment non-interacting KE calculated from the approximated functionals is different from that computed using the fragment orbitals, so the left-hand side and the right-hand side of Eq. 8.7 do not match when the approximated functionals are used for the left-hand side. Interestingly, vW, the worst NAKE approximation for He_2, yields the accurate Virial

Table 8.1.
Comparison in the non-additive KE. Exact XC functional and partition potential are used for H_2^+ and LDA XC functional is used for all other systems. $K_{\rm I}^{\rm nad}$ is calculated from the wavefunctions for H_2^+ and from Eq. 8.11 for the rest of the systems. $K_{\rm II}^{\rm nad}$ is calculated using Eq. 8.10.

System	$K_{\rm I}^{\rm nad}$	$K_{\rm II}^{\rm nad}$	$K_{\rm I}^{\rm nad}/K_{\rm II}^{\rm nad}$
H_2^+	$-8.522\,33\times10^{-2}$	$-8.529\,64\times10^{-2}$	0.999 14
H_2	$-1.257\,07\times10^{-1}$	$-1.257\,16\times10^{-1}$	0.999 93
Li_2	$1.716\,12\times10^{-2}$	$1.695\,15\times10^{-2}$	1.012 37
He_2	$1.107\,03\times10^{-3}$	$1.106\,75\times10^{-3}$	1.000 25
Ne_2	$2.999\,46\times10^{-3}$	$2.988\,51\times10^{-3}$	1.003 66
Ar_2	$4.423\,86\times10^{-3}$	$4.405\,50\times10^{-3}$	1.004 17

Table 8.2.
Comparison in the NAKE. LDA is used as the XC functional. $T_{\rm s,I}^{\rm nad}$ is obtained from the inversion method. $T_{\rm s,II}^{\rm nad}$ is calculated using Eq. 8.12.

System	$T_{\rm s,I}^{\rm nad}$	$T_{\rm s,II}^{\rm nad}$	$T_{\rm s,I}^{\rm nad}/T_{\rm s,II}^{\rm nad}$
H_2	$-1.520\,69\times10^{-1}$	$-1.520\,73\times10^{-1}$	0.999 97
Li_2	$4.916\,58\times10^{-3}$	$4.899\,30\times10^{-3}$	1.003 53
He_2	$9.930\,00\times10^{-4}$	$9.930\,00\times10^{-4}$	1.000 14
Ne_2	$2.749\,80\times10^{-3}$	$2.743\,24\times10^{-3}$	1.002 39
Ar_2	$4.050\,44\times10^{-3}$	$4.040\,77\times10^{-3}$	1.002 39

relation. This means although a good Virial relation is required for an accurate NAKE approximation, having an accurate Virial relation does not necessarily mean the NAKE approximation is good. TF has the best Virial relation for the rest of the approximations, with R-PBE following not far behind.

Table 8.3.
Comparison in the NAKE of He_2 when approximated functionals are used. LDA is used as the XC functional. $T_{s,I}^{nad}$ is calculated directly from the approximated functionals. $T_{s,II}^{nad}$ is calculated using Eq. 8.12, where the approximated NAKE functionals are used in calculating the partition potential.

Functional	$T_{s,I}^{nad}$	$T_{s,II}^{nad}$	$T_{s,I}^{nad}/T_{s,II}^{nad}$
TF	$1.197\,88 \times 10^{-3}$	$1.402\,35 \times 10^{-3}$	0.854 19
vW	$-3.782\,34 \times 10^{-2}$	$-3.782\,37 \times 10^{-2}$	0.999 99
GEA2	$-1.560\,68 \times 10^{-3}$	$-1.146\,27 \times 10^{-3}$	1.361 54
TW02I	$1.135\,78 \times 10^{-3}$	$1.444\,03 \times 10^{-3}$	0.786 54
LC94	$5.653\,53 \times 10^{-4}$	$8.119\,41 \times 10^{-4}$	0.696 30
R-PBE	$9.951\,43 \times 10^{-4}$	$1.195\,87 \times 10^{-3}$	0.832 15

9. SUMMARY

P-DFT is a computational method that potentially has better computational efficiency than standard KS-DFT and showed some success in solving delocalization and state-correlation errors. In this dissertation, we developed the formalism of the P-DFT with spin-polarized fragment densities. We focused on explicit functional approximations of the NAKE, which are required for efficient P-DFT calculations. The uniqueness of the NAKE in P-DFT makes the study of the exact behavior of the NAKE and the development of general approximations easier.

Two types of systems were used to study the NAKE in this dissertation, the weakly-interacting rare-gas dimers and the covalent bonds. The fragment-fragment interactions of these systems are very different, so by studying them, we can get a more general idea of the behavior of the NAKE. Unfortunately, similar to the approximations to the non-interacting KE, approximations to the NAKE also lack transferability as no approximation yields accurate NAKE for both types of systems. This makes designing approximations to the NAKE a huge challenge.

Besides that, the decomposable approximations constructed from the approximations to the non-interacting KE typically behave worse than non-decomposable approximations designed to approximate the NAKE. This is expected because the former is optimized for the non-interacting KE while the latter is optimized for the NAKE. We showed that the decomposable approximations yield terrible NAKE for covalent bonds, with most of them worse than setting NAKE to 0. These facts indicate that developing non-decomposable approximations to the NAKE is necessary.

In this dissertation, we proposed three new approximations to the NAKE: R-PBE, which uses PBE enhancement factor but re-parameterized with a set of NAKE data of rare-gas dimers, greatly improved the binding behavior for rare-gas dimers; 2OA, a physically motivated approximation designed for two-orbital systems, yields accurate

asymptotic behavior for rare-gas dimers; the covalent approximation, inspired from the accurate behavior of the vW functional in regions dominated by one orbital, shows accurate binding energy for stretched alkali dimers.

We also derived two Virial relations for P-DFT. Numerical calculations verified both relations, even when the partition potential is calculated with approximations to the XC energy. However, the relation regarding the NAKE is not preserved when approximations to the NAKE are used, except for the case of vW. The Virial relations can be used as an exact constraint in designing better approximations to the NAKE.

REFERENCES

[1] W. Kohn and L. J. Sham. Self-Consistent Equations Including Exchange and Correlation Effects. *Physical Review*, 140(4A):A1133–A1138, 1965.

[2] Morrel H. Cohen and Adam Wasserman. On the Foundations of Chemical Reactivity Theory. *The Journal of Physical Chemistry A*, 111(11):2229–2242, 2007.

[3] Peter Elliott, Kieron Burke, Morrel H. Cohen, and Adam Wasserman. Partition density-functional theory. *Physical Review A*, 82(2):024501, 2010.

[4] Jonathan Nafziger and Adam Wasserman. Density-Based Partitioning Methods for Ground-State Molecular Calculations. *The Journal of Physical Chemistry A*, 118(36):7623–7639, 2014.

[5] Samuel Fux, Christoph R. Jacob, Johannes Neugebauer, Lucas Visscher, and Markus Reiher. Accurate frozen-density embedding potentials as a first step towards a subsystem description of covalent bonds. *The Journal of Chemical Physics*, 132(16):164101, 2010.

[6] Jason D. Goodpaster, Nandini Ananth, Frederick R. Manby, and Thomas F. Miller III. Exact nonadditive kinetic potentials for embedded density functional theory. *The Journal of Chemical Physics*, 133(8):084103, 2010.

[7] C. Huang, M. Pavone, and E. A. Carter. Quantum mechanical embedding theory based on a unique embedding potential. *The Journal of Chemical Physics*, 134(15):154110, 2011.

[8] Jonathan Nafziger, Qin Wu, and Adam Wasserman. Molecular binding energies from partition density functional theory. *The Journal of Chemical Physics*, 135(23):234101, 2011.

[9] Jonathan Nafziger, Kaili Jiang, and Adam Wasserman. Accurate reference data for the nonadditive, noninteracting kinetic energy in covalent bonds. *Journal of Chemical Theory and Computation*, 13(2):577–586, 2017.

[10] Daniel S. Jensen and Adam Wasserman. Numerical methods for the inverse problem of density functional theory. *International Journal of Quantum Chemistry*, pages e25425–n/a, 2017.

[11] Yan Alexander Wang and Emily A Carter. Orbital-free kinetic-energy density functional theory. In *Theoretical methods in condensed phase chemistry*, pages 117–184. Springer, 2002.

[12] Adam Wasserman, Jonathan Nafziger, Kaili Jiang, Min-Cheol Kim, Eunji Sim, and Kieron Burke. The importance of being inconsistent. *Annual Review of Physical Chemistry*, 68:555–581, 2017.

[13] Kaili Jiang, Jonathan Nafziger, and Adam Wasserman. Non-additive non-interacting kinetic energy of rare gas dimers. *The Journal of Chemical Physics*, 148(10):104113, 2018.

[14] P. Hohenberg and W. Kohn. Inhomogeneous Electron Gas. *Physical Review*, 136(3B):B864–B871, 1964.

[15] Klaus Capelle. A bird's-eye view of density-functional theory. *Brazilian Journal of Physics*, 36(4A):1318–1343, 2006.

[16] TL Gilbert. Hohenberg-kohn theorem for nonlocal external potentials. *Physical Review B*, 12(6):2111, 1975.

[17] Walter Kohn. v-representability and density functional theory. *Physical Review Letters*, 51(17):1596, 1983.

[18] Mel Levy. Electron densities in search of hamiltonians. *Physical Review A*, 26(3):1200, 1982.

[19] Elliott H Lieb. Density functionals for coulomb systems. *International Journal of Quantum Chemistry*, 24(3):243–277, 1983.

[20] Roy G Gordon and Yung Sik Kim. Theory for the forces between closed-shell atoms and molecules. *The Journal of Chemical Physics*, 56(6):3122–3133, 1972.

[21] Gaetano Senatore and KR Subbaswamy. Density dependence of the dielectric constant of rare-gas crystals. *Physical Review B*, 34(8):5754, 1986.

[22] Pietro Cortona. Self-consistently determined properties of solids without band-structure calculations. *Physical Review B*, 44(16):8454, 1991.

[23] T. A. Wesołowski and A. Warshel. Frozen density functional approach for ab initio calculations of solvated molecules. *The Journal of Physical Chemistry*, 97(30):8050–8053, 1993.

[24] Tomasz Adam Wesolowski and Jacques Weber. Kohn-sham equations with constrained electron density: an iterative evaluation of the ground-state electron density of interacting molecules. *Chemical Physics Letters*, 248(1-2):71–76, 1996.

[25] Johannes Neugebauer. Chromophore-specific theoretical spectroscopy: From subsystem density functional theory to mode-specific vibrational spectroscopy. *Physics Reports*, 489(1-3):1–87, 2010.

[26] Eduardo Fabiano, Savio Laricchia, and Fabio Della Sala. Frozen density embedding with non-integer subsystems particle numbers. *The Journal of Chemical Physics*, 140(11):114101, 2014.

[27] John P. Perdew, Robert G. Parr, Mel Levy, and Jose L. Balduz. Density-Functional Theory for Fractional Particle Number: Derivative Discontinuities of the Energy. *Physical Review Letters*, 49(23):1691–1694, 1982.

[28] Aron J. Cohen, Paula Mori-Sánchez, and Weitao Yang. Fractional spins and static correlation error in density functional theory. *The Journal of Chemical Physics*, 129(12):121104, 2008.

[29] Morrel H. Cohen and Adam Wasserman. On Hardness and Electronegativity Equalization in Chemical Reactivity Theory. *Journal of Statistical Physics*, 125(5-6):1121–1139, 2006.

[30] Martín A. Mosquera and Adam Wasserman. Partition density functional theory and its extension to the spin-polarized case. *Molecular Physics*, 111(4):505–515, 2013.

[31] Jonathan Nafziger. *Partition density functional theory*. PhD thesis, Purdue University, 2015.

[32] Christoph R. Jacob and Johannes Neugebauer. Subsystem density-functional theory. *Wiley Interdisciplinary Reviews: Computational Molecular Science*, 4(4):325–362, 2014.

[33] Frederick R Manby, Martina Stella, Jason D Goodpaster, and Thomas F Miller III. A simple, exact density-functional-theory embedding scheme. *Journal of Chemical Theory and Computation*, 8(8):2564–2568, 2012.

[34] Eunji Sim, Joe Larkin, Kieron Burke, and Charles W. Bock. Testing the kinetic energy functional: Kinetic energy density as a density functional. *The Journal of Chemical Physics*, 118(18):8140–8148, 2003.

[35] Mojdeh Banafsheh and Tomasz Wesolowski. Nonadditive kinetic potentials from inverted Kohn–Sham problem. *International Journal of Quantum Chemistry*, 2017.

[36] Andreas W. Götz, S. Maya Beyhan, and Lucas Visscher. Performance of Kinetic Energy Functionals for Interaction Energies in a Subsystem Formulation of Density Functional Theory. *Journal of Chemical Theory and Computation*, 5(12):3161–3174, 2009.

[37] T. A. Wesołowski and A. Savin. Non-Additive Kinetic Energy and Potential in Analytically Solvable Systems and Their Approximated Counterparts. *Recent Progress in Orbital-free Density Functional Theory*, 6:275, 2013.

[38] Alex Borgoo, Andrew M. Teale, and David J. Tozer. Revisiting the density scaling of the non-interacting kinetic energy. *Physical Chemistry Chemical Physics*, 16(28):14578–14583, 2014.

[39] Christoph R. Jacob, S. Maya Beyhan, and Lucas Visscher. Exact functional derivative of the nonadditive kinetic-energy bifunctional in the long-distance limit. *The Journal of Chemical Physics*, 126(23):234116, 2007.

[40] Qin Wu and Weitao Yang. A direct optimization method for calculating density functionals and exchange–correlation potentials from electron densities. *The Journal of Chemical Physics*, 118(6):2498–2509, 2003.

[41] L. H. Thomas. The calculation of atomic fields. *Mathematical Proceedings of the Cambridge Philosophical Society*, 23(5):542–548, 1926.

[42] Enrico Fermi. Un metodo statistico per la determinazione di alcune priorieta dell'atome. *Rendiconti. Accademia Nazionale dei Lincei*, 6(602-607):32, 1927.

[43] C. F. v Weizsäcker. Zur theorie der kernmassen. *Zeitschrift Für Physik a Hadrons and Nuclei*, 96(7):431–458, 1935.

[44] F. Tran and T. A. Wesołowski. Semilocal approximations for the kinetic energy. *Recent Progress in Orbital-free Density Functional Theory*, pages 429–442, 2013.

[45] Eduardo V Ludeña and Valentin V Karasiev. Kinetic energy functionals: History, challenges, and prospects. *Reviews of Modern Quantum Chemistry*, 1, 2002.

[46] A. S. Kompaneets and E. S. Pavlovsky. Self-consistent equations for atoms. *Journal of Experimental and Theoretical Physics*, 31:427, 1956.

[47] D. A. Kirzhnits. Quantum corrections to the thomas-fermi equation. *Journal of Experimental and Theoretical Physics*, 5, 1957.

[48] Sidney Golden. Statistical theory of many-electron systems. general considerations pertaining to the thomas-fermi theory. *Physical Review*, 105:604–615, 1957.

[49] Katsumi Yonei and Yasuo Tomishima. On the weizsäcker correction to the Thomas-Fermi theory of the atom. *Journal of the Physical Society of Japan*, 20(6):1051–1057, 1965.

[50] R. Baltin. The energy-density functional of an electron gas in locally linear approximation of the one-body potential. *Zeitschrift Für Naturforschung A*, 27(8-9):1176–1186, 1972.

[51] Elliott H. Lieb. Thomas-fermi and related theories of atoms and molecules. *Reviews of Modern Physics*, 53(4):603–641, 1981.

[52] N. H. March and R. Santamaria. Non-local relation between kinetic and exchange energy densities in hartree–fock theory. *International Journal of Quantum Chemistry*, 39(4):585–592, 1991.

[53] Hsing Lee, Chengteh Lee, and Robert G. Parr. Conjoint gradient correction to the Hartree-Fock kinetic- and exchange-energy density functionals. *Physical Review A*, 44(1):768–771, 1991.

[54] John P. Perdew, Kieron Burke, and Matthias Ernzerhof. Generalized Gradient Approximation Made Simple. *Physical Review Letters*, 77(18):3865–3868, 1996.

[55] Fabien Tran and Tomasz A. Wesołowski. Link between the kinetic- and exchange-energy functionals in the generalized gradient approximation. *International Journal of Quantum Chemistry*, 89(5):441–446, 2002.

[56] Lucian A. Constantin, E. Fabiano, S. Laricchia, and F. Della Sala. Semiclassical Neutral Atom as a Reference System in Density Functional Theory. *Physical Review Letters*, 106(18):186406, 2011.

[57] S. Laricchia, E. Fabiano, L. A. Constantin, and F. Della Sala. Generalized Gradient Approximations of the Noninteracting Kinetic Energy from the Semiclassical Atom Theory: Rationalization of the Accuracy of the Frozen Density Embedding Theory for Nonbonded Interactions. *Journal of Chemical Theory and Computation*, 7(8):2439–2451, 2011.

[58] P. Fuentealba and O. Reyes. Further evidence of the conjoint correction to the local kinetic and exchange energy density functionals. *Chemical Physics Letters*, 232(1):31–34, 1995.

[59] A. D. Becke. Density-functional exchange-energy approximation with correct asymptotic behavior. *Physical Review A*, 38:3098–3100, 1988.

[60] Ajit J. Thakkar. Comparison of kinetic-energy density functionals. *Physical Review A*, 46(11):6920–6924, 1992.

[61] A. Lembarki and H. Chermette. Obtaining a gradient-corrected kinetic-energy functional from the Perdew-Wang exchange functional. *Physical Review A*, 50(6):5328–5331, 1994.

[62] Chengteh Lee and Robert G. Parr. Gaussian and other approximations to the first-order density matrix of electronic systems, and the derivation of various local-density-functional theories. *Physical Review A*, 35(6):2377–2383, 1987.

[63] Hui Ou-Yang and Mel Levy. Approximate noninteracting kinetic energy functionals from a nonuniform scaling requirement. *International Journal of Quantum Chemistry*, 40(3):379–388, 1991.

[64] Erik William Pearson. *THEORY AND APPLICATION OF THE ELECTRON GAS MODEL.* PhD thesis, Harvard Univeristy, 1983.

[65] Erik W. Pearson and Roy G. Gordon. Local asymptotic gradient corrections to the energy functional of an electron gas. *The Journal of Chemical Physics*, 82(2):881–889, 1985.

[66] Daniel J. Lacks and Roy G. Gordon. Tests of nonlocal kinetic energy functionals. *The Journal of Chemical Physics*, 100(6):4446–4452, 1994.

[67] John P. Perdew. Generalized gradient approximation for the fermion kinetic energy as a functional of the density. *Physics Letters A*, 165(1):79–82, 1992.

[68] L. Vitos, H. L. Skriver, and J. Kollár. Kinetic-energy functionals studied by surface calculations. *Physical Review B*, 57(19):12611–12615, 1998.

[69] L. Vitos, B. Johansson, J. Kollár, and H. L. Skriver. Local kinetic-energy density of the Airy gas. *Physical Review A*, 61(5):052511, 2000.

[70] M. Ernzerhof. The role of the kinetic energy density in approximations to the exchange energy. *Journal of Molecular Structure: THEOCHEM*, 501502:59–64, 2000.

[71] A. D. Becke. Numerical Hartree–Fock–Slater calculations on diatomic molecules. *The Journal of Chemical Physics*, 76(12):6037–6045, 1982.

[72] Leif Laaksonen, Pekka Pyykkö, and Dage Sundholm. Two-dimensional fully numerical solutions of molecular Schrödinger equations. I. One-electron molecules. *International Journal of Quantum Chemistry*, 23(1):309–317, 1983.

[73] Jacek Kobus, Leif Laaksonen, and Dage Sundholm. A numerical Hartree-Fock program for diatomic molecules. *Computer Physics Communications*, 98(3):346–358, 1996.

[74] T. Grabo, T. Kreibich, and E. K. U. Gross. Optimized Effective Potential for Atoms and Molecules. *Molecular Engineering*, 7(1-2):27–50, 1997.

[75] Adi Makmal, Stephan Kümmel, and Leeor Kronik. Fully Numerical All-Electron Solutions of the Optimized Effective Potential Equation for Diatomic Molecules. *Journal of Chemical Theory and Computation*, 5(7):1731–1740, 2009.

[76] Miguel AL Marques, Micael JT Oliveira, and Tobias Burnus. Libxc: A library of exchange and correlation functionals for density functional theory. *Computer Physics Communications*, 183(10):2272–2281, 2012.

[77] Susi Lehtola, Conrad Steigemann, Micael JT Oliveira, and Miguel AL Marques. Recent developments in libxc—a comprehensive library of functionals for density functional theory. *SoftwareX*, 7:1–5, 2018.

[78] M. Valiev, E.J. Bylaska, N. Govind, K. Kowalski, T.P. Straatsma, H.J.J. Van Dam, D. Wang, J. Nieplocha, E. Apra, T.L. Windus, and W.A. de Jong. Nwchem: A comprehensive and scalable open-source solution for large scale molecular simulations. *Computer Physics Communications*, 181(9):1477–1489, 2010.

[79] W. Koch and M. C. Holthausen. *A chemist's guide to density functional theory*. John Wiley & Sons, 2015.

[80] David C Langreth, Max Dion, Henrik Rydberg, Elsebeth Schröder, Per Hyldgaard, and Bengt I Lundqvist. Van der waals density functional theory with applications. *International Journal of Quantum Chemistry*, 101(5):599–610, 2005.

[81] Oleg A Vydrov and Troy Van Voorhis. Nonlocal van der waals density functional: The simpler the better. *The Journal of Chemical Physics*, 133(24):244103, 2010.

[82] Fabien Tran and Tomasz A. Wesołowski. Introduction of the explicit long-range nonlocality as an alternative to the gradient expansion approximation for the kinetic-energy functional. *Chemical Physics Letters*, 360(34):209–216, 2002.

[83] Aron J Cohen, Paula Mori-Sánchez, and Weitao Yang. Insights into current limitations of density functional theory. *Science*, 321(5890):792–794, 2008.

[84] Jianwei Sun, Bing Xiao, Yuan Fang, Robin Haunschild, Pan Hao, Adrienn Ruzsinszky, Gábor I Csonka, Gustavo E Scuseria, and John P Perdew. Density functionals that recognize covalent, metallic, and weak bonds. *Physical Review Letters*, 111(10):106401, 2013.

[85] Juan Maria Garcia Lastra, Jakub W. Kaminski, and Tomasz A. Wesolowski. Orbital-free effective embedding potential at nuclear cusps. *The Journal of Chemical Physics*, 129(7):074107, 2008.

[86] Jonathan Nafziger and Adam Wasserman. Fragment-based treatment of delocalization and static correlation errors in density-functional theory. *The Journal of Chemical Physics*, 143(23):234105, 2015.

[87] Mel Levy and John P. Perdew. Hellmann-feynman, virial, and scaling requisites for the exact universal density functionals. shape of the correlation potential and diamagnetic susceptibility for atoms. *Physical Review A*, 32:2010–2021, 1985.

[88] SK Ghosh and Vijay A Singh. Energy theorems in constrained density-functional theory. *Journal of Physics: Condensed Matter*, 1(11):1971, 1989.

[89] Juan I. Rodríguez, Paul W. Ayers, Andreas W. Götz, and F. L. Castillo-Alvarado. Virial theorem in the Kohn–Sham density-functional theory formalism: Accurate calculation of the atomic quantum theory of atoms in molecules energies. *The Journal of Chemical Physics*, 131(2):021101, 2009.

A. SUPPLEMENTARY MATERIALS

Table A.1.: The error in the NAKE in Ha of various KE functionals at LDA equilibrium for He_2, Ne_2, and Ar_2. For each system, the best result is in boldface and the worst is in italics.

Functional	He_2	Ne_2	Ar_2
$T_S^{nad} = 0$	-9.929×10^{-4}	-2.750×10^{-3}	-4.050×10^{-3}
TF	2.049×10^{-4}	1.527×10^{-3}	7.250×10^{-4}
vW	*-3.882×10^{-2}*	*-7.857×10^{-2}*	*-8.139×10^{-2}*
TFvW	-3.448×10^{-2}	-6.591×10^{-2}	-6.649×10^{-2}
GEA2	-2.554×10^{-3}	-3.885×10^{-3}	-4.806×10^{-3}
Golden	-7.526×10^{-3}	-1.362×10^{-2}	-1.469×10^{-2}
YT65	-4.953×10^{-3}	-8.588×10^{-3}	-9.588×10^{-3}
Baltin	-1.630×10^{-2}	-3.074×10^{-2}	-3.185×10^{-2}
Lieb	-4.561×10^{-3}	-7.820×10^{-3}	-8.809×10^{-3}
R-PBE	$\mathbf{2.206 \times 10^{-6}}$	6.267×10^{-4}	2.600×10^{-4}
revAPBEKint	-5.027×10^{-5}	6.394×10^{-4}	-6.547×10^{-4}
APBEKint	1.353×10^{-4}	1.148×10^{-3}	-2.377×10^{-5}
revAPBEK	-2.446×10^{-5}	7.142×10^{-4}	-5.628×10^{-4}
APBEK	1.551×10^{-4}	1.209×10^{-3}	5.637×10^{-5}
TW02I	1.429×10^{-4}	1.178×10^{-3}	2.080×10^{-5}
TW02II	2.005×10^{-4}	1.347×10^{-3}	2.461×10^{-4}
TW02III	1.321×10^{-4}	1.148×10^{-3}	$\mathbf{-1.615 \times 10^{-5}}$
TW02IV	1.251×10^{-4}	1.128×10^{-3}	-4.019×10^{-5}

continued on next page

Table A.1.: *continued*

Functional	He_2	Ne_2	Ar_2
LLP	-2.362×10^{-4}	4.397×10^{-4}	-6.508×10^{-4}
FR(B88)	-2.055×10^{-4}	5.109×10^{-4}	-5.720×10^{-4}
T92	-3.764×10^{-4}	7.418×10^{-5}	-1.112×10^{-3}
LC94	-4.276×10^{-4}	$\mathbf{4.412 \times 10^{-6}}$	-1.125×10^{-3}
FR(PW86)	6.607×10^{-5}	1.098×10^{-3}	3.809×10^{-5}
LP	2.433×10^{-4}	1.647×10^{-3}	8.716×10^{-4}
OL1	-1.514×10^{-3}	-1.848×10^{-3}	-2.735×10^{-3}
OL2	-2.553×10^{-3}	-3.883×10^{-3}	-4.804×10^{-3}
P82	2.973×10^{-4}	1.818×10^{-3}	1.139×10^{-3}
P92	3.578×10^{-4}	2.055×10^{-3}	1.563×10^{-3}
VSK98	-2.912×10^{-2}	-5.025×10^{-2}	-4.787×10^{-2}
VJKS00	1.013×10^{-2}	1.934×10^{-2}	1.699×10^{-2}
E00	-1.260×10^{-2}	-1.957×10^{-2}	-1.832×10^{-2}

Table A.2.: The error in the NAKE in Ha of various KE functionals at LDA equilibrium for HeNe, HeAr, and NeAr. For each system, the best result is in boldface and the worst is in italics.

Functional	HeNe	HeAr	NeAr
$T_{\mathrm{S}}^{\mathrm{nad}} = 0$	-1.845×10^{-3}	-1.802×10^{-3}	-3.152×10^{-3}
TF	1.057×10^{-3}	3.683×10^{-4}	1.054×10^{-3}
vW	*-5.862×10^{-2}*	*-5.338×10^{-2}*	*-7.917×10^{-2}*
TFvW	-5.034×10^{-2}	-4.572×10^{-2}	-6.520×10^{-2}
GEA2	-3.069×10^{-3}	-3.322×10^{-3}	-4.246×10^{-3}

continued on next page

Table A.2.: *continued*

Functional	HeNe	HeAr	NeAr
Golden	-1.049×10^{-2}	-9.965×10^{-3}	-1.380×10^{-2}
YT65	-6.653×10^{-3}	-6.529×10^{-3}	-8.855×10^{-3}
Baltin	-2.353×10^{-2}	-2.165×10^{-2}	-3.060×10^{-2}
Lieb	-6.068×10^{-3}	-6.006×10^{-3}	-8.103×10^{-3}
R-PBE	2.556×10^{-4}	$\mathbf{8.108 \times 10^{-5}}$	6.251×10^{-4}
revAPBEKint	4.926×10^{-4}	-1.749×10^{-4}	6.305×10^{-5}
APBEKint	8.411×10^{-4}	1.434×10^{-4}	5.909×10^{-4}
revAPBEK	5.429×10^{-4}	-1.289×10^{-4}	1.424×10^{-4}
APBEK	8.812×10^{-4}	1.807×10^{-4}	6.573×10^{-4}
TW02I	8.591×10^{-4}	1.608×10^{-4}	6.254×10^{-4}
TW02II	9.727×10^{-4}	2.662×10^{-4}	8.056×10^{-4}
TW02III	8.388×10^{-4}	1.423×10^{-4}	5.945×10^{-4}
TW02IV	8.255×10^{-4}	1.301×10^{-4}	5.744×10^{-4}
LLP	2.915×10^{-4}	-3.353×10^{-4}	-7.291×10^{-5}
FR(B88)	3.429×10^{-4}	-2.892×10^{-4}	$\mathbf{-1.301 \times 10^{-6}}$
T92	4.031×10^{-5}	-5.651×10^{-4}	-4.573×10^{-4}
LC94	$\mathbf{-2.455 \times 10^{-5}}$	-6.178×10^{-4}	-5.070×10^{-4}
FR(PW86)	7.790×10^{-4}	9.946×10^{-5}	5.751×10^{-4}
LP	1.134×10^{-3}	4.366×10^{-4}	1.185×10^{-3}
OL1	-1.516×10^{-3}	-1.933×10^{-3}	-2.252×10^{-3}
OL2	-3.068×10^{-3}	-3.321×10^{-3}	-4.244×10^{-3}
P82	1.248×10^{-3}	5.516×10^{-4}	1.385×10^{-3}
P92	1.396×10^{-3}	6.957×10^{-4}	1.646×10^{-3}
VSK98	-3.965×10^{-2}	-3.629×10^{-2}	-4.877×10^{-2}
VJKS00	1.514×10^{-2}	1.280×10^{-2}	1.798×10^{-2}

continued on next page

Table A.2.: *continued*

Functional	HeNe	HeAr	NeAr
E00	-1.610×10^{-2}	-1.495×10^{-2}	-1.901×10^{-2}

Table A.3.: The error in the self-consistent density defined in Eq. 6.2 of various KE functionals at LDA equilibrium for He_2, Ne_2, and Ar_2. For each system, the best result is in boldface and the worst is in italics.

Functional	He_2	Ne_2	Ar_2
$T_{\mathrm{S}}^{\mathrm{nad}} = 0$	5.349×10^{-3}	1.063×10^{-2}	2.143×10^{-2}
TF	1.731×10^{-3}	4.568×10^{-3}	7.352×10^{-3}
vW	*1.364 × 10⁻¹*	*2.364 × 10⁻¹*	*3.270 × 10⁻¹*
TFvW	1.207×10^{-1}	2.007×10^{-1}	2.694×10^{-1}
GEA2	1.099×10^{-2}	1.639×10^{-2}	2.328×10^{-2}
Golden	3.082×10^{-2}	5.033×10^{-2}	6.948×10^{-2}
YT65	2.076×10^{-2}	3.315×10^{-2}	4.611×10^{-2}
Baltin	6.266×10^{-2}	1.042×10^{-1}	1.420×10^{-1}
Lieb	1.919×10^{-2}	3.046×10^{-2}	4.245×10^{-2}
R-PBE	1.510×10^{-3}	2.989×10^{-3}	$\mathbf{6.047 \times 10^{-3}}$
revAPBEKint	2.965×10^{-3}	5.794×10^{-3}	1.171×10^{-2}
APBEKint	1.780×10^{-3}	3.084×10^{-3}	7.922×10^{-3}
revAPBEK	2.811×10^{-3}	5.410×10^{-3}	1.119×10^{-2}
APBEK	1.693×10^{-3}	2.853×10^{-3}	7.492×10^{-3}
TW02I	1.743×10^{-3}	2.939×10^{-3}	7.597×10^{-3}
TW02II	$\mathbf{1.454 \times 10^{-3}}$	$\mathbf{2.316 \times 10^{-3}}$	6.402×10^{-3}
TW02III	1.798×10^{-3}	3.056×10^{-3}	7.778×10^{-3}

continued on next page

Table A.3.: *continued*

Functional	He_2	Ne_2	Ar_2
TW02IV	1.835×10^{-3}	3.135×10^{-3}	7.898×10^{-3}
LLP	2.775×10^{-3}	4.058×10^{-3}	8.409×10^{-3}
FR(B88)	2.628×10^{-3}	3.777×10^{-3}	8.065×10^{-3}
T92	3.703×10^{-3}	6.194×10^{-3}	1.177×10^{-2}
LC94	3.756×10^{-3}	5.864×10^{-3}	1.069×10^{-2}
FR(PW86)	1.675×10^{-3}	2.357×10^{-3}	6.428×10^{-3}
LP	1.875×10^{-3}	4.985×10^{-3}	7.891×10^{-3}
OL1	6.671×10^{-3}	9.049×10^{-3}	1.339×10^{-2}
OL2	1.099×10^{-2}	1.638×10^{-2}	2.327×10^{-2}
P82	2.423×10^{-3}	7.021×10^{-3}	1.221×10^{-2}
P92	3.978×10^{-3}	1.090×10^{-2}	1.753×10^{-2}
VSK98	7.158×10^{-2}	9.057×10^{-2}	1.100×10^{-1}
VJKS00	3.416×10^{-2}	4.693×10^{-2}	5.270×10^{-2}
E00	3.396×10^{-2}	4.398×10^{-2}	5.640×10^{-2}

Table A.4.: The error in the self-consistent density defined in Eq. 6.2 of various KE functionals at LDA equilibrium for HeNe, HeAr, and NeAr. For each system, the best result is in boldface and the worst is in italics.

Functional	HeNe	HeAr	NeAr
$T_S^{nad} = 0$	8.493×10^{-3}	1.125×10^{-2}	1.453×10^{-2}
TF	3.048×10^{-3}	3.885×10^{-3}	5.585×10^{-3}
vW	*1.891 × 10⁻¹*	*2.106 × 10⁻¹*	*2.756 × 10⁻¹*
TFvW	1.631×10^{-1}	1.811×10^{-1}	2.313×10^{-1}

continued on next page

Table A.4.: *continued*

Functional	HeNe	HeAr	NeAr
GEA2	1.421×10^{-2}	1.724×10^{-2}	1.945×10^{-2}
Golden	4.144×10^{-2}	4.725×10^{-2}	5.867×10^{-2}
YT65	2.764×10^{-2}	3.203×10^{-2}	3.880×10^{-2}
Baltin	8.486×10^{-2}	9.509×10^{-2}	1.208×10^{-1}
Lieb	2.548×10^{-2}	2.966×10^{-2}	3.570×10^{-2}
R-PBE	2.265×10^{-3}	$\mathbf{3.764 \times 10^{-3}}$	$\mathbf{4.458 \times 10^{-3}}$
revAPBEKint	4.739×10^{-3}	7.346×10^{-3}	8.638×10^{-3}
APBEKint	2.723×10^{-3}	5.127×10^{-3}	5.817×10^{-3}
revAPBEK	4.463×10^{-3}	7.062×10^{-3}	8.267×10^{-3}
APBEK	2.551×10^{-3}	4.924×10^{-3}	5.530×10^{-3}
TW02I	2.627×10^{-3}	5.007×10^{-3}	5.628×10^{-3}
TW02II	$\mathbf{2.107 \times 10^{-3}}$	4.396×10^{-3}	4.728×10^{-3}
TW02III	2.721×10^{-3}	5.119×10^{-3}	5.771×10^{-3}
TW02IV	2.785×10^{-3}	5.192×10^{-3}	5.864×10^{-3}
LLP	3.787×10^{-3}	6.190×10^{-3}	6.513×10^{-3}
FR(B88)	3.570×10^{-3}	5.958×10^{-3}	6.249×10^{-3}
T92	5.323×10^{-3}	7.878×10^{-3}	8.807×10^{-3}
LC94	5.197×10^{-3}	7.663×10^{-3}	8.261×10^{-3}
FR(PW86)	2.267×10^{-3}	4.516×10^{-3}	4.784×10^{-3}
LP	3.295×10^{-3}	4.012×10^{-3}	6.002×10^{-3}
OL1	8.299×10^{-3}	1.077×10^{-2}	1.104×10^{-2}
OL2	1.420×10^{-2}	1.723×10^{-2}	1.944×10^{-2}
P82	4.538×10^{-3}	4.815×10^{-3}	8.644×10^{-3}
P92	7.215×10^{-3}	7.294×10^{-3}	1.323×10^{-2}
VSK98	8.226×10^{-2}	9.089×10^{-2}	1.001×10^{-1}

continued on next page

Table A.4.: *continued*

Functional	HeNe	HeAr	NeAr
VJKS00	4.091×10^{-2}	4.238×10^{-2}	4.991×10^{-2}
E00	3.982×10^{-2}	4.421×10^{-2}	4.833×10^{-2}

Table A.5.: The error in the NAKE in Ha of various KE functionals at LDA equilibrium for H_2, Li_2, and Be_2. ENS treatment is used. For each system, the best result is in boldface and the worst is in italics.

Functional	H_2	Li_2	Be_2
$T_{\rm S}^{\rm nad} = 0$	1.521×10^{-1}	$\mathbf{-4.797 \times 10^{-3}}$	-6.036×10^{-2}
TF	-1.944×10^{-1}	-1.299×10^{-2}	8.250×10^{-3}
vW	**0**	-2.243×10^{-1}	-2.145×10^{-1}
TFvW	*-3.703×10^{-1}*	-2.144×10^{-1}	*-1.101×10^{-1}*
GEA2	-2.130×10^{-1}	-3.131×10^{-2}	-3.551×10^{-3}
Golden	-2.433×10^{-1}	-6.280×10^{-2}	-2.319×10^{-2}
YT65	-2.281×10^{-1}	-4.672×10^{-2}	-1.326×10^{-2}
Baltin	-2.899×10^{-1}	-1.149×10^{-1}	-5.428×10^{-2}
Lieb	-2.257×10^{-1}	-4.424×10^{-2}	-1.170×10^{-2}
R-PBE	-1.965×10^{-1}	-1.435×10^{-2}	7.106×10^{-3}
revAPBEKint	-2.180×10^{-1}	-1.285×10^{-2}	1.644×10^{-3}
APBEKint	-2.189×10^{-1}	-1.206×10^{-2}	3.339×10^{-3}
revAPBEK	-2.234×10^{-1}	-1.274×10^{-2}	1.911×10^{-3}
APBEK	-2.241×10^{-1}	-1.200×10^{-2}	3.641×10^{-3}
TW02I	-2.234×10^{-1}	-1.206×10^{-2}	3.583×10^{-3}
TW02II	-2.240×10^{-1}	-1.189×10^{-2}	4.287×10^{-3}

continued on next page

Table A.5.: *continued*

Functional	H_2	Li_2	Be_2
TW02III	-2.231×10^{-1}	-1.211×10^{-2}	3.486×10^{-3}
TW02IV	-2.230×10^{-1}	-1.214×10^{-2}	3.424×10^{-3}
LLP	-2.236×10^{-1}	-1.501×10^{-2}	3.096×10^{-3}
T92	-2.174×10^{-1}	-1.524×10^{-2}	$\mathbf{7.264 \times 10^{-4}}$
FR(B88)	-2.246×10^{-1}	-1.483×10^{-2}	3.287×10^{-3}
LC94	-2.225×10^{-1}	-1.624×10^{-2}	2.026×10^{-3}
FR(PW86)	-2.227×10^{-1}	-1.305×10^{-2}	3.608×10^{-3}
LP	-2.167×10^{-1}	-1.361×10^{-2}	9.953×10^{-3}
OL1	-2.088×10^{-1}	-2.449×10^{-2}	7.979×10^{-4}
OL2	-2.133×10^{-1}	-3.132×10^{-2}	-3.527×10^{-3}
P82	-2.274×10^{-1}	-1.334×10^{-2}	9.538×10^{-3}
P92	-1.724×10^{-1}	-1.341×10^{-2}	1.308×10^{-2}
VSK98	-1.981×10^{-1}	$\textit{-2.346} \times \textit{10}^{-1}$	-3.959×10^{-2}
VJKS00	-2.390×10^{-1}	6.003×10^{-2}	2.689×10^{-2}
E00	-2.056×10^{-1}	-1.037×10^{-1}	-1.805×10^{-2}

Table A.6.: The error in the self-consistent density defined in Eq. 6.2 of various KE functionals at LDA equilibrium for H_2, Li_2, and Be_2. ENS treatment is used. For each system, the best result is in boldface and the worst is in italics.

Functional	H_2	Li_2	Be_2
$T_S^{nad} = 0$	8.933×10^{-2}	$\mathbf{1.135 \times 10^{-1}}$	7.072×10^{-1}
TF	2.227×10^{-1}	2.226×10^{-1}	5.644×10^{-1}

continued on next page

Table A.6.: *continued*

Functional	H_2	Li_2	Be_2
vW	**0**	2.815×10^{-1}	*1.107*
TFvW	2.305×10^{-1}	3.042×10^{-1}	7.274×10^{-1}
GEA2	2.204×10^{-1}	2.155×10^{-1}	5.736×10^{-1}
Golden	2.183×10^{-1}	2.147×10^{-1}	5.936×10^{-1}
YT65	2.191×10^{-1}	2.134×10^{-1}	5.827×10^{-1}
Baltin	2.196×10^{-1}	2.354×10^{-1}	6.343×10^{-1}
Lieb	2.193×10^{-1}	2.135×10^{-1}	5.811×10^{-1}
R-PBE	2.225×10^{-1}	2.218×10^{-1}	5.653×10^{-1}
revAPBEKint	2.268×10^{-1}	2.023×10^{-1}	5.779×10^{-1}
APBEKint	2.273×10^{-1}	2.035×10^{-1}	5.776×10^{-1}
revAPBEK	2.267×10^{-1}	2.023×10^{-1}	5.779×10^{-1}
APBEK	2.266×10^{-1}	2.022×10^{-1}	5.779×10^{-1}
TW02I	2.270×10^{-1}	2.022×10^{-1}	5.782×10^{-1}
TW02II	2.259×10^{-1}	2.003×10^{-1}	5.788×10^{-1}
TW02III	2.253×10^{-1}	2.027×10^{-1}	5.777×10^{-1}
TW02IV	2.242×10^{-1}	2.011×10^{-1}	5.780×10^{-1}
LLP	2.270×10^{-1}	2.075×10^{-1}	5.756×10^{-1}
T92	2.274×10^{-1}	2.073×10^{-1}	5.757×10^{-1}
FR(B88)	2.214×10^{-1}	2.014×10^{-1}	5.796×10^{-1}
LC94	2.261×10^{-1}	2.079×10^{-1}	5.757×10^{-1}
FR(PW86)	2.255×10^{-1}	2.055×10^{-1}	5.799×10^{-1}
LP	2.343×10^{-1}	2.278×10^{-1}	5.638×10^{-1}
OL1	2.220×10^{-1}	2.170×10^{-1}	5.702×10^{-1}
OL2	2.205×10^{-1}	2.155×10^{-1}	5.736×10^{-1}
P82	2.301×10^{-1}	2.232×10^{-1}	5.722×10^{-1}

continued on next page

Table A.6.: *continued*

Functional	H_2	Li_2	Be_2
P92	2.210×10^{-1}	2.401×10^{-1}	$\mathbf{5.545 \times 10^{-1}}$
VSK98	1.986×10^{-1}	*3.094* $\times$ *10*$^{-1}$	5.606×10^{-1}
VJKS00	*2.446* $\times$ *10*$^{-1}$	2.024×10^{-1}	5.844×10^{-1}
E00	2.108×10^{-1}	2.202×10^{-1}	5.728×10^{-1}

VITA

Kaili Jiang

Education

Aug 2012 - Aug 2018	Ph.D., Physics,
	Purdue University, West Lafayette, IN
	Advisor: Prof. Adam Wasserman
Sep 2007 - Jul 2011	B.S., Physics,
	Peking University, Beijing, China

Research Experience

May 2013 - present	Department of Physics and Astronomy,
	Purdue University
	Supervisor: Prof. Adam Wasserman
Aug 2011 - May 2012	School of Physics,
	Peking University
	Supervisor: Prof. Jing Lu

Refereed Journal Publications

1. **Jiang, K.**, Nafziger, J., Wasserman, A., "Non-additive Non-interacting Kinetic Energy of Rare Gas Dimers" *J. Chem. Phys.*, **148**, 104113 (2018).

2. Nafziger, J., **Jiang, K.**, Wasserman, A., "Accurate Reference Data for the Non-additive, Noninteracting Kinetic Energy in Covalent Bonds.", *J. Chem. Theory Comput.* **13**, 577 (2017).
3. Wasserman, A., Nafziger, J., **Jiang, K.**, Kim, M., Sim, E., Burke, K., "The Importance of Being Inconsistent.", *Annu. Rev. Phys. Chem.* **68**, 555 (2017)
4. Pan, F., Wang, Y, **Jiang, K.**, Ni, Z., Ma, J., Zheng, J. Quhe, R. Shi, J., Yang, J., Chen, C., Lu, J., "Silicene nanomesh.", *Sci. Rep.* **5**, 9075 (2015)

Papers in Preparation

1. **Jiang, K.**, Nafziger, J., Wasserman, A., "Constructing Non-additive Non-interacting Kinetic Energy for Covalent Bonds from Exact Conditions."
2. **Jiang, K.**, Mosquera, M. A., Wasserman, A., "Virial Relations in Fragment-based Density-functional Theory."

Presentations

- APS March Meeting, Los Angles, CA — Mar 2018
- APS March Meeting, Baltimore, MD — Mar 2016
- Purdue Quantum Center, West Lafayette, IN — Oct 2015
- Midwest Theoretical Chemistry Conference, Evanston, IL — Jun 2014